A Method to Evaluate the Thermal Stress Management of Firefighters' Protective Clothing

A Thesis Submitted to the College of Graduate and Postdoctoral Studies

In Partial Fulfilment of the Requirements

For the Degree of Master of Science

In the Department of Mechanical Engineering

University of Saskatchewan

Saskatoon

By

Tamsaki Asawo

Permission to Use

In presenting this dissertation in partial fulfilment of the requirements for a Postgraduate degree from the University of Saskatchewan, I agree that the Libraries of this University may make it freely available for inspection. I further agree that permission for copying of this dissertation in any manner, in whole or in part, for scholarly purposes may be granted by the professor or professors who supervised my dissertation work or, in their absence, by the Head of the Department or the Dean of the College in which my thesis work was done. It is understood that any copying or publication or use of this thesis/dissertation or parts thereof for financial gain shall not be allowed without my written permission. It is also understood that due recognition shall be given to me and to the University of Saskatchewan in any scholarly use which may be made of any material in my dissertation.

Requests for permission to copy or to make other uses of materials in this dissertation in whole or part should be addressed to:

Head of the Department of Mechanical Engineering,
University of Saskatchewan,
Room 3B48 Engineering Building,
57 Campus Drive,
Saskatoon, SK S7N 5A9,
Canada.

OR

Dean, College of Graduate and Postdoctoral Studies,
University of Saskatchewan,
Room 116 Thorvaldson Building,
110 Science Place,
Saskatoon, SK S7N 5C9,
Canada.

Disclaimer

The names of certain commercial products were exclusively used to meet the thesis and/or exhibition requirements for the degree of Master of Science at the University of Saskatchewan. Reference in this dissertation to any specific commercial products, process, or service by trade name, trademark, manufacturer, or otherwise, does not constitute or imply its endorsement, recommendation, or favoring by the University of Saskatchewan. The views and opinions of the author expressed herein do not necessarily state or reflect those of the University of Saskatchewan and shall not be used for advertising or product endorsement purposes.

Abstract

The clothing worn by firefighters is essential in ensuring their safety. One of the tradeoffs that is made when designing apparel for firefighting is between its ability to protect the individual from high external heat and its ability to manage the thermal stress of the firefighter. More research is required to evaluate the thermal stress management of firefighters' protective clothing. Some of the methods that have been used in the past to assess the thermal stress management of firefighters' protective clothing include the sweating hot plate test, the sweating thermal manikin test and the dry manikin test. The planar geometry of the flat plate does not provide a very realistic representation of the human body while the complexity in the design and testing of the thermal manikin makes it more involved than the hot plate and expensive to obtain thermal resistance values for different fabric ensembles. So a testing method that could be simpler than the heated manikin test but provides a better representation of the human body than the hot plate test is required. This led to the development of the heated cylinder method presented in this thesis.

The method makes use of a heated cylinder in a wind tunnel. In the present research, a finite-height cylinder with a free end at the top causing a 3D airflow, and an infinitely long cylinder that spanned the height of the wind tunnel to create two-dimensional (2D) flow, were used. The fabric specimens were wrapped around the heated sections of these two cylinder models and the Nusselt number and thermal resistance values for the 2D and three-dimensional (3D) fabric-covered cylinders were obtained by subjecting the fabric and cylinder ensemble to airflow at different speeds in a wind tunnel and measuring the temperatures in the different layers of the ensemble. The results for the Nusselt number and thermal resistance data showed the impact of fabric permeability on the heat transfer from the surface of the fabric-covered cylinder and the thermal stress management of the fabric ensembles. This method was developed as a proof of concept; the results from this thesis research would be used in the development of a more realistic but relatively simple method to test the thermal stress management of firefighters' protective clothing.

Acknowledgements

Table of Contents

List of Tables

List of Figures

Nomenclature

English Symbols

A	Area [m^2]
A_{side}	Area of side surface of 3D cylinder [m^2]
A_{total}	Total area of the top and side surface of 3D cylinder [m^2]
AR	Aspect ratio
Bi	Biot number
C_D	Drag force coefficient
c_p	Specific heat [J/(kg·K)]
D	Diameter of the bare cylinder [m]
D'	Diameter of the fabric covered cylinder [m]
F_D	Drag force [N]
H	Length of the cylinder [m]
H_{2D}	Length of 2D cylinder [m]
H_{3D}	Length of 3D cylinder [m]
k	Thermal conductivity [W/(m·K)]
k_{air}	Thermal conductivity of air [W/(m^2·K)]
L	Thickness of the segment used in developing the 1D model [m]
Nu	Nusselt number
Nu_m	Overall Nusselt number for a 3D finite-height cylinder
Nu_r	Nusselt number for the free end of a 3D finite-height cylinder
Nu_s	Nusselt number for the side surface of a 3D finite-height cylinder
P_∞	Freestream absolute static pressure [kPa]
Pr	Prandtl number
q	Heat transfer rate [W]
q''	Heat flux [W/m^2]
q_∞	Dynamic pressure of the freestream [Pa]
q_{cond}	Rate of heat transfer by conduction [W]
q_{conv}	Rate of heat transfer by convection [W]

q_g	Rate of thermal energy generation [W]
q_{in}	Rate of heat transfer into the control volume [W]
q_{st}	Rate of thermal energy storage [W]
Δr	Radial distance between neighboring temperature nodes [mm]
r	Radial dimension in cylinder [m]
R	Gas constant for air [J/kg·K]
R_1	Radius of the first layer of a composite cylinder [mm]
Re_D	Reynolds number
R_f	Fabric thermal resistance [m²· °C/W]
R_i	Internal radius of a composite cylinder [mm]
R_o	External radius of a composite cylinder [m]
Δt	Interval between time steps [s]
T_{avg}	Average temperature on the surface of the cylinder [°C]
T_∞	Temperature of the freestream [°C]
T_m^p	Temperature node at time p and radial location m [°C]
T_{m+1}^p	Temperature node at time p and to the right of T_m^p [°C]
T_{m-1}^p	Temperature node at time p and to the left of T_m^p [°C]
T_m^{p+1}	Temperature node at time $p+1$ and radial location m [°C]
T_{TC}	Internal temperature of the cylinder [°C]
U_∞	Freestream velocity [m/s]
$U(x)$	Uncertainty in x
$u(z)$	Mean streamwise velocity profile of the boundary layer [m/s]
x, y, z	Directions of movement of the traversing wing [mm]

Greek Symbols

δ	Boundary layer thickness [mm]
θ	Angle of segment in 1D model development [degrees]
μ_∞	Dynamic viscosity of the freestream [kg/(m·s)]
ρ_∞	Density of the freestream [kg/m³]

List of Abbreviations and Acronyms

1D	One-dimensional
2D	Two-dimensional
3D	Three-dimensional
ASTM	American Society for Testing and Materials
FDM	Finite-difference model
FF	Firefighters'
IR	Infrared
ISO	International Organization for Standardization
OSHA	Occupational Safety and Health Administration
PBI	Polybenzimidazole
PPE	Personal Protective Equipment
RS	Ripstop

Chapter 1 – Introduction

1.1 Background

The evolution of technology has led to the development of multiple building materials which may increase aesthetic value and provide better insulation for buildings. However, these materials may be susceptible to quicker ignition and more rapid flame spread than traditional materials. This has made the job of a firefighter more challenging today. Some factors are very important in the job of a firefighter. These include but are not limited to, time to fire site, access to fire hydrants and other firefighting equipment, setup time, complexity of the design of the building, fire behavior of building materials, and the personal protective equipment (PPE) worn by the firefighters (OSHA, 2015).

The clothing worn by firefighters is extremely important in ensuring their safety. A typical firefighters' protective coat is made up of three major layers: the outer layer that protects the individual from flames and abrasion from sharp objects, the moisture barrier that obstructs the flow of liquid towards the individual but strives to allow moisture from the body to escape, and finally the thermal liner that protects the individual from excessive heat transfer in hot or cold environments. The arrangement of the composite fabric can be seen in Figure 1.1 with the thermal liner closest to the body, followed by the moisture barrier and the outer shell.

Figure 1.1: Basic layers of a complete firefighters' protective coat.

The clothing worn by firefighters should be capable of protecting the individual from the high heat fluxes and temperatures present at fire sites to avoid skin burns (thermal protection). This requires the resistance to heat transfer through the clothing to be relatively high. However,

the high thermal resistance of the clothing makes it difficult for the heat that is produced by the body to escape. The direct exposure of the body to these high amounts of thermal energy for an elongated period of time could lead to thermal stress. This could prompt the development of fatigue that could cause slips, trips, falls and heat burns while on the job, or in the long term, contribute to more severe problems such as cardiac or cancer-related deaths (University of Illinois Fire Service Institute, 2008). According to Fahy et al. (2020), there has been a 9% increase in cancer cases for firefighters and a 14% increase in cancer-related deaths when compared to the general population of the United States. The tradeoff that occurs between the thermal protection and the thermal stress management is an integral factor in the design process of firefighters' clothing.

While there has been a lot of work done on the thermal protection of firefighters, more research is required to study the thermal stress management of the clothing. Several factors such as the fit of clothing and rate of perspiration make it challenging to create an accurate representation of the situation encountered by firefighters experimentally. Various methods have been used in the past to test the thermal stress management of fabrics. These include the sweating hot plate test in the ASTM F1868 (ASTM International, 2017) and ISO 11092 (ISO, 2014) standards, the sweating thermal manikin test in the ASTM F1291 standard (ASTM International, 2016), and the dry manikin test in the ISO 15831 test standard (ISO, 2004; Nazare and Madrzykowski, 2015). For the hot plate method, the fabric or fabric ensemble to be tested is placed over a heated test plate and the edges are taped for stability. The other surface of the fabric ensemble that is not in direct contact with the hot plate is exposed to extremely low-speed airflow and the experimental chamber is maintained at a constant predetermined temperature and humidity. The temperatures on both sides of the fabric ensemble are measured during the experiment. At steady state, these temperatures are used to calculate the thermal resistance of the fabric ensemble. For this test method, the flat test plate is used to represent the human body. However, due to its planar geometry it is not a very realistic representation. This could lead to less accurate results. A study was conducted by Su et al. (2019) to investigate the thermal protection capability of firefighters' protective clothing and the level of agreement between the results obtained from planar and cylindrical configurations. It was observed that the times to second degree burns predicted by the planar and cylindrical configurations were significantly different despite the similarity in experimental setup and procedure. Also, due to the fact that the

fabric specimen is often only secured to the test plate by tape at the edges, there is a tendency of the fabric specimen randomly bulging upwards during the test thereby producing misleading results.

The thermal manikin method involves using an artificial model of a human being to perform heat transfer tests that are similar to those performed with the hot plate setup, to obtain a thermal resistance value that pertains to the fabric specimen. Although the thermal manikin method makes use of the most realistic representation of the human body – the manikin – it can be very expensive and complex to perform as the thermal resistance of the clothing on each body part has to be obtained and used to derive an average value for the entire body of clothing. This can be seen in a review article by McLellan and Selkirk (2006) for the Toronto Fire Service where selected firefighters' protective clothing samples were tested using a heated manikin. The thermal resistance and water vapor permeability coefficients associated with each fabric were obtained and used in collaboration with a heat strain model to predict the rate of increase of body core temperatures under different environmental conditions.

The method proposed in this thesis uses a heated cylinder as the major test apparatus to model the human body being exposed to high temperatures. It is a less expensive and simpler method to quantify the thermal stress management of fabrics than the thermal manikin, and a more realistic and potentially more accurate representation of the human body than the hot plate test. This proposed heated cylinder method can also be extended to solve a similar problem in performance clothing such as that worn by athletes performing physical activities in cold or hot weather environments for an extended period of time.

1.2 Motivation

Due to the various problems still faced by firefighters today, it is important to continue the advancement of research to improve their health and safety, which is significantly dependent on the capability of their personal protective clothing. As was stated earlier, research in the past has been heavily focused on the thermal protection offered by their clothing leaving the heat stress management aspect somewhat overlooked. Although current research has begun addressing this component, there is still room for progress. The goal of the research described in this thesis is to contribute to the development of more realistic and less expensive methods to

characterize the thermal stress management of firefighters' protective clothing as well as to measure convective heat transfer coefficients of fabric covered cylinders.

1.3 Objectives

To achieve this goal, the following objectives were developed for this research:

- To measure the thermal resistance of various fabrics used for firefighters' protective clothing,
- To measure the effects that changes in airflow conditions and temperature have on the convective heat transfer coefficient of a three-dimensional and two-dimensional cylinder with and without a fabric,
- To contribute to the development of a method and equipment to evaluate the thermal stress management of various fabrics, and
- To obtain drag force coefficient data on the flow around a three-dimensional and two-dimensional cylinder covered with various fabrics.

1.4 Scope and Outline of Thesis

This thesis contains information about a method to test the thermal stress management of various fabrics. However, emphasis is placed on the fabrics used by firefighters and the environments they usually operate in. To fully represent the thermal situation faced by both firefighters and athletes, it is important to include the effect of sweat in the analysis of the thermal stress management of the clothing. However, since this is the first step in the development of the heated cylinder test method, the effect of sweating on the thermal comfort of the individual was neglected and was therefore outside the scope of the research. The analyses of the thermal stress management shown in the thesis therefore only include sensible heat transfer through the clothing specimen. Therefore, the method proposed by the author cannot be used in determining the absolute thermal resistance of the test specimen. However, it can be helpful in obtaining relative values of thermal resistance and heat loss that can be used to rank multiple fabrics based on their ability to manage thermal stress.

Furthermore, due to the constraints of the wind tunnel and other instrumentation used in this research, the tests were only performed for specific Reynolds numbers and temperature

differences between the cylinder and the freestream in the wind tunnel; this matter is discussed further in later sections of this thesis.

In Chapter 2, a more detailed literature review of the various standards that have been developed in the past to measure the thermal stress management of firefighters' protective clothing, as well as the various research studies that have been performed using these standards, are documented. The literature review also includes a presentation of studies done in the past on the flow around heated three-dimensional (3D) and two-dimensional (2D) cylinders in a wind tunnel, the theories obtained from these investigations that were applied to this research, and the gaps present in these studies. The method, instrumentation and procedure that were employed during this research are stated in detail in Chapter 3. In Chapters 4 and 5, the experimental and numerical results obtained are presented and explained, respectively. Finally, the conclusions drawn from the results are presented in Chapter 6 along with some recommendations for future work.

Chapter 2 – Literature Review

The comfort experienced by individuals wearing a particular type of clothing is strongly influenced by the thermal stress management of the clothing. A situation where the body's temperature deviates from the normal could cause thermal stress. When the body's core temperature increases to about 39.5℃, the body's thermoregulation starts to fail and the effectiveness of the individual becomes compromised; a temperature of greater than 42℃ could be fatal (Ding, 2010). Due to the thickness and hence thermal resistance of firefighters' protective gear, the capability of their clothing to manage thermal stress is crucial in ensuring they can perform their jobs effectively and also prevent serious health problems.

For most fabrics the ability to protect an individual from high external heat energy conflicts greatly with its thermal stress management. Jin et al. (2018) developed total performance indices to rank five materials used to manufacture firefighters' protective clothing based on their combined thermal protection and thermal stress management capability. It was observed that the resistance to external heat conflicted with the ability of the fabric to dissipate heat generated internally. Therefore, a fabric with a higher resistance to external heat had a low rating in terms of thermal stress management. This made it somewhat difficult to rank the materials tested. The thermal stress management of various types of clothing have been tested using various methods in the past as stated in the introduction. This includes the sweating hot plate test in the ASTM F1868 (ASTM International, 2017) and ISO 11092 (ISO, 2014) standards, the sweating thermal manikin test in the ASTM F1291 standard (ASTM International, 2016), and the dry manikin test in the ISO 15831 test standard (ISO, 2004; Nazare and Madrzykowski, 2015).

2.1 Hot Plate Test

According to ASTM F1868 (ASTM International, 2017), the hot plate test involves the use of a heated flat plate called the test plate, guarded by a metallic ring around and below it, all maintained at a constant temperature with the aid of an electric current. The fabric specimen to be tested is placed over the test plate and air at a very low velocity (between 0.5 and 1.0 m/s) is allowed to flow over the exposed surface of the fabric. The plate and fabric assembly as well as all the instrumentation are located in an environmental chamber where the air is maintained at a predetermined temperature between 4 and 25℃ (with fluctuations of no more than $\pm$ 0.1℃

during test) and relative humidity between 20 and 80% (with fluctuations of no more than $\pm$ 4% during the test). When the entire test environment reaches steady state, the thermal resistance of the fabric can be obtained by measuring the air and plate's surface temperature as well as the power required to keep the plate at that particular temperature. According to ASTM F1868 (ASTM International, 2017), the evaporative resistance represents the resistance to the flow of moisture vapor from a saturated surface to an environment with a lower vapor pressure. This can be obtained by introducing water to the hot plate test and measuring the water vapor pressures on the test plate and in the surrounding air at steady state. This helps to quantify the contribution of sweat to thermal stress management of a fabric. The total heat loss through a fabric (or ensemble) can also be obtained from the hot plate test.

Various researchers have used the hot plate tests for testing all three parameters (the thermal resistance, evaporative resistance and total heat loss). These include but are not limited to the following. Bakshi et al. (2015) developed breathable and waterproof fabrics by coating them with silicone oil and polyurethane binder and the sweating hot plate test was used to quantify the breathability of the fabrics by measuring the evaporative resistance pertaining to each layer of fabric as well as comparing the effects that the different types of coating have on the thermal resistance of the newly developed fabric. From the results of these tests, it was noted that although the thermal resistances pertaining to each newly developed fabric were similar, the evaporative resistance differed depending on the type of coating that was used. For the newly developed fabrics, it was noted that the fabrics with a higher thickness and a lower thermal conductivity had the highest thermal resistance for the most part. This is expected as thickness and thermal conductivity of a fabric material are the two most important factors that influence conduction heat transfer and hence its intrinsic thermal resistance.

Huang (2006) discussed the factors affecting the measurement of thermal and evaporative resistance by a hot plate. According to Huang (2006), it is important to note that the speed of the air flowing over the specimen surface should be high enough to minimize the effects of radiation heat loss and the resistance of the air layer directly above the specimen. The direction of airflow, either parallel to the specimen surface (horizontal flow) or normal to the specimen surface (vertical flow) is also important. If the airflow is vertical and the fabric being tested is permeable,

the air could penetrate the surface and affect the air gap size underneath the specimen's surface. This could influence the overall thermal resistance measured.

Huang (2006) also reports that the problem of air penetration through the fabric is minimized if an airflow parallel to the specimen surface is used, however for horizontal flow the leading edge of the test plate is exposed to the flow first, therefore it is usually cooler than the rest of the plate. This creates a non-uniform temperature distribution over the face of the test specimen which could cause a variation in thermal resistance at different spots on the fabric. Huang (2006) also contends that for horizontal flow, it is necessary to ensure that the boundary layer developed on the fabric-covered plate is similar to that for the bare plate as their values of thermal resistance need to be subtracted to obtain the intrinsic thermal resistance pertaining to the fabric specimen. Therefore, the surface characteristics of the test plate and fabric specimen tested should be identical. Since the method reported in the present research thesis required the use of a flow normal to the surface of the cylinder, these factors had to be taken into account during the design of the experimental procedure.

Kim et al. (2014) researched how effectively the total heat loss values obtained from a hot plate test and thermal manikin tests predicted the thermal stress management of personal protective equipment. These results were also compared to body temperature and heart rate measurements of humans performing physical activities under two different environmental conditions. It was noticed that although the material that had the higher total heat loss value in the sweating hot plate test showed a similar behavior in the sweating thermal manikin test, the results of total heat loss obtained from the sweating hot plate test were significantly higher than the results obtained when an entire ensemble of the fabric was tested using the sweating thermal manikin. Also, the difference between the total heat loss values for the two fabrics obtained in the sweating hot plate test was not proportional to the difference between the results obtained in the sweating thermal manikin test.

The sweating hot plate test was performed according to ASTM F1868 (ASTM International, 2009) under standard conditions at an environmental temperature of 25℃ and 65% RH while the sweating thermal manikin test was performed according to ASTM F1291 and ASTM F2370 (ASTM International, 2010) with an environmental temperature of 20℃ and 40% RH. Recognizing the differences in environmental test conditions between the sweating hot plate

and sweating thermal manikin tests, the total heat loss values were adjusted accordingly. This caused the total heat loss values measured by the sweating thermal manikin test to decrease. However, the difference in total heat loss values between the two materials as given by the sweating hot plate and sweating thermal manikin test did not change significantly. Therefore, it was concluded that a large difference between the total heat loss values of two materials obtained using a sweating hot plate may not reflect the difference in the total heat loss measured when the fabrics are used to make complete coveralls and tested using the sweating thermal manikin. From the human tests, it was noticed that the environmental conditions have a larger impact on the comfort of thermal stress experienced by an individual than the thermal characteristics of the fabrics worn. Also, using the results from the sweating hot plate test, linear relationships showing the rate of increase of body core temperature in mild (21℃, 65% RH) and hot (39℃, 35% RH) conditions were developed. However, the comprehensiveness of this linear relationship is uncertain since only two different types of fabrics were used. Manshahia and Das (2014) also studied the effects that the filament shape factor, the fabric loop length and the elastane linear density have on the thermophysiological comfort properties of a polyester elastane-plated fabric by measuring the thermal resistances and the evaporative resistances using a sweating guarded hot plate.

Wen et al. (2016) investigated the difference between the results of heat stress obtained from the sweating hot plate test and the thermal manikin test and checked which is more informative in predicting the physiological response of a human with respect to heat stress. The tests were carried out on four chemical protective coveralls and it was noted that the thermal resistance of the fabrics depended significantly more on the thickness of their layers than on the materials' thermal conductivity, as the volume of air enclosed in the fabric layers is significantly more than the volume of fibers that make up the fabric. It was also observed that although the rankings of fabrics based on thermal resistance results were in agreement between the sweating thermal manikin and sweating hot plate tests, the exact values were quite different. This agrees with the conclusion derived from the results of total heat loss reported in Kim et al. (2014) and is most likely due to the fact that the sweating hot plate is flat and does not account for three-dimensional effects, drape and fit that are much better represented in the sweating thermal manikin test. This is highlighted in the research performed by Holmer and Nilsson (1995).

9

From the studies stated above, it can be observed that while the hot plate test can be used to characterize the level of comfort provided by different types of fabrics by producing relative values of thermal resistance, evaporative resistance and total heat loss, it does not take into account the effect of clothing fit and the three-dimensionality of the test body on the heat transfer. Although the thermal manikin method as shown in Kim et al. (2014) and Wen et al. (2016) includes these factors, it is complex and can be expensive to perform. Furthermore, hot plate tests are performed in an environmental chamber with low speed airflow that is parallel to the fabric being tested, therefore the impact of air penetration on the thermal resistance of the fabric is not always evident. This does not portray all conditions experienced by firefighters when performing tasks and could lead to misleading results for the thermal resistance of fabrics in conditions where there are higher air speeds; hence, the need for a method relatively simpler than the thermal manikin test that involves the use of a round three-dimensional test model subjected to airflow at varying speed.

2.2 Flow around Bare Cylinders

Since the majority of the human body parts are more cylindrical than flat, it is expected that a cylindrical model would be a more realistic tool to measure the thermal stress management of fabrics. A lot of research has been done to study fluid flow around a cylinder as well as the rate of heat transfer from a heated cylinder in cross flow. The findings from some of these past research studies helped in the design of the experimental model and procedure for the present research.

The flow around a cylinder can be characterized by the Reynolds number,

$$Re_D = \rho_\infty U_\infty D / \mu_\infty \tag{2.1}$$

for a cylinder with diameter, D, and a fluid with density, ρ_∞, viscosity μ_∞, and freestream velocity, U_∞. This represents the ratio of inertial forces to viscous forces within a fluid. In the research stated in this thesis, a two-dimensional cylinder and a three-dimensional cylinder were used as models for studying the thermal stress management of fabrics. To obtain two-dimensional (2D) flow around a cylinder, the ratio of the length H of the cylinder and the diameter D should be very large, (i.e. $H >> D$). On the other hand, a three-dimensional cylinder has an aspect ratio $AR = H/D$ where the wind tunnel wall and/or the free end of the cylinder

affect the flow around it. End plates are used to promote 2D flow around a model. Based on the study for the optimization of end plates performed by Stansby (1974), it was noted that the interference effects of end plates span $3.5D$ from the edge of the plate, therefore 2D flow can be approximated in the section of the cylinder that is at least $3.5D$ from the edge of the end plates. Fox and West (1990) also confirmed this in their study.

The blockage of a 2D cylinder represents the ratio of the diameter of the cylinder to the width of the tunnel across the flow. If the blockage is too large, the boundary layers on the wind tunnel walls may impact the flow around the cylinder. West and Apelt (1982) did some research to study the effects of tunnel blockage and aspect ratio on the flow past a circular cylinder for a Reynolds number range of 10^4 - 10^5. It was reported that for blockage ratios less than 6%, the effects of blockage on the flow characteristics (pressure distribution and drag coefficient) are small, therefore it is important to ensure that the blockage of the flow caused by the cylinder is below 6%. This helped in determining the diameter of the 2D cylinder that would be tested during this research.

2.2.1 Flow around Bare 2D Heated Cylinders

Heated cylinders have been used by various researchers to study various theories or model some real life phenomena. Some of the research on heat transfer from two-dimensional cylinders is documented here. The Nusselt number for a cylinder Nu_D is the ratio of convection heat transfer to conduction between the cylinder and the surrounding fluid. It yields a quantification of the convective heat transfer that occurs at the cylinder's surface and is represented by the equation

$$Nu_D = hD/k,$$
(2.2)

where h represents the convective heat transfer coefficient associated with the flow around the cylinder, D is the diameter of the cylinder, and k is the thermal conductivity of the fluid (Bergman et al., 2011).

Schmidt et al. (1943) performed some experiments to study the local heat transfer from the surface of a cylinder in cross flow using air as the fluid over a Reynolds number range of $5 \times 10^3 - 10^5$. It was noticed that the percent of the overall heat transfer associated with the rear of the cylinder steadily increased with Reynolds number. Although a correlation was not proposed

for the overall Nusselt number, the results were compared to those by Hilpert (1933) and were found to be similar despite some minor variations at lower Reynolds numbers. Achenbach (1975) studied the total and local heat transfer from a smooth two-dimensional copper cylinder in cross flow over a Reynolds number range of $Re_D = 3 \times 10^4 - 4 \times 10^6$.

The effects of the cylinder's boundary layer on the heat transfer from a cylinder has been well-studied. The variation of the Nusselt number has been studied for subcritical, critical, supercritical and transcritical flow. The effect of surface roughness on the pressure drag coefficient and the heat transfer from a circular cylinder in cross flow was also studied by Achenbach (1977). It was observed that for relative surface roughness, k_s/D (where k_s represents the sand-grain roughness height) up to 300×10^{-5} and $Re_D < 10^{-5}$, the pressure drag coefficient is independent of surface roughness and Reynolds number. As the surface roughness increases, the critical Reynolds number where the drag coefficient is minimum decreases. Furthermore, at lower Re_D, the overall Nusselt number values were independent of surface roughness as expected from the drag force results. However, a deviation is noticed at the critical Reynolds number and the Nusselt number increases with surface roughness. Nusselt number correlations for the smooth cylinder as well as the cylinder with specific roughness values were proposed for different ranges of Re_D and $Pr = 0.72$.

Sanitjai and Goldstein (2004) studied the forced convection heat transfer from the surface of a circular cylinder in cross flow for $Re_D = 2 \times 10^3 - 9 \times 10^4$ and a range of Prandtl number, $Pr = 0.7 - 176$ by using different fluids such as air, water and mixtures of ethylene glycol and water. Local Nusselt number correlations based on Re_D and Pr were developed for heat transfer in three different flow regions that were observed at different angular locations θ around the circumference of the cylinder. This includes the laminar boundary layer region ($0° < \theta < 85°$), the reattachment of shear layer region ($85° < \theta < 135°$) and the periodic vortex flow region ($135° < \theta < 180°$). Furthermore, an overall Nusselt number correlation was computed by numerically integrating the local Nusselt number values and it was found to be in agreement with the other results from the literature.

Churchill and Bernsein (1977) developed a comprehensive correlation for the average Nusselt number that characterizes the convection heat transfer from the surface of an entire circular cylinder for all Re_D and Pr. This was done by combining correlations that have been

obtained previously for the various flow regimes. The correlation obtained was compared to experimental data stated in past literature and was observed to provide a lower bound for the Nusselt numbers obtained in the experiment for $Re_D Pr > 0.2$ as the impact of free convection, tunnel blockage and end effects were ignored. As the correlation was obtained for a large range of Re_D and Pr, its accuracy for lower Reynolds numbers ($Re_D < 4 \times 10^5$) is not certain, hence correlations specific to that flow regime would yield more accurate results.

2.2.2 Flow around Bare 3D Heated Cylinders

Sparrow and Samie (1981) performed experiments to obtain heat transfer coefficients for a finite cylinder in cross flow. It was reported that the heat transfer coefficient at the free end was higher than the heat transfer coefficient at the portion of the cylinder that is not influenced by end effects. Chyu and Natarajan (1996) examined the local heat transfer from five different protruding geometries (cube, cylinder, hemisphere, diamond and pyramid) at $Re_D = 1.7 \times 10^4$. It was noted that the upstream horseshoe vortex system and the vortices in the downstream wake have a large impact on the convective heat transfer from the geometries.

Finnigan and Longstaff (1982) examined the heat transfer from finite cylinders in cross flow undergoing forced convection in a wind tunnel. These cylinders were used as models to represent cylindrical grain storage bins. Correlations for Nusselt number as a function of Reynolds number were reported. The tops of the cylinders were conically shaped and were reported to have the highest amount of heat transfer from the protrusion. Kawamura et al. (1984) also studied the heat transfer from a finite cylinder in cross flow. A correlation that can be used to obtain the Nusselt number as a function of the Reynolds numbers and the dimensions of the cylinder was developed.

Tsutsui et al. (2000) investigated the fluid flow characteristics as well as the heat transfer from a cylinder of $AR = 0.35$ mounted on a flat plate. This was used as a model to study the heat transfer from fuel oil storage tanks. Correlations used to estimate the Nusselt number as a function of Reynolds number for the top of the cylinder as well as the circular surface were developed and reported. An expression to calculate the overall Nusselt number of the finite height cylinder was developed for a situation where the Nusselt numbers on the free end and on the cylindrical side as well as the aspect ratio of the cylinder are known. This information was

used in the current research to obtain the Nusselt number for the side surface of the finite height cylinder.

Rodiger et al. (2007) also studied the flow on the surface of a finite cylinder mounted normal to a ground plate with $AR = 2$. The flow characteristics were visualized using the oil-film visualization technique and pressure and heat flux fluctuation measurements were made. These measurements helped to determine the boundary layer transition on the surface of the cylinder.

Tsutsui and Kawahara (2006) studied the heat transfer around a cylinder with a low aspect ratio in cross flow. The effects of the boundary layer thickness and the aspect ratio of the cylinder on heat transfer were investigated. It was reported that the maximum heat transfer from the cylinder occurred when the ratio of the cylinder's height to the boundary layer thickness was 0.24. It was also reported that the local Nusselt number on the free end reaches a maximum at the reattachment point and a minimum value in the separation bubble region.

Garcia-Villalba et al. (2014) studied the heat transfer caused by forced convection from a finite cylinder with $AR = 2.3$ and $Re_D = 4.4 \times 10^4$ using a large eddy simulation. It was stated that the free end of the cylinder largely affects the heat transfer coefficient. Due to the low pressure at the top of the cylinder, the flow was downwashed behind the cylinder and hence, vortex shedding did not occur in that region. This led to a low rate of heat transfer in that region. However, vortex shedding occurred in the lower parts of the cylinder thereby causing a higher heat transfer rate.

Giordano et al. (2012) performed experiments to study the heat transfer from the base surface on which a finite cylinder in cross flow is mounted as well as the flow downstream of the cylinder. The effects of aspect ratio and Reynolds number on the heat transfer of the flow were studied by testing at $Re_D = 4 \times 10^3, 8 \times 10^3, 1.6 \times 10^4, 3.2 \times 10^4$ and $AR = 1, 2, 4, 8$. The presence of some high heat transfer zones in the cylinder's wake were reported and the heat transfer from these zones increased as the Reynolds number increased. However, the overall heat transfer decreased as the aspect ratio was increased. It was also reported that there was a zone with low heat transfer downstream of the cylinder which was due to the recirculation in the flow field.

2.3 Fabric Covered Cylinders

Some research has been performed on cylinders covered with a porous layer with and without various air gaps between the cylinder and the covering, as the results from this composite cylinder can be applied to filtering and separation technology as well as human clothing. This can be seen in the research by Takeuchi et al. (1984) where the heat transfer from a 2D cylinder covered with close-fitting fabrics was studied. The results obtained showed that the thickness of a fabric as well as the amount of the fabric that is in contact with an object are major contributors to its intrinsic thermal resistance. The less contact between the fabric and the cylinder, the lower the potential for heat transfer as air provides insulation between the fabric and the cylinder. Also, it was observed that the smaller the fabric thickness and contact with the cylinder, the less the variation between the rate of local heat transfer from the cylinder at the front stagnation point and at the rear end as the Reynolds number increases. Therefore, the thickness and contact layer of the fabric enhanced the effect that wind penetration had on the uniformity of heat transfer around the heated cylinder. This was explained further in Takeuchi et al. (1982).

It was also observed that the mean overall heat transfer measured for the fabric-covered cylinder can provide an indication of the order of magnitude of the resistance to heat transfer of the various fabrics. However, these results could be misleading as it was noticed that some fabrics that produced higher overall heat transfer resistance values, had lower values when measured at the front stagnation point. In the context of clothing material, this could mean cold or hot spots for otherwise well performing fabrics.

Sobera et al. (2003) studied the heat transfer from a cylinder covered by a porous layer. The effects of the thickness of the porous layer, the size of the air gap between the layer and the heated cylinder, and the Reynolds number, on the rate of heat and mass transfer from the cylinder, were investigated. It was observed that when the thickness of the porous layer, the permeability of the layer as well as the Reynolds number of the flow are high, the heat transfer resembles that of the bare cylinder as the flow can easily penetrate the porous layer. It was also noticed that when these three parameters are small the results of heat transfer from the covered cylinder are also similar to that of a bare cylinder. It was for intermediate values that a disparity between the results of the covered and bare cylinder can be observed. An empirical correlation

was developed to obtain the average Nusselt number of a covered cylinder if its physical parameters and the Nusselt number of a similar bare cylinder are known.

The research by Kind et al. (1991) showed the impact of fabric permeability on the heat transfer from a cylinder. An internally-heated cylinder covered by a fabric with an air gap in between was tested at multiple air speeds in a wind tunnel and it was observed that the heat loss from the cylinder is higher when the fabric is more permeable and the external air speed is high. This is in agreement with the results presented in Sobera et al. (2003). The results reported in Foncesca and Breckenridge (1965) agree with this and also show how the use of two moderately permeable fabrics with a space between them can provide better resistance to heat loss than a single fabric with low permeability by specific arrangement of the fabric layers.

Gibson (2009) used a computational fluid dynamics (CFD) model to simulate the resistance to heat and mass transfer through a fabric covered cylinder. The effects of thermal resistance, air permeability and water vapor diffusion resistance on the rate of heat transfer through a fabric covered cylinder was investigated. This study is possible with the aid of computational modelling as specific parameters can be easily varied without changing any other parameter at each time unlike in an experiment where varying a specific property of a fabric would most likely lead to a change in another (e.g. in order to change the thermal conductivity of a fabric, another fabric which may have a different air permeability or thickness would have to be used). The results of the simulation showed that the air permeability of a fabric is the most significant factor in determining the rate of heat transfer through a fabric in windy conditions and small variance in fabric intrinsic thermal resistance had little effect on the rate of heat transfer in a windy environment. The results for only three types of fleece materials were reported in this research paper, therefore it is uncertain that the same trend would be observed for other types of fabrics.

Most of the research on fabric covered cylinders focuses on how the heat loss from a cylinder is affected by the thickness and permeability of the fabric as well as the air gap between the cylinder and the fabric. A lot less information has been published regarding the convective heat transfer coefficient for a fabric covered cylinder. The overall heat transfer coefficient referred to in most of the literature represents the rate of heat transfer between the ambient air and the cylinder, not the fabric. Kamata et al. (1988) show the effect of fabrics on the convective

heat transfer coefficients on a heated cylinder. The fabric covered cylinder was tested in an open circuit wind tunnel and the local and mean Nusselt number pertaining to cylinders covered by four different fabrics was presented. It was noticed that the mean Nusselt number for the nylon material agreed very well with the Nusselt number for a two-dimensional bare cylinder. This is expected as the nylon material is relatively smooth compared to the rest of the fabrics, therefore its surface is most similar to that of the cylinder. The knitted fabric (which had the largest thickness) agreed with the results of the bare cylinder until higher velocities where it surpassed the Nusselt number of the bare cylinder. The other two fabrics (tweed and denim) had lower Nusselt number values than the nylon material and the knitted fabric.

One of the reasons suggested for the discrepancy in Nusselt numbers for the various fabrics is due to the variation in air permeability. The tweed and denim materials are more resistant to air penetration than the other fabrics studied. Therefore, it was reported that this resistance to air penetration would inhibit the rate of heat transfer from the cylinder as compared to when it is covered by the other fabrics that are more permeable. However, the convection from the surface of the fabric-covered cylinder should be independent of the heat transfer occurring within the cylinder-fabric ensemble. Although the Nusselt number for the fabric covered cylinders was calculated using the temperature on the outer surface of the fabric, this temperature value was obtained by extrapolation from the internal temperature profile. This may have led to some errors in the results as the method did not account for the airflow through the fabric. The temperature on the surface of the fabric-covered cylinder used in the present research was measured using an infra-red camera, therefore the Nusselt number results should be able to check the conclusion about the effect of permeability reached by Kamata et al. (1988).

Ulijaszek and Henneberg (2012) did some research on epidemiological studies of blood pressure and how they relate to arm size. This study is important to the present thesis research as it reported the arm sizes of adult men and women. These data were used in conjunction with the average wind speeds experienced by firefighters and athletes to determine the Reynolds numbers that would be tested during the course of this research.

2.4 Heat Transfer Model

In the present thesis research, a numerical method was developed to complement the experiments performed in the study of the heat stress management of firefighters' protective clothing. The development of the model can be found in Section 5.1. Numerical and analytical methods are popular for solving non-homogenous differential equations. These include the finite difference, finite element and boundary element method, separation of variables and Laplace transforms. They have also been used repeatedly in the past to solve the transient heat conduction equation. Below are some examples relevant to the thesis research.

Yang and Liu (2017) investigated an analytical solution for one-dimensional transient heat conduction through a two-dimensional composite cylinder with general boundary conditions, and an infinite number of layers. The method allows for a transient and steady state condition as well as a case that involves heat generation. This was done by applying a Laplace transform to both the governing heat conduction equation and the general boundary conditions, obtaining the eigenvalues of the composite cylinder and using the combined results to develop an infinite series solution for the problem. The problem of thermal resistance between layers was also addressed, however this is only possible if the conductance coefficient between the layers is known. In a research study by Lu et al. (2005), the Laplace transform was also used to develop a closed form analytical solution for the temperature on different layers on a hollow composite cylinder in transient heat conduction with outer and inner boundary temperatures that change with time. This was done by applying the time-dependent boundary conditions approximately using a Fourier series to the transient differential heat conduction equation in cylindrical coordinates. The analytical solution obtained can be used to compute temperatures at the centre of each layer assuming the entire layer of the cylinder is at the same temperature.

Delouei et al. (2012) also studied a two-dimensional steady state conduction heat transfer through a composite cylinder with varying fiber orientation. The Fourier field equation in cylindrical coordinate system for an orthotropic material as well as general boundary conditions were used to develop an exact general solution for the composite cylinder and to study the effects of the angles of the fibres on the temperature distribution of the composite cylinder in conjunction with Laplace transforms.

18

Lee et al. (2001) focused on the transient temperature distribution and thermal stresses on an infinitely long, multi-layered hollow cylinder. This one-dimensional temperature change and thermal stresses were induced by the deformation of the elastic materials that make up the composite cylinder. A finite element method was used to develop discretized temperature and stress equations and the Laplace transform method was used to obtain an algebraic system of these equations which are solved to obtain a numerical solution for the stresses and temperature distribution in the radial direction. Najibi and Talebitooti (2017) also studied the heat-induced stresses in a hollow single-layer finite length cylinder under transient conduction as well as the temperature distribution through the cylinder. Applying convection boundary conditions and the specific initial conditions to the differential equations of transient heat conduction in both the radial and axial directions and using a finite element method, a numerical solution giving the temperature distribution in the radial and axial directions as a function of time was developed.

Just like Lee et al. (2001) and Najibi and Talebitooti (2017), Jacquemini and Vautrin (2004) developed a method to determine the temperature in the walls of pipe layers. The problem involved a multi-layer composite pipe with the inner and outer surfaces experiencing convection heat transfer with a fluid and perfect thermal contact between the adjacent layers of the cylinder. The Laplace transform theorem was used to convert the heat conduction differential equations as well as the boundary conditions into algebraic equations and the residue theory method was used to obtain a solution in the time and space domain after the coefficients of the expression had been determined. The result is an analytical solution that can be used to obtain the temperature in an infinite number of layers at any desired time.

Tamene et al. (2006) developed a mathematical model to study the temperature distribution and the thermal contact resistance on a two-layer composite cylinder. Specific temperature boundary conditions and initial conditions at the interfaces of all the layers were applied to the governing equations pertaining to transient conduction in the cylindrical coordinate system. The separation of variables method was used to obtain an analytical solution for the temperature distribution as a function of time and radius for each layer in the cylinder. The contact resistance between the two layers was calculated for known temperature values on the surface of each layer and thermal resistance values pertaining to each layer of the composite cylinder. The method is suitable for a small number of layers as separate analytical equations

19

pertaining to each layer have to be developed and would be more tedious than the other methods presented as the number of layers increase.

Furthermore, Burleson and Eppes (1965) developed solutions to transient heat transfer problems for flat plates, cylinders and spheres using the finite difference method. Of interest to the present research are the solutions for one-dimensional transient heat transfer problems through a multi-layered cylinder. The solution was derived using the energy balance method for various boundary conditions. Although multiple adaptations had to be made, the method described by Burleson and Eppes (1965) was consulted during the development of the computational model used in the current thesis research as describes later in Section 5.1.

In the present research, a finite difference model of a composite cylinder that comprises of multiple concentric layers was developed with the aid of Microsoft Excel software. The concentric layers were modeled according to the properties of the various layers of the firefighters' protective gear and the temperature distribution through the clothing was obtained for various environmental conditions. The results from the computational simulation in the present research was compared and agreed with the results from the models developed by Yang and Liu (2017) as well as the results of the experiments performed. This provides some confidence that the simulation framework is correct and results of similar test scenarios should be reasonable. The model is discussed in more detail in Section 5.1.

Chapter 3 – Experimental Approach

To study the thermal stress management of fabrics, their thermal resistance was measured. The thermal resistance represents the opposition to the flow of thermal energy from a heated surface to a cooler region (ASTM International, 2017). This was studied with the aid of a 3D finite-height cylinder and a 2D infinitely long cylinder (i.e. spanning the entire height of the wind tunnel). The wind tunnel facility and instrumentation used, the fabric samples tested, cylinder models, as well as the experimental procedure followed to measure the thermal resistance of the various fabrics, are explained in this section.

3.1 Wind Tunnel

The experiments performed for the heated cylinder tests were carried out in a wind tunnel located at the University of Saskatchewan. The wind tunnel is a low-speed closed loop type (i.e. when in operation, there is no exchange with the air in the surroundings). It has a low-speed and a high-speed test section that can be used depending on the speed of the airflow required for a specific experiment as well as the size of the model being tested. The speed of the airflow in the high speed test section (where the present experiments were conducted) is reliably controlled between 10 - 40 m/s by a constant-speed, variable-pitch fan powered by an electric motor. The rotational speed of the fan remains constant and the velocity of the airflow is varied by changing the pitch angle of the blades using a swashplate whose motion is controlled by a servo motor. The high-speed test section of the wind tunnel is a 910 x 1130 x 1960 mm (height x width x length) channel with an aluminium ground plane on its floor and plexi-glass doors and roof. A schematic of the wind tunnel can be seen in Figure 3.1.
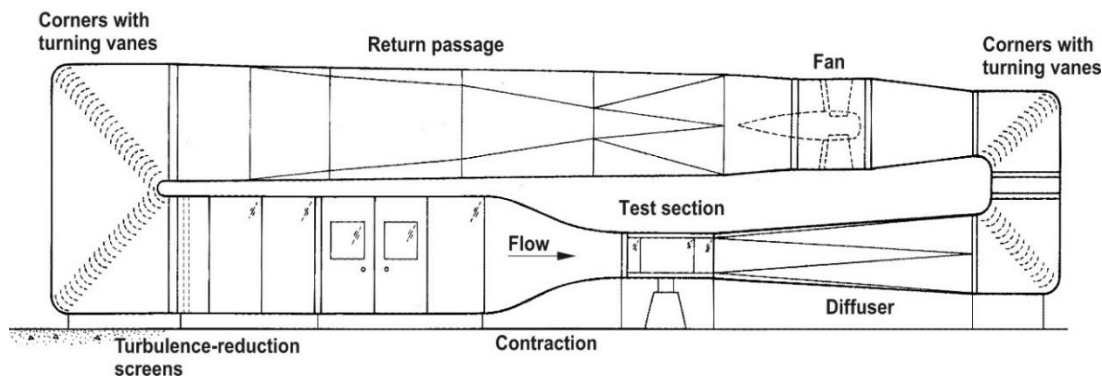

Figure 3.1: Schematic of closed-loop wind tunnel

The freestream conditions in the wind tunnel were measured using a 3.2-mm-diameter United Sensor Pitot-static probe containing a 24 AWG type-T thermocouple (to measure the freestream air temperature, T_∞), a Datametrics Barocel Type 590 differential pressure transducer (model no. 590D-10W-2Q8-V1X-4D) with a thermal base (range of 254 mm H$_2$O) to measure the dynamic pressure of the freestream, q_∞, and a Datametrics Barocel Type 600 absolute pressure transducer (model no. 600A-1000T-S13-H21X-4, range of 1000 Torr) to measure the freestream absolute static pressure, P_∞. The velocity of the freestream is obtained from the dynamic pressure using the formula

$$U_\infty = \sqrt{2q_\infty/\rho_\infty} \,, \tag{3.1}$$

where ρ_∞ is the density of the freestream calculated using the ideal gas law,

$$\rho_\infty = P_\infty/RT_\infty, \tag{3.2}$$

and R is the gas constant for air.

A traversing wing capable of moving in three directions (x, y, z planes) was mounted in the test section of the wind tunnel where instruments can be fitted for measuring the airflow conditions at various locations. Specific programs written using the Labview software installed on a personal computer were used to control various operations of the wind tunnel such as changing the speed of the airflow, controlling the motion of the instrumentation located on the traversing wing, as well as displaying data obtained through the PCIe-6259 16 bit data acquisition board.

3.2 Velocity Boundary Layer Measurement

The velocity boundary layer represents the region in a flow where the velocity of the airflow is influenced by shear forces on the plane over which it flows over and its thickness is denoted by the normal distance from the surface where the velocity of the airflow is 99% of the velocity of the freestream. The boundary layer thickness at the location of the cylinder in the test section was measured using a single-wire hot-wire probe (Dantec 55P15).

The sensor on the probe is platinum-plated tungsten wire with diameter of 5 µm. The calibration of the hot-wire probe was done by exposing the heated hot-wire to the flow and measuring the voltage required to keep the sensor at a constant temperature for multiple airflow

speeds. These data points were used to develop a mathematical correlation relating the voltage measured and the velocity of the freestream. The hot-wire probe was fitted to the traverse system and used to measure the velocity of the airflow at 1 mm vertical intervals for the first 50 mm from the surface of the ground plane and 100 mm intervals for the next 200 mm. The measurement was performed at the center of the high speed test section where the model to be studied was located and data were collected at a sampling frequency of 1 kHz for 20 s. At this location, there was a turbulent boundary layer on the ground plane with a thickness $\delta = 48$ mm $\pm$ 1 mm, yielding a thickness-to-diameter ratio of $\delta/D = 1.0$ over the range of Reynolds numbers tested. This thickness is important for characterizing the flow around the 3D cylinder model (Beitel et al., 2019).

3.3 Fabric Samples

Seven apparel systems (involving single fabrics and ensembles) were tested by wrapping them around the 3D and 2D cylinder models in the wind tunnel. These included two materials used for the outer shell of firefighters' protective clothing, RS Black and PBI Max tested individually, RS Black and cotton in an assembly, PBI Max and cotton, fleece and cotton, a winter jacket material and cotton, and an ensemble of the complete firefighters' protective gear (Firefighters' (FF) PPE and cotton) consisting of RS Black as the outer shell, Stedair 3000 as the moisture barrier, and XE-289 as the thermal liner. The pictures of the various fabric layers are shown in Appendix A. For the 3D (finite-height) cylinder, the samples had a size of 151 mm $\times$ 144 mm while the samples for the 2D (infinitely long) cylinder had a size of 151 mm $\times$ 300 mm.

These fabric samples were made into sleeves by joining the two ends using a "Peel*n*Stick" fabric fuse double-sided tape and placed around the surfaces of the cylinders. The connection point of the fabric sleeves was located at the rear of the cylinder to minimize its impact on the airflow. The dimensions of the samples were chosen to ensure that the cylindrical surface was completely covered by the fabric and there was negligible air gap between the cylinder and the fabric. Table 3.1 shows the individual fabrics that make up the multi-layer fabric systems and the physical properties associated with them. The thicknesses and air permeability values of the individual fabric layers were obtained using a Thickness Compression Recovery Tester (Custom Scientific Instruments Inc., Whippany, NJ, US) and Frazier Air Permeability Tester - high pressure differential air permeability machine (Frazier Precision Instrument

Company, Hagerstown, MD, US) respectively, both located at the University of Alberta. The air permeability was measured using a differential pressure of 12.7 mm H_2O between the two surfaces of the fabric. The mass of the fabrics was measured using an Ohaus Corporation's mass balance (model number VP6102CN) and the thermal conductivity values were obtained from similar fabrics in the literature with references also stated in Table 3.1.

Table 3.1: Physical and thermal properties of individual fabrics used to make the multiple fabric systems (permeability was measured according to CAN/CGSB-4.2, No.36-M89 (CGSB, 2013))

Multi-layer fabric systems	Fabric	Thickness (mm)	Mass/unit area (g/m^2)	Permeability (L/m^2·s)	k (W/m·K)	References
PBI Max and cotton	PBI Max	0.54	260	50.1	0.040	Torvi (1997)
	Cotton	0.45	158	1048.0	0.060	Bergman et al. (2011)
RS Black and cotton	RS Black	0.80	274	69.2	0.040	Torvi (1997)
	Cotton	0.45	158	1048.0	0.060	Bergman et al. (2011)
Fleece and cotton	Fleece	4.28	246	1086.0	0.050	Gunesoglu and Meric (2006)
	Cotton	0.45	158	1048.0	0.060	Bergman et al. (2011)
Winter jacket and cotton	Winter jacket	0.25	165	0.0	NA	NA
	Cotton	0.45	158	1048.0	0.060	Bergman et al. (2011)
Firefighters' PPE and cotton	RS Black	0.8	260	69.2	0.040	Torvi (1997)
	Moisture barrier	0.85	178	0.0	0.036	Lawson et al. (2005)
	Thermal liner	1.65	249	404.0	0.036	Lawson et al. (2005)
	Cotton	0.45	158	1048.0	0.060	Bergman et al. (2011)

The physical properties of the fabric ensembles that were tested can be seen in Table 3.2. The thickness for a multi-layer fabric system was obtained by simply adding the thicknesses of the individual fabrics that make up the ensemble and the air permeability was calculated using the method for total permeability of multi-layer cylindrical structures stated in Ganat (2020). Equation (3.3) shows the final equation for a cylindrical fabric ensemble consisting of n – layers

with outer radius R_o, radius of first layer R_1 (which is the brass cylinder's radius in this case) and total permeability P_T using the radii and air permeability of the individual layers of the ensemble.

$$P_T = \frac{\ln(R_o/R_1)}{\sum_{j=1}^{n}\left[\frac{\ln(R_j/R_{j-1})}{P_j}\right]} \tag{3.3}$$

For the sake of this research, the total air permeability for multi-layer fabric systems that include a material with an air permeability value of zero was calculated using the radii and permeability values of the layers that are on the outside of that layer in the fabric structure. For example, the Firefighters' PPE and cotton ensemble contains a moisture barrier that has an air permeability of zero. Since only the RS Black material was located before it in the structure, the total air permeability was calculated as such:

$$P_{Firefighters'\,PPE\,and\,cotton} = \frac{\ln(R_{Firefighters'\,PPE\,and\,cotton}/R_{cylinder})}{\frac{\ln(R_{Firefighters'\,PPE\,and\,cotton}/R_{moisture\,barrier})}{P_{RS\,Black}}} = \frac{0.1452}{\frac{0.02925}{69.2}}$$

$$= 343.4 \text{ L/m}^2\text{·s}$$

Table 3.2: Physical properties of fabric systems tested

Fabric	Thickness (mm)	Permeability (L/m²·s)
PBI Max	0.54	50.1
RS Black	0.80	69.2
PBI max and cotton	0.99	89.1
RS Black and cotton	1.25	105.1
Fleece and cotton	4.73	1081.9
Winter jacket and cotton	0.70	0
Firefighters' PPE and cotton	3.75	343.4

3.4 Cylinder Models

In addition to obtaining information about the fluid dynamics around a fabric covered 3D (finite-height) cylinder, the tests performed on the 3D cylinder were done as a precursor to the tests done on the 2D cylinder as it was more readily available and the 2D cylinder required a significantly longer time to manufacture. The results and experience obtained from performing the 3D cylinder tests informed the design and manufacture of the model as well as the instrumentation used and procedure followed to complete the 2D cylinder test in a more efficient manner.

3.4.1 3D Cylinder Model

The model used was an internally heated cylinder with a height of H_{3D} = 144 mm, a diameter of D = 48 mm, and an aspect ratio of AR = H_{3D}/D = 3. This can be seen in Figure 3.2 and Figure 3.3.
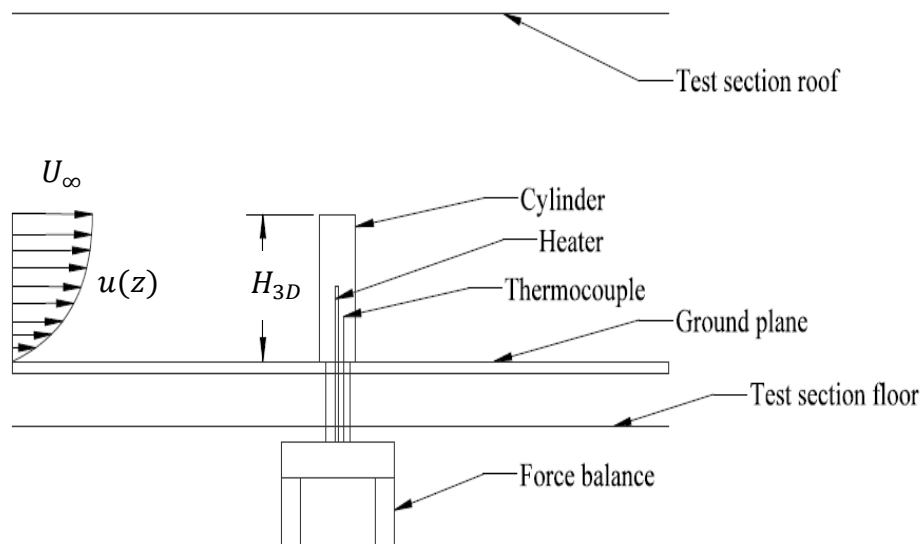
Figure 3.2: Side view schematic for the 3D (finite-height) cylinder in the wind tunnel, where H_{3D} = 144 mm and $u(z)$ is the mean streamwise velocity profile of the boundary layer.

.
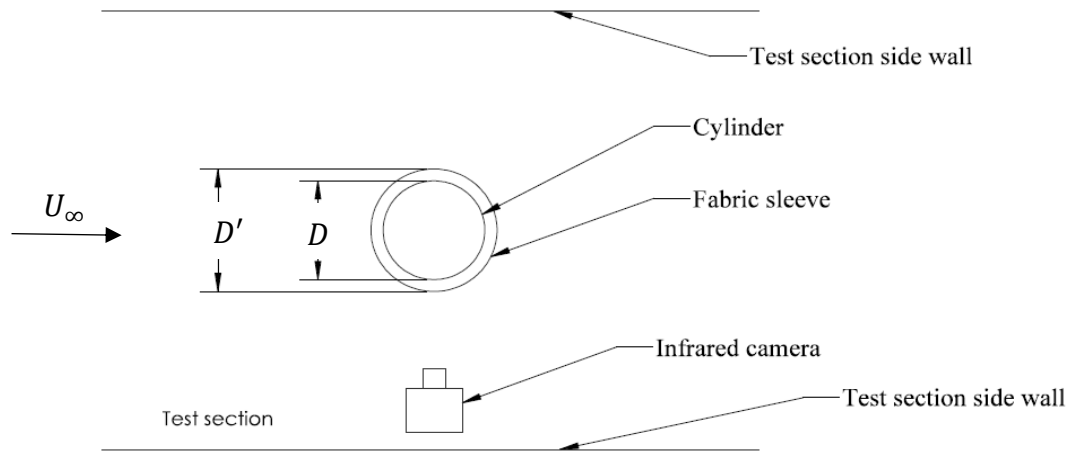
Figure 3.3: Top view schematic of the 3D finite-height cylinder in the wind tunnel where $D = 48$ mm is replaced by D' when the cylinder is covered with a fabric.

The 3D cylinder was made from brass, which has a relatively high thermal conductivity thereby ensuring that the maximum Biot number ($Bi = hr/2k$) was less than 0.1 for the range of Reynolds numbers tested. The Biot number represents the ratio of the resistance to conduction to the resistance to convection heat transfer from a solid (Bergman et al., 2011). It was important that the Biot number for the airflow and cylinder combination was small so that the temperature gradient through the cylinder would be negligible during each test. The brass cylinder was heated using an Omega stainless steel sheath cartridge heater (model no. CSH-104400) with a maximum rating of 400 W. The cylinder was also painted black using a Rust-oleum paint for metals to ensure that its emissivity was about 0.95 (Bergman et al., 2011).

3.4.2 2D Cylinder Model

The model used for the 2D cylinder was an 881 mm long assembly comprised of three major parts. This can be seen in Figure 3.4. The heated section was the main focus of the experiment and was located in the middle of the cylinder, at equal distance away from the roof and floor of the wind tunnel test section. Two other cylindrical parts of equal diameter were added at the top and bottom of the heated section to ensure the assembly spanned the entire height of the test section thereby minimizing the three-dimensional effects of the flow around the ends of the cylinder. The entire assembly was secured at the top with an aluminium cap bolted to the roof of the wind tunnel and at the bottom with a bracket attached to the force balance below the wind tunnel. A ring similar in similar size to the top cap was placed around the bottom of the cylinder on the ground plane to ensure ideal similarity between the top and bottom of the structure.
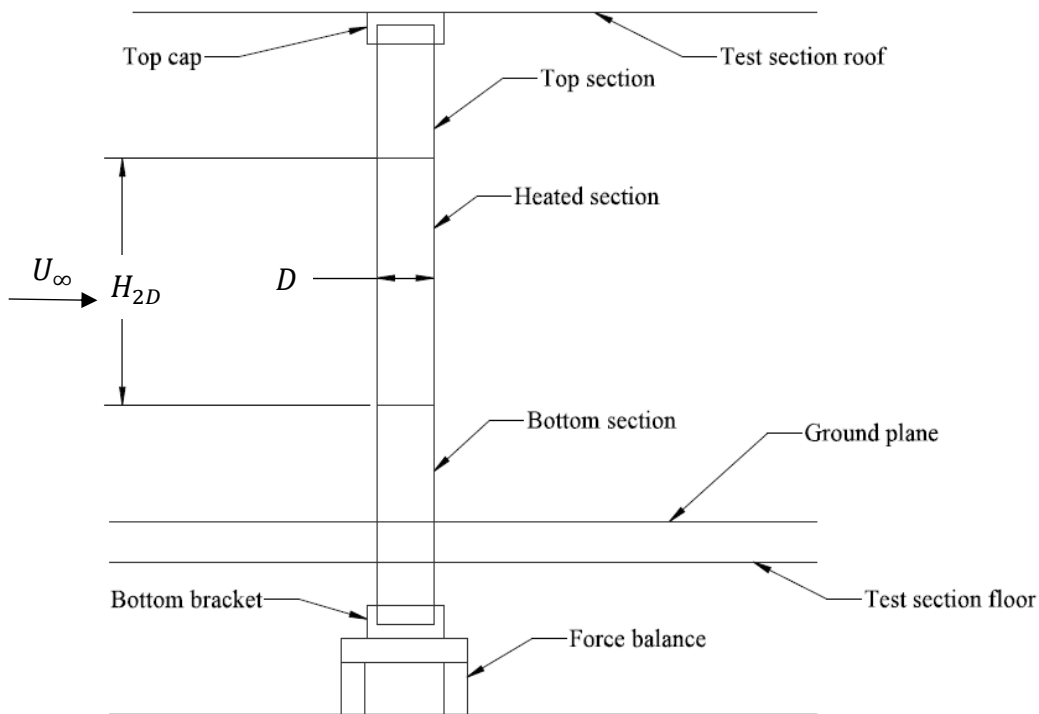

Figure 3.4: Schematic of the 2D (infinitely-long) cylinder in the wind tunnel where $H_{2D} = 288$ mm.

The top and bottom sections were fabricated from chlorinated polyvinyl chloride (CPVC) plastic pipes while the middle section was made from solid brass because of its high thermal conductivity of about 110 W/m·K (Bergman et al., 2011) to ensure that, just like the 3D cylinder, there was a negligible temperature gradient within the heated section. The heated section had a height of $H_{2D} = 288$ mm, diameter of $D = 48$ mm an aspect ratio of $AR = H_{2D}/D = 6$, and was heated internally using an Omega high watt density cartridge heater with a nominal diameter of 3/8 in and a maximum power rating of 600 W (model no. CIR-2100).

3.5 Experimental Setup

The experimental setups for both cylinder tests were identical. For both models, the entire cylindrical structure was mounted normal to the ground plane in the test section of the wind tunnel as can be seen in Figures 3.2 and 3.4. Samples of the fabrics that were tested were made into sleeves and placed in a tight fit around the cylinder. However, since a sleeve was used, the free end at the top of the 3D (finite-height) cylinder was uncovered by the fabric and was therefore exposed to the flow. For the 2D (infinitely long) cylinder, the sleeves covered the entire heated section and extended about 6.35 mm onto the top and bottom CPVC sections.

An Omega Extech clamp meter (model no. MA61) was used to measure the current and voltage required to produce the power used to heat the cylinders. An Omega type-K thermocouple (24 AWG wire size) was placed inside each cylinder at a distance of about 3 mm from the centre to measure its temperature, and another Omega type-K thermocouple (30 AWG wire size) was attached to the inner surface of each fabric sleeve that was tested. The thermocouples on the fabric layers were positioned at approximately 90° or 270° from the flow direction and for multi-layered fabrics they were placed on opposite sides of the cylinder to ensure that they do not come in contact with each other. A FLIR one infrared camera (model no. E64501) was used to monitor and, at steady state, obtain images showing the temperature distribution around the surface of the bare or fabric-covered cylinder. The average temperature on the surface of the cylinder was derived from these images with the aid of the FLIR tools software (version 5.13.18031.2002). For the 3D cylinder tests, the infrared camera was mounted inside the wind tunnel, far enough from the cylinder that it did not interfere significantly with the flow as can be seen in Figure 3.3.

The drag force coefficient,

$$C_D = 2F_D/(\rho_\infty U_\infty^2 D H_{3D}),\qquad\qquad(3.4)$$

where F_D is the drag force of the 3D fabric-covered cylinder was obtained using a six-component force balance. The force balance comprises of six HBM PLC single-point load cells each with a maximum capacity of 50 N. Three of the load cells measure vertical forces and moments while the other three measure drag and twisting forces. This allows for the measurement of lift, normal, and drag forces as well as rolling, yawing and pitching moments. However, only drag forces were measured during this research.

Images of the 3D (finite-height) and the 2D (infinitely-long) cylinder experiments inside the wind tunnel can be seen in Figure 3.5 and Figure 3.6, respectively.
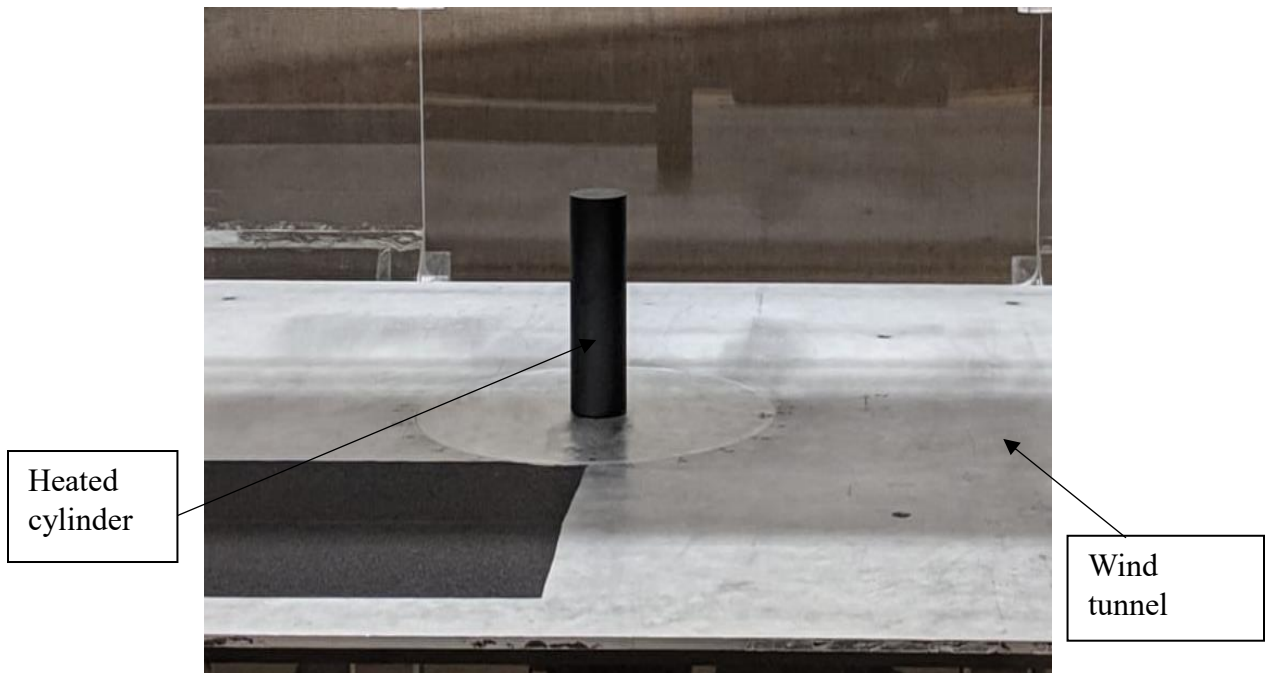

Figure 3.5: Image of the 3D cylinder in the wind tunnel (airflow is from left to right).

Figure 3.6: The 2D cylinder in the wind tunnel with PBI Max fabric wrapped around it (airflow is from left to right).

Tests were conducted for five different Reynolds numbers, $Re_D = 3.8\times10^4$, 6.1×10^4, 8.6×10^4, 1.0×10^5, and 1.3×10^5. Five temperature differences between the cylinder (with surface temperature T_s) and the air in the wind tunnel (with freestream temperature T_∞) were used, $T_s - T_\infty$ = 10°C, 20°C, 30°C, 40°C, and 50°C. The Reynolds numbers were chosen based on information about the average human arm size documented in Ulijaszek and Henneberg (2012) and the historical wind speeds experienced in Saskatoon from Saskatoon weather stats (2018). The diameter of the cylinder was chosen to be 48 mm to ensure that the above stated Reynolds numbers can be achieved in the wind tunnel while also ensuring that a blockage ratio of less than 6% was maintained according to West and Apelt (1982).

Using internal heating, the cylinder was kept at a constant temperature while being subjected to airflow at different speeds, U_∞. The convective heat transfer coefficient h [W/(m$^2\cdot$K)] pertaining to each fabric surface and freestream condition was calculated from

$$q = hA(T_s - T_\infty), \tag{3.5}$$

where q [W] is the power required by the heater to keep the temperature difference between the cylinder and the freestream constant and A [m^2] is the surface area. While equation (3.5) is based on the assumption that there is no air penetration through the surface of the cylinder such as in

the case of the bare cylinder, it is also used in this research for the situation where the surface is permeable to airflow as is the case for the fabric-covered cylinders. The penetration of the airflow through the fabric would result in additional energy transfer through advection and other mechanisms. The effects of permeability and this additional energy transfer will be discussed in Sections 4.2 and 4.3.

Due to the presence of the free end at the top of the 3D finite-height cylinder, the overall Nusselt number obtained from the experiment was for both the side surface of the cylinder which was covered by the test fabrics and the top which was uncovered and therefore directly exposed to the flow. This had to be adjusted to obtain the Nusselt number for only the side surface of the cylinder. To do this, the heat transfer rate through the free end was subtracted from the total heat transfer rate into the cylinder. This was done by first obtaining the Nusselt number for the free end (Nu_r) using equation (3.6), from Tsutsui et al. (2000), then calculating the heat transfer rate from the free end using equation (3.5), and then subtracting that value from the total heat transfer rate measured in the experiment.

$$Nu_r = Nu_m(1 + 4AR) - 4ARNu_s, \tag{3.6}$$

Nu_r is the average Nusselt number on the free end, Nu_m is the overall average Nusselt number for both the side surface and the free end, and Nu_s is the average Nusselt number on the side surface of the cylinder. Nu_m was calculated from the experimental data using a combination of equations (3.5) and (2.2) and Nu_s was obtained from the Nusselt number correlation for a 2D cylinder by Churchill and Bernstein (1977) shown in equation (3.7).

The Nusselt numbers obtained from the present experiments were compared to that of a two-dimensional cylinder from Churchill and Bernstein (1977), in equation (3.4) where Pr is the Prandtl number (which represents the ratio of momentum diffusivity to thermal diffusivity).

$$Nu = 0.3 + \frac{0.62Re_D^{\frac{1}{2}}Pr^{\frac{1}{3}}}{(1+[\frac{0.4}{Pr}]^{\frac{2}{3}})^{\frac{1}{4}}}\left(1 + \left[\frac{Re_D}{28200}\right]^{\frac{5}{8}}\right)^{\frac{4}{5}}.$$

(3.7)

Furthermore, the resistance to conduction heat transfer pertaining to each fabric was calculated similar to the methods used in the hot plate tests stated in ASTM F1868 (ASTM International, 2017),

32

$$R_f = (T_1 - T_2)A/q, \tag{3.8}$$

where R_f [m²·K/W] is the resistance to conduction heat transfer through a particular layer of fabric, T_1 is the temperature on the inner surface of the fabric or outer surface of the cylinder obtained from the reading of the thermocouple located on that surface, T_2 is the temperature on the outer surface of the fabric obtained from the temperature readings of the IR camera and A [m²] is the surface area of the fabric exposed to the flow.

The steady state temperature value on the surface of the bare 2D cylinder as well as on the surfaces of the cylinder and fabric for the 2D fabric-covered cylinders were compared to a theoretical closed form solution for a hollow cylinder obtained using the one-dimensional Fourier heat equation in cylindrical coordinates. The cylinder is bounded internally by a constant heat flux (q'') and externally by convection (h, T_∞) as is the case in the experiment. For the bare cylinder case, a single-layer cylinder is used while a two-layer cylinder model was used for the fabric-covered cylinders. A two-layer cylinder was used to simplify the solution for the fabric-covered cylinder. One layer represented the cylinder and the other layer represented the entire fabric ensemble. For the multi-layer fabrics the layers were combined into one and an average value of their thermal conductivities (shown in Table 3.1) was used. This simplification is valid because the thermal conductivities of the different fabrics are very similar (as can be seen in Table 3.1). This closed form solution also helped in exploring the effect of fabric thickness and thermal conductivity on the temperature on the surface of the cylinder and hence, the thermal resistance of the fabric.

The Fourier heat equation, the boundary conditions that are representative of the experimental situation as well as the final form of the steady state solution obtained for the bare cylinder are shown in equations (3.9a) – (3.9d) and in equations (3.10a) to (3.10h) for the fabric covered cylinder.

For the bare cylinder, the Fourier heat equation is:

$$\frac{1}{r}\frac{d}{dr}\left(k_c r \frac{dT(r)}{dr}\right) = 0, \tag{3.9a}$$

The boundary conditions are:

$$-k_c \frac{dT(r)}{dr} = q'', \qquad at \ r = r_i \tag{3.9b}$$

$$-k_c \frac{dT(r)}{dr} = h(T(r_o) - T_\infty), \qquad at\ r = r_o \qquad\qquad (3.9c)$$

where k_c is the thermal conductivity of the cylinder, r_i and r_o are the internal and external radii of the cylinder. After integrating equation (3.9a) twice and including the effect of the boundary conditions in equations (3.9b) and (3.9c), equation (3.9d) was obtained for the temperature distribution in the bare cylinder.

$$T(r) = \frac{-q''r_i}{k_c}\ln(r) + \frac{q''r_i}{hr_o} + \frac{q''r_i}{k_c}\ln(r_o) + T_\infty, \qquad\qquad (3.9d)$$

For the fabric-covered cylinder, two equations were developed for the temperature distribution in the cylinder and in the fabric.

The Fourier heat equations are:

$$\frac{1}{r}\frac{d}{dr}\left(k_c r \frac{dT_c(r)}{dr}\right) = 0, \qquad r_i \le r \le r_1 \qquad\qquad (3.10a)$$

for the brass cylinder layer, and

$$\frac{1}{r}\frac{d}{dr}\left(k_f r \frac{dT_f(r)}{dr}\right) = 0, \qquad r_1 \le r \le r_o \qquad\qquad (3.10b)$$

for the fabric; where $T_c(r)$ and $T_f(r)$ are the temperature in the brass cylinder layer and fabric layer respectively, k_f is the thermal conductivity of the fabric and r_1 is the radius of the cylindrical layer.

The boundary conditions are:

$$-k_c \frac{dT_c(r)}{dr} = q'', \qquad at\ r = r_i \qquad\qquad (3.10c)$$

$$-k_c \frac{dT_c(r)}{dr} = -k_f \frac{dT_f(r)}{dr}, \qquad at\ r = r_1 \qquad\qquad (3.10d)$$

$$T_c(r) = T_f(r), \qquad at\ r = r_1 \qquad\qquad (3.10e)$$

$$-k_f \frac{dT_f(r)}{dr} = h(T_f(r) - T_\infty). \qquad at\ r = r_o \qquad\qquad (3.10f)$$

The final form of the steady state solution is shown below. The temperature distribution in the brass cylindrical layer is:

$$T_c(r) = \frac{-q''r_i}{k_c}\ln(r) - \frac{q''r_i}{k_c}\ln(r_1) + \frac{q''r_i}{k_f}\ln(r_1) + \frac{q''r_i}{r_o h} + \frac{q''r_i}{k_f}\ln(r_o) + T_\infty, \qquad (3.10g)$$

$$\text{for} \quad r_i \le r \le r_1,$$

and the temperature distribution in the fabric layer is:

$$T_f(r) = \frac{-q''r_i}{k_f}\ln(r) + \frac{q''r_i}{r_o h} + \frac{q''r_i}{k_f}\ln(r_o) + T_\infty. \qquad (3.10h)$$

$$\text{for} \quad r_i \le r \le r_1$$

3.6 Experimental Procedure

Prior to each test the fabric specimens were conditioned according to ASTM D1776 (ASTM International, 2016) at about $22 \pm 2°C$ and $65 \pm 5\%$ RH for a minimum of 24 hours. The conditioning was done using a small conditioning chamber that contained a mixture of magnesium chloride and water $(0.6 - 0.8$ g/L salt concentration) according to the method stated in ASTM E104 (ASTM International, 2012). Based on the size of the cylinder and properties of the material used to manufacture it, the power required to keep the cylinder at a particular temperature difference was estimated and set until the temperature of the cylinder reached the intended value. This value of power was adjusted until the temperature difference was within $2°C$ of the intended value.

The system was allowed to run until steady state. Steady state was said to have been attained if for 5 min, the temperature difference between the cylinder and the freestream changed by less than $0.5°C$. At steady state, the temperature difference between the cylinder and the freestream, the power required, and the temperature on the inner and outer surfaces of each layer of fabric sleeve were recorded. These steps were repeated three times for each case scenario.

3.7 Sweating Hot Plate Tests

The sweating hot plate test is a method stated in the ASTM F1868 (ASTM International, 2017) standard that is used to measure both the thermal resistance and the evaporative resistance of a thickness of fabric as well as the total heat loss through that fabric. The evaporative resistance denotes the opposition to the flow of moisture vapour from a region of higher vapour pressure to a region with lower vapour pressure (ASTM International, 2017). The thermal and evaporative resistance of an item of clothing can be used to quantify the thermal comfort experienced by an individual wearing that clothing, in an environment with a specific

temperature and humidity. Since this research focuses on the transfer of dry heat through a thickness of fabric, only the thermal resistance tests were performed.

The hot plate tests were performed at the University of Alberta's Human Ecology Department using a Measurement Technology Northwest sweating guarded hot plate (model no. SGHP – 8.2). The hot plate equipment comprises a square test plate that is 203.2 mm (8 in) in length with a 50.8 mm (2 in) guard ring around it requiring a square fabric sample with length of about 304.8 mm (12 in). Prior to the test, the fabric samples were conditioned at the University of Alberta in an environmentally controlled room where the air is maintained at a temperature of $22 \pm 2°C$ and $65 \pm 5\%$ RH according to ASTM D1776 (ASTM International, 2016). During the test, the entire hot plate and test samples were enclosed in an environmental chamber where the temperature and relative humidity were maintained at $20 \pm 0.1°C$ and $65 \pm 4\%$ RH, respectively. The procedure followed for the hot plate test is stated in Part C of the ASTM F1868 (ASTM International, 2017) standard and the results of thermal resistance obtained from the hot plate tests were compared to the results from both heated cylinder tests. Labelled images of the hot plate equipment can be seen in Figure 3.7 below.
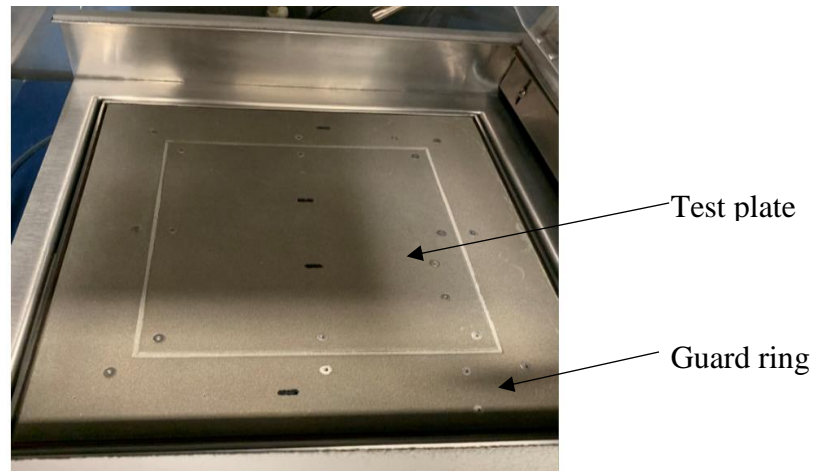
(a) Hot plate without specimen

Figure 3.7: Hot plate equipment used for alternate thermal resistance measurement.
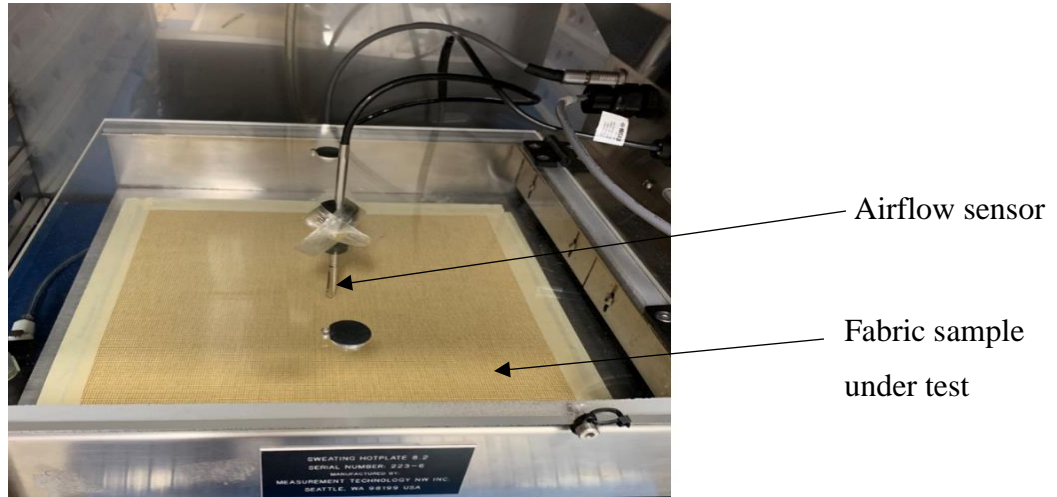
(b) Hot plate with specimen

Figure 3.7: Hot plate equipment used for alternate thermal resistance measurement.

3.8 Measurement Uncertainty

The uncertainties associated with the various parameters tested and results obtained in this research are described in this section. The speed of the airflow in the wind tunnel, U_∞ was set manually to be within 0.2 m/s, however due to fluctuations that may have occurred during the test, a conservative value of 0.5 m/s can be estimated for the uncertainty in U_∞. To measure the boundary layer thickness, δ, the single-wire hot wire probe was moved up in increments of 1 mm; therefore, the uncertainty in the measurement of the boundary layer thickness is 1 mm. Type-K thermocouples were used to measure the temperature of the cylinder and the various fabric layers. According to the manufacturer, Omega, the uncertainty in the measurements of the thermocouples is about 2.2% of the measured value. The accuracy of the Omega Extech clamp meter used for measuring the electric power that heats the cylinder is 2.5% + 0.8 W.

Since the Nusselt number, *Nu,* is calculated using equations (2.2) and (3.5), its uncertainty is dependent on the uncertainty of the parameters stated in those equations. The uncertainties pertaining to each parameter comprises of Type A (that accounts for random errors during measurement) and Type B errors (that represents systematic errors during measurements). The uncertainty in *Nu* was calculated by first obtaining the uncertainty in *h* by combining the contributions of the parameters that yield *h* in equation (3.5), then propagating it using the

parameters that yield *Nu* in equation (2.2). This was done using the propagation of uncertainties technique stated in Kline (1985) as shown below:

$$U(h) = \sqrt{\left(\frac{\partial h}{\partial q}U(q)\right)^2 + \left(\frac{\partial h}{\partial A}U(A)\right)^2 + \left(\frac{\partial h}{\partial(\Delta T)}U(\Delta T)\right)^2}, \qquad (3.11)$$

$$U(Nu) = \sqrt{\left(\frac{\partial Nu}{\partial h}U(h)\right)^2 + \left(\frac{\partial Nu}{\partial D}U(D)\right)^2}, \qquad (3.12)$$

where $U(x)$ is the uncertainty in x. The same method was used to obtain the uncertainty in the thermal resistance of the fabrics, R_f.

$$U(R_f) = \sqrt{\left(\frac{\partial R_f}{\partial q}U(q)\right)^2 + \left(\frac{\partial R_f}{\partial A}U(A)\right)^2 + \left(\frac{\partial R_f}{\partial(\Delta T)}U(\Delta T)\right)^2}, \qquad (3.13)$$

The uncertainty values for the important parameters and results in this thesis research are stated in Table 3.2 below.

Table 3.3: Experimental uncertainty values associated with specific parameters and results

| Parameter	Uncertainty ($\pm$)
Airflow speed, U_∞	0.5 m/s
Temperature, T	2.2% of measured value
Power measure, q	2.5% of measured value + 0.8 W
Nusselt number, Nu	23% of measured value
Thermal resistance, R_f	18% of measured value

Chapter 4 – Results and Discussion

After the experiments were completed, the data obtained were analysed and used to calculate the Nusselt number pertaining to each fabric/fabric ensemble and airflow combination as well as the thermal resistance of each apparel system.

4.1 Infrared (IR) Camera Images

Some of the images obtained from the infrared camera are shown in this section. Figure 4.1 shows examples of the side view of the IR images for the 2D and 3D bare and fabric-covered cylinders. Images similar to Figure 4.1 were obtained at steady state for every test to ensure uniformity of the temperature distribution around the cylinder with and without the fabric. The temperature distribution around the bare 2D and 3D cylinders can be seen to be relatively uniform although there is some variability between the temperatures measured at the top, middle and bottom of the heated section, especially for the fabric-covered cylinders. This can be seen in the IR images shown in Figure 4.1 and in Appendix B. For the 2D cylinder, this is due to the difference between the length of the heater (254 mm) and the length of the heated section (288 mm). The heater is located in the middle of the heated section causing the slightly lower heating rate at the ends (top and bottom) of the cylinder. The same is the case for the 3D cylinder.

For the bare cylinder in both cases, a maximum temperature variation of about 8% is noticed along the length of the cylinder, but for the fabric-covered cylinder, this rises to about 23% for the 3D cylinder and 13% for the 2D cylinder. Since the cylinder was made of brass that has a high thermal conductivity (110 W/(m·K) (Bergman et al. (2011)), the temperature on the surface of the bare cylinder remains relatively uniform despite the difference in heat transfer rate between the ends and the middle of the cylinder. On the other hand, the introduction of the fabric in the fabric-covered cylinder leads to a larger temperature variation around the surface as the non-uniformity in heat transfer is enhanced by the airflow through the fabric. In addition to the difference in heating rate caused by the length of the heater, the free end at the top of the 3D cylinder also causes further non-uniformity of the heat transfer in the cylinder. Furthermore, the temperature variation along the height of the fabric-covered cylinder is significantly affected by the airflow speed and hence the rate of convection from the cylinder. As the rate of convection from the surface of the fabric-covered cylinder increases, the difference between the rate of heat transfer by conduction at the ends and in the middle within the cylinder becomes more apparent
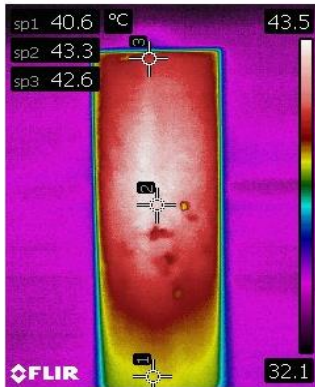
thereby leading to a larger temperature variation on the surface of the cylinder. This can also be seen in Figures B.2 and B.4 in Appendix B.
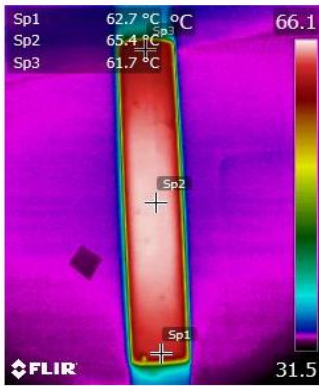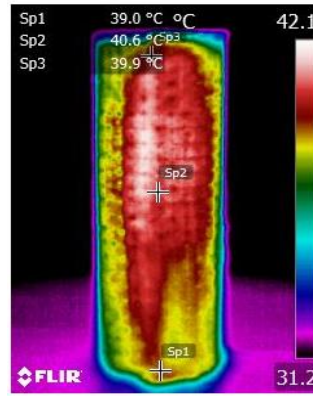

(a) Bare 2D cylinder ($U_\infty = 11.8$ m/s, $\Delta T = 30°C$, $T_{avg} = 63.9°C$, $T_{TC} = 65.2°C$)
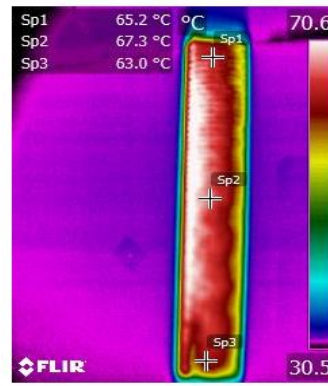
(b) RS Black fabric-covered 2D cylinder ($U_\infty = 32$ m/s, $\Delta T = 50°C$, $T_{avg} = 65.5°C$, $T_{TC} = 83.6°C$)

(c) Bare 3D cylinder ($U_\infty = 26.5$ m/s, $\Delta T = 10°C$, $T_{avg} = 42.3°C$, $T_{TC} = 42.3°C$)

(d) RS Black and cotton fabric-covered 3D cylinder ($U_\infty = 11.8$ m/s, $\Delta T = 10°C$, $T_{avg} = 38.9°C$, $T_{TC} = 43.5°C$)

Figure 4.1: Temperature distribution on the side face of the 2D and 3D bare and fabric-covered cylinders for different testing scenarios (airflow is from left to right).

Since, the focus of the convective heat transfer in this thesis research is on the overall Nusselt number, the weighted average temperature on the surface of the cylinder, T_{avg} measured by the IR camera was used in the calculation of the Nusselt number for the cylinder. T_{avg} was

obtained using the FLIR tools software to calculate a weighted average temperature from the temperature values at every point on the surface of the cylinder. The reading of the thermocouple placed inside the cylinder, T_{TC}, is also shown for each scenario. T_{TC} and T_{avg} can be seen for all the test cases for the bare 2D cylinder in Table C.1 in Appendix C.

From Figure 4.1 (a) and (c), as well as Table C.1, it can be seen that the temperature measured by the thermocouple is within 6% of the average temperature measured by the IR camera and the differences in the values could be due to the fact that the thermocouple measures temperature at a particular point and since the temperature on the surface of the cylinder varies with angle, there may be some differences between the average temperature measured by the IR camera and the temperature measured by the thermocouple based on where the thermocouple is located inside the cylinder. For the fabric-covered cylinders, T_{TC} is higher than T_{avg} and the difference depends on the fabric ensemble that is being tested as the resistance of the fabric would lead to a lower rate of conduction heat transfer, thereby causing a reduction in the temperature across its thickness. This can be seen in Table C.2 to C.7 in Appendix C.

4.2 Relationship between Nusselt Number and Reynolds Number for the Fabric-Covered Cylinders

4.2.1 Results of Nusselt Number Relationship to Reynolds Number

Figure 4.2 shows the relationship between the Nusselt number and Reynolds number for the 3D cylinder without any fabric sleeve (bare cylinder), the 3D cylinder when covered with the RS Black fabric, and when covered with the PBI max fabric. The solid symbols represent the total heat transfer from both the side surface covered with fabrics and the uncovered free end at the top of the cylinder while the hollow symbols represent only the heat transfer from the side of the fabric covered cylinder. Figure 4.2 also shows how these results compare to the correlation proposed by Churchill and Bernstein (1977) for a bare 2D cylinder. Churchill and Bernstein (1977) states that the correlation should be viewed as a lower bound for forced convection from 2D cylinders and Bergman et al. (2011) states that an accuracy of 20% can be safely assumed for the correlation. This is represented by the error bars in Figure 4.2.
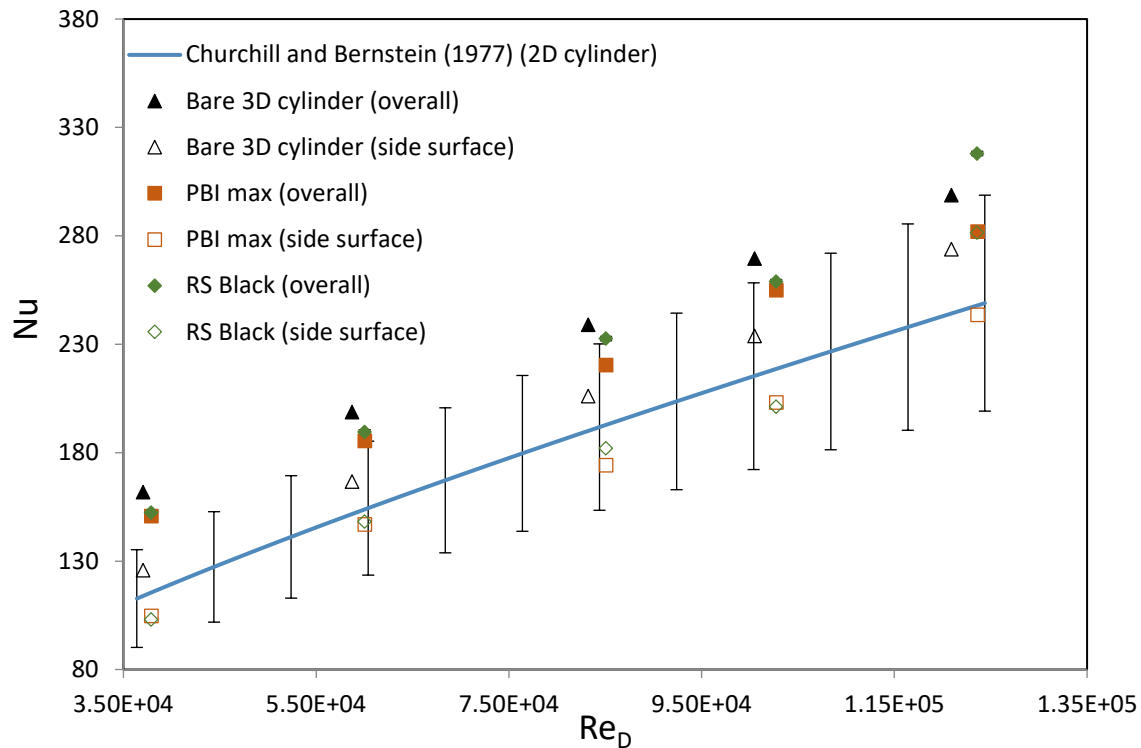
Figure 4.2: Relationship between Nusselt number and Reynolds number for some of the fabrics tested on the 3D cylinder.

From Figure 4.2 it can be seen that, as expected, the Nusselt number of the 3D cylinder increases with Reynolds number for all cases. The correction method proposed by Tsutsui et al. (2000) was used to obtain the Nusselt number value for the side surface of the 3D cylinder from the overall Nusselt number obtained in the experiment. It can be seen that the corrected values are in better agreement and fully within the error limits of the 2D cylinder correlation of Churchill and Bernstein (1977). When the heat transfer from the free end is included, the Nusselt number pertaining to the bare 3D cylinder is 15 – 25% higher than that for the side surface only. For the PBI max and RS Black fabrics, however, the overall Nusselt number is about 25 – 40% higher than the Nusselt number for the side only. Tsutsui et al. (2000) reported that for a finite cylindrical protuberance of $AR = 0.35$, the overall heat transfer is twice as much as that from its side surface which is similar to that of a two-dimensional cylinder. Since the cylinder explored in the present thesis research has an aspect ratio of $AR = 3$, it is expected that the fraction of heat transfer from the side surface is higher than that for the cylinder used in Tsutsui et al. (2000), which indeed was the case.

42

Consider the area ratio,

$$\frac{A_{side}}{A_{total}} = \frac{\pi D H}{\frac{\pi D^2}{4} + \pi D H} = \frac{H}{\frac{D}{4} + H} \tag{4.1}$$

dividing the numerator and denominator by *D,* equation (4.1) becomes

$$\frac{A_{side}}{A_{total}} = \frac{AR}{AR + 0.25} \tag{4.2}$$

As *AR* increases, the area ratio tends to unity, which means the overall heat transfer would be dominated by the heat transfer from the side surface of the cylinder as the heat transfer from the free end would be quite small. Therefore, the heat transfer from the side surface would tend towards the overall heat transfer from both the side and the the top surface. The 3D cylinder used in this thesis research has *AR* = 3, an area ratio of 0.923 and the overall Nusselt number is about 15 – 40% higher than the Nusselt number for only the side surface for the bare and fabric-covered cylinders while the cylinder used in Tsutsui et al. (2000) has *AR* = 0.35, an area ratio of 0.583 and the overall Nusselt number is about twice the Nusselt number for the side surface only.

Figure 4.3 shows how the Nusselt number results for the side surface of the 3D cylinder obtained using the correction technique reported by Tsustsui and Kawahara (2006) compare to the results of the 2D cylinder.
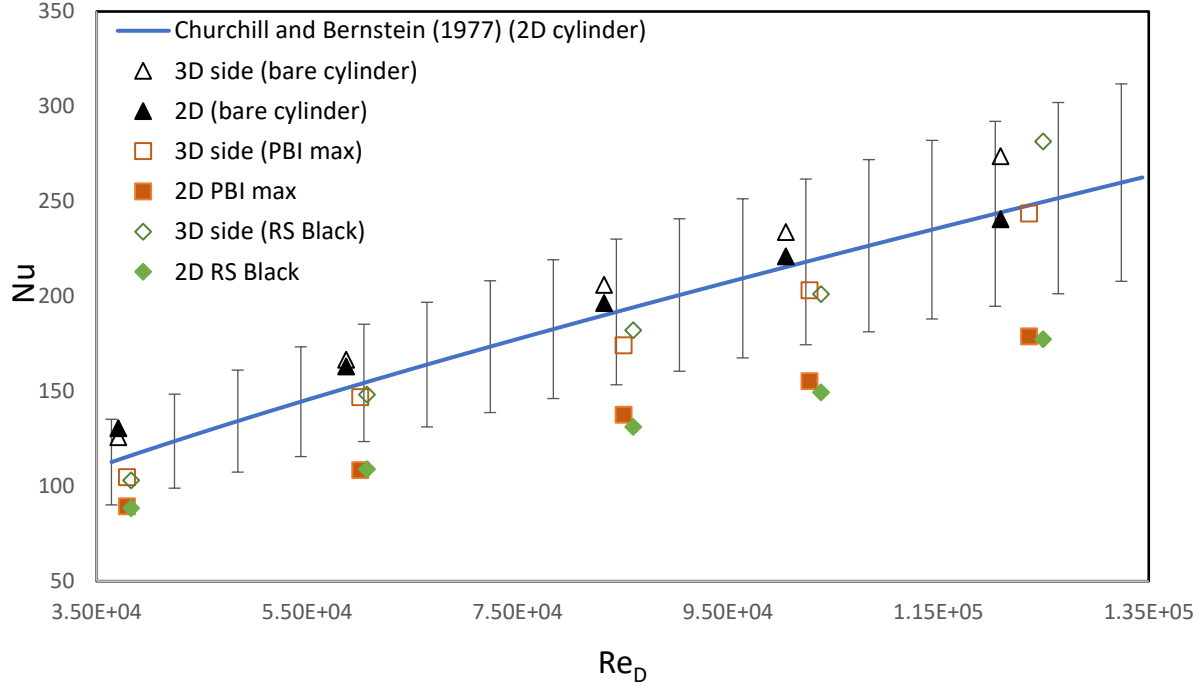
Figure 4.3: Nusselt number results for the 2D cylinder and the side surface of the 3D cylinder.

From Figure 4.3, it can be observed that the Nusselt number values for the 2D fabric-covered cylinders are much lower than those for the side surface of the 3D cylinder obtained using the correction technique proposed by Tsutsui et al. (2000). While the 2D and 3D side surface results for the bare cylinder are in good agreement (less than 13% difference), the results for the fabric-covered cylinders vary between 15 – 45%. This shows that while the correction technique is valid for a bare cylinder (or a cylinder with an impermeable surface), it may not be applicable for a fabric covered cylinder. More explanation of the reason is shown later with the aid of Figure 4.4. Figure 4.4 shows the Nusselt number results for the bare and fabric-covered cylinders obtained using the 2D cylinder. It also includes the Nusselt number obtained when the RS Black fabric-covered 2D cylinder is covered with an aluminum shimstock to minimize wind penetration into the fabric. This is denoted as 2D RS Black with shimstock in Figure 4.4.
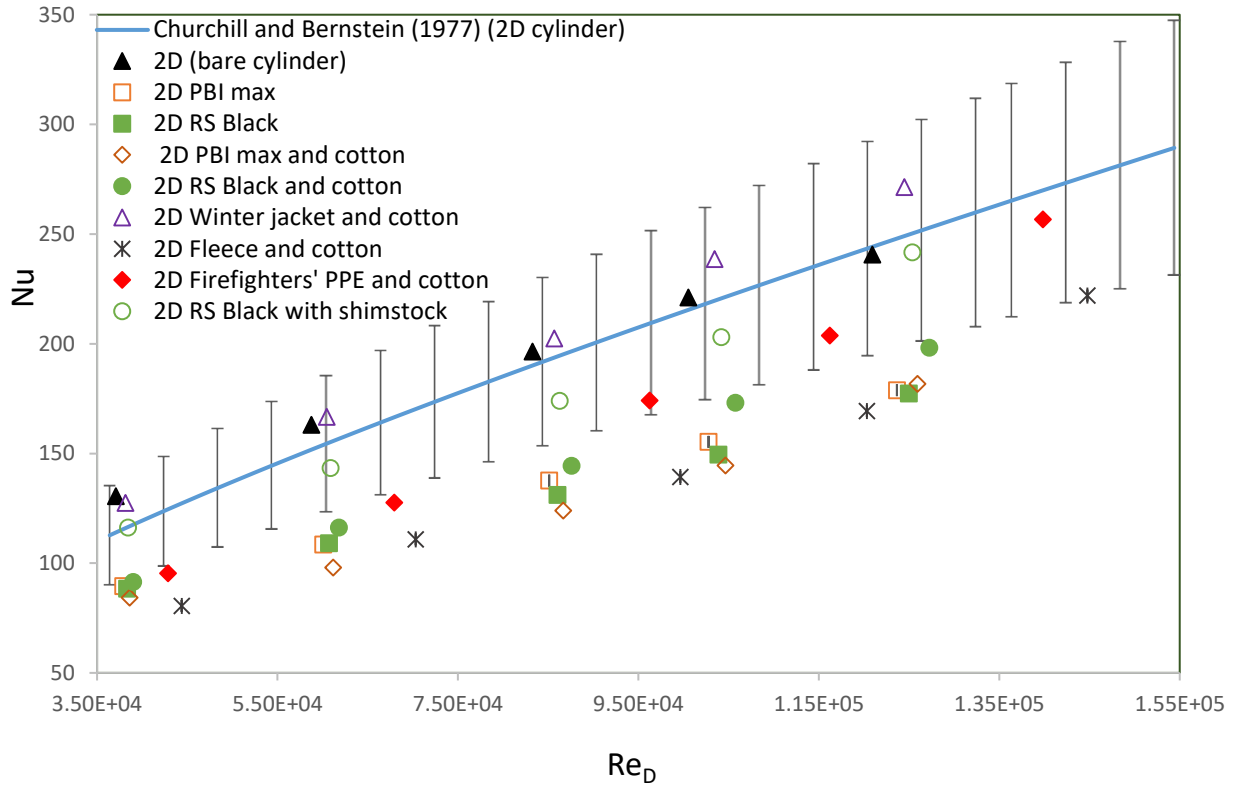
Figure 4.4: Nusselt number results for the various fabrics tested on the 2D cylinder.

From Figure 4.4, it can be seen that the Nusselt numbers for most of the fabric-covered 2D cylinders are significantly lower than that for the bare 2D cylinder similar to what was shown for the corrected 3D cylinders in Figures 4.2 and 4.3. The geometry and texture of an object's surface play an important role in determining the rate of convection heat trasfer from that surface, so drag force measurements were performed on the 3D cylinder when covered with the different fabrics to determine if the difference in surface of each fabric was enough to cause a significant variation in the rate of convection heat transfer as shown by the Nusselt numbers for the 2D cylinder in Figure 4.4. The drag force coefficient (C_D) behavior for three samples of each of the various fabrics and fabric ensembles over a range of Reynolds numbers is shown in Figure 4.5.
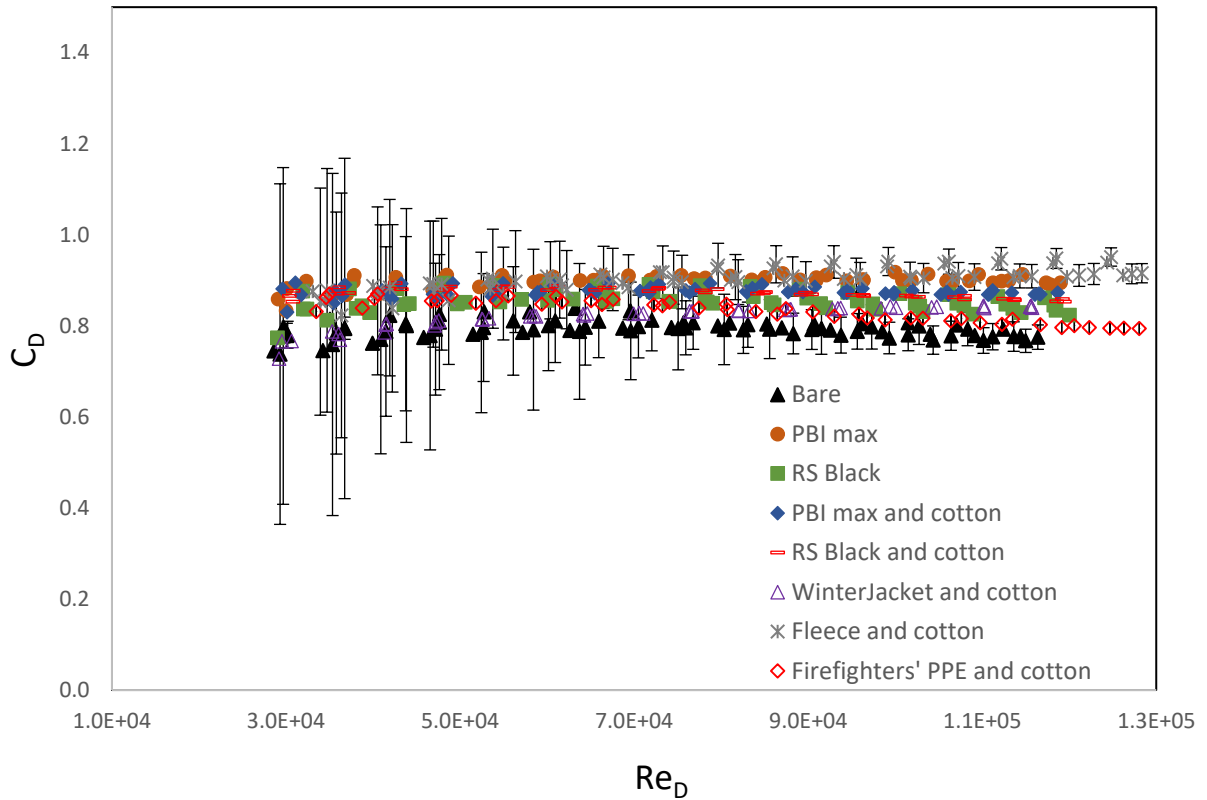
Figure 4.5: Drag force coefficient data for the 3D cylinders with the different fabrics and fabric ensembles. Representative error bars shown for the bare cylinder and the fleece and cotton ensemble only, for clarity.

For all of the configurations, the drag coefficients are relatively independent of Reynolds number. Small differences can be seen in the C_D values between the different fabric-covered cylinders especially at the highest values of Reynolds number where the uncertainty in C_D is the smallest. A maximum of 14% difference was observed between the C_D values and this was between the values for the bare cylinder and the fleece and cotton fabric covered cylinder. Therefore, fabric surface features may have an influence on the airflow and hence, the Nusselt number obtained for the different fabrics. The measured C_D values for the bare cylinder are consistent with published results for bare finite cylinders, as shown in Table 4.1.

Table 4.1: Comparison of drag coefficient data for surface-mounted 3D (finite-height) cylinders (without fabric)

Study	Re_D	δ/D	C_D
Beitel et al. (2019)	6.5×10^4	0.60	0.82
Sakamoto and Oiwake (1984)	5.64×10^4	2.00	0.69
Okamoto and Yagita (1973)	1.3×10^4	0.23	0.74
Current study (3D cylinder)	3.8×10^4 to 1.3×10^5	1.00	0.79

A fabric feature that may be responsible for the significant difference between the Nusselt number of the bare and fabric-covered cylinders is the fabric air permeability. According to ASTM D 123 (ASTM International, 2019), air permeability is the rate of airflow passing perpendicular through an area under a particular air pressure differential between two surfaces of a material. In the present case, due to the penetration of some of the airflow through the surface of the fabric, the airflow in the cylinder's boundary layer will be disturbed compared to that for a bare cylinder. This may lead to a reduction in the rate of convection heat transfer from the surface of the fabric-covered cylinder itself (and an enhancement of the heat transfer from the internal brass cylinder). Furthermore, the air that penetrates and flows through the fabric creates another significant pathway of heat transfer by advection. In this case, the energy balance around the fabric becomes:

$$q = hA(T_s - T_\infty) + \dot{m}_a c_{p,a}\left(T_{air,s} - T_\infty\right) \tag{4.3}$$

where $\dot{m}_a$ represents the mass flow rate of air through the fabric, $c_{p,a}$ represents the specific heat of air, $T_{air,s}$ represents the temperature of air as it exits the fabric. The advection term was not included in the analysis of Nusselt number performed for this thesis research and that could have contributed to the reduced values that were obtained for the fabric-covered cylinders. Similar to the present research, the results of Kamata et al. (1988) show a reduction in Nusselt number values when a cylinder is covered with fabrics.

To further investigate the effect of air penetration in the convection from the surface of a fabric-covered cylinder, an aluminium shimstock with thickness of 0.0762 mm and length equal to the length of the heated section of the 2D cylinder model was wrapped on the outside of the RS Black fabric covered 2D cylinder as a shield to restrict air penetration through the fabric. The high thermal conductivity of aluminium keeps the intrinsic thermal resistance of the entire fabric ensemble reasonably the same despite the addition of another layer of material. The result of this test can be seen by the hollow green data points in Figure 4.4. It was noticed that the values for Nusselt number increased by a maximum of about 31% with the addition of the impermeable shimstock and can be seen to be well within the error limits of the 2D cylinder correlation. Also, the Nusselt number values for the Winter jacket and cotton fabric ensemble are higher than the other fabrics and within the error limits of the 2D cylinder correlation. This is expected as its air permeability is zero (as can be seen in Table 3.1); therefore it can be treated as an impermeable surface compared to the other fabrics tested that have high air permeability values. Figure 4.6 shows the relationship between Nusselt number and Reynolds numbers for only the permeable fabric-covered cylinders along with the error bars that are representative of the uncertainty in Nusselt number (shown in Table 3.2). For clarity, the error bars are shown for only the PBI Max and the fleece and cotton fabric-covered cylinders. From Figure 4.6, it can be seen that the Nusselt number values for the different permeable fabric-covered cylinders are within the uncertainty limits as represented by the error bars on the graph. This shows that small differences in air permeability may not significantly affect the Nusselt number and a similar behavior in convection would occur as long as there is some air penetration through the fabric. The concept of air permeability also explains why the correction technique to obtain the Nusselt number for the side surface of the 3D cylinder from Tsutsui et al. (2000), is accurate for the bare cylinder but not applicable to the fabric covered cylinders shown in Figure 4.3. This is because it does not take into consideration the penetration of airflow through the surface of the fabrics.
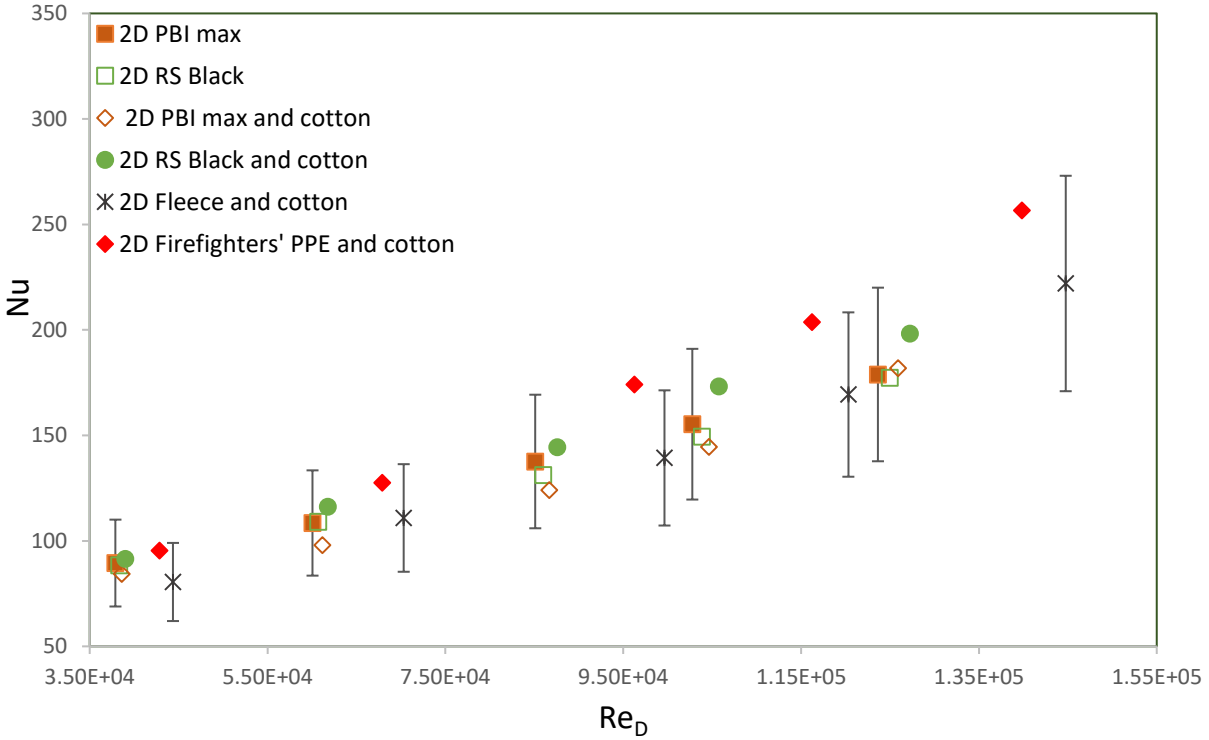
Figure 4.6: Relationship between Nusselt number and Reynolds number for the permeable fabrics tested on the 2D cylinder.

4.2.2 Summary of Nusselt Number Relationship with Reynolds Number

The rate of convective heat transfer for the 2D and 3D bare and fabric-covered cylinders is represented above by the Nusselt number values. In summary, it should be noted that the rate of forced convection from a particular fabric-covered cylinder is quite different than that from a bare cylinder. The major reason for this is the permeability of the fabric. A permeable fabric allows some airflow to penetrate the surface, thereby leading to a difference in the behavior of the airflow on the surface of the fabric-covered cylinder as compared to the airflow on the surface of a bare cylinder with an impermeable surface. Although this could lead to a higher overall rate of heat transfer from the internal cylinder surface, as shall be seen in Section 4.3, the rate of convective heat transfer from the surface of the external fabric itself was seen to be decreased based on the method of analysis used in this thesis research. This also explains why the correction technique proposed by Tsutsui et al. (2000) works for the bare cylinder but is not applicable to the fabric-covered cylinders.

49

4.3 Thermal Resistance of Fabrics

4.3.1 Results of Thermal Resistance of Fabrics

The intrinsic thermal resistance values of each fabric measured using the hot plate test, and the wind tunnel tests of the 2D and the 3D heated cylinders, are shown in Table 4.2.

Table 4.2: Resistance values of each fabric or fabric ensemble from the hot plate and heated cylinder tests

Fabric	Average thickness (mm)	R_f (m^2·C/W)			$R_f/R_{f\,(PBI\,max)}$		
		Hot plate	3D Heated cylinder	2D Heated cylinder	Hot plate	3D heated cylinder	2D heated cylinder
PBI max	0.54	0.022	0.006	0.004	1.0	1.0	1.0
RS Black	0.80	0.022	0.007	0.006	1.0	1.2	1.4
PBI max and cotton	0.99	0.033	0.009	0.015	1.5	1.5	3.4
RS Black and cotton	1.25	0.032	0.010	0.015	1.4	1.7	3.5
Fleece and cotton	4.73	0.129	0.015	0.040	5.8	2.5	9.1
Winter jacket and cotton	0.70	N/A	0.010	0.013	N/A	1.6	3.0
Firefighters' PPE and cotton	3.75	N/A	0.025	0.060	N/A	4.1	13.4

It is observed from Table 4.2, that although the thermal resistance values from the hot plate and heated cylinder tests are not the same, the trend in the ranking of the thermal resistance of the fabrics from highest to lowest is similar. This trend can be seen better in Figure 4.7. The firefighters' PPE and cotton ensemble has the highest thermal resistance value, followed by the Fleece and cotton, then the ensembles of RS Black and cotton, PBI max and cotton and Winter jacket and cotton. The singular RS Black and PBI max fabrics have the lowest thermal resistance values. For both the hot plate and heated cylinder tests, the PBI max and RS Black fabrics have similar thermal resistance values singularly and when each is combined with cotton.
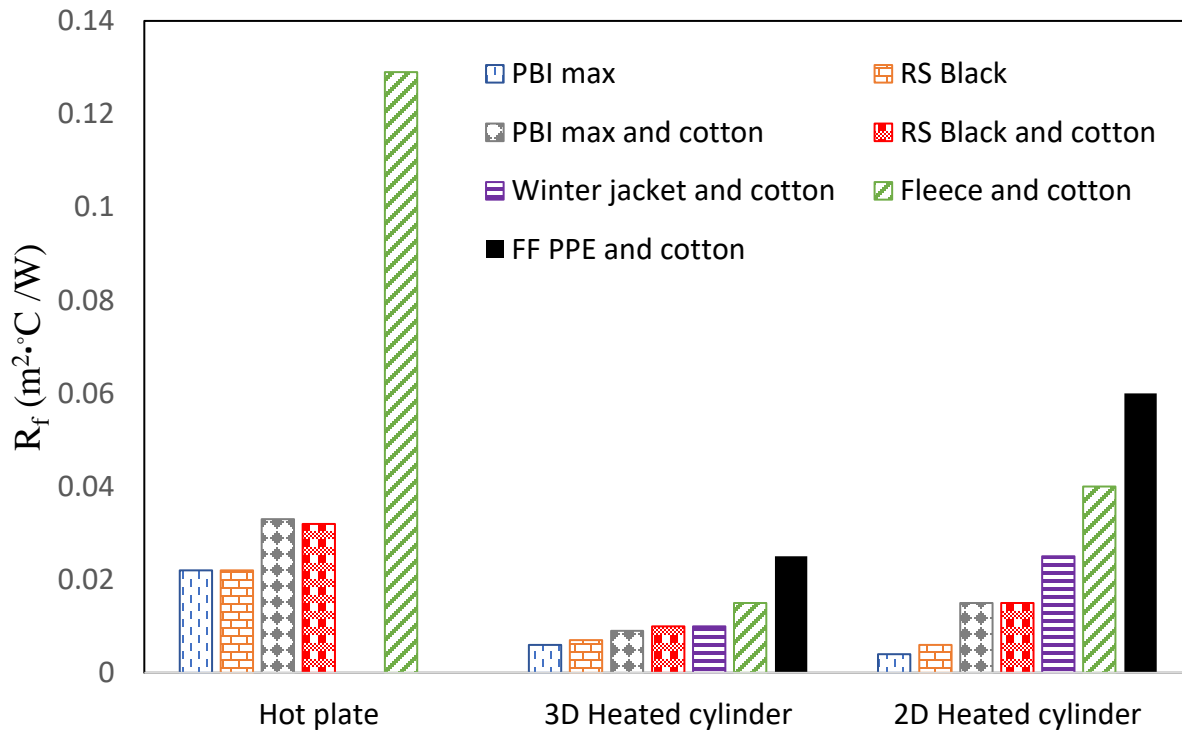
Figure 4.7: Bar chart showing the thermal resistance values for the different fabrics.

This is expected because they have similar thicknesses and thermal conductivitities (see Table 3.1) as they are both outer layers of firefighter's protective clothing. When cotton is included with either of the firefighters' outer layer fabrics (PBI max/RS Black), the thermal resistance is increased by about 40% for the 3D heated cylinder test and the hot plate test. For the 3D heated cylinder tests, the thermal resistance for the fleece and cotton ensemble is more than double the thermal resistance of the singular PBI max and RS Black fabrics. A similar trend can be noticed for the hot plate tests. This is expected because, although fabric thermal conductivity and thickness are generally the two major factors influencing thermal resistance, thickness is usually the more dominant factor as the volume of the fabric occupied by air is much more than that occupied by the fabric strands and for most of the fabrics tested in this research, their thermal conductivities vary only slightly (see Table 3.1).

The influence of fabric thickness and thermal conductivity on the thermal resistance of a fabric was further explored by using the closed form solution from equation (3.10) to obtain temperature values at the surface of the brass cylinder as well as on the outer surface of the fabric

for the range of thickness and thermal conductivity values of the materials used in this research. Then the thermal resistance per unit length (R_f/H) where H is the height of the cylinder was obtained for each case using equation (3.8). This is shown in Table 4.3 and Table 4.4. The study was performed for a heat transfer rate of 30 W, internal cylinder diameter of 9.53 mm, an external cylinder diameter of 48 mm, a convective heat transfer coefficient of 100 W/m²·K and an ambient temperature of 36.9℃.

Table 4.3: Effect of thickness on cylinder temperature

q (W)	k_c (W/m·K)	k_f (W/m·K)	Fabric thickness (mm)	$T_{cylinder}$(℃)	T_{fabric}(℃)	$\dfrac{R_f}{H}$ (W/m·K)
30	110	0.0453	0.5	51.2	43.7	0.038
30	110	0.0453	1.0	58.5	43.5	0.075
30	110	0.0453	1.5	65.7	43.4	0.112
30	110	0.0453	2.0	72.6	43.3	0.147
30	110	0.0453	2.5	79.4	43.2	0.182
30	110	0.0453	3.0	86.1	43.0	0.217
30	110	0.0453	4.7	108.5	42.7	0.331
30	110	0.0453	5.0	111.8	42.6	0.348
30	110	0.0453	10.0	169.2	41.8	0.640

Table 4.4: Effect of thermal conductivity on cylinder temperature

q (W)	k_c (W/m·K)	Fabric thickness (mm)	k_f (W/m·K)	$T_{cylinder}$(℃)	T_{fabric}(℃)	$\dfrac{R_f}{H}$ (W/m·K)
30	110	3	0.0350	98.8	43.0	0.280
30	110	3	0.0450	86.4	43.0	0.218
30	110	3	0.0455	86.0	43.0	0.216
30	110	3	0.0460	85.5	43.0	0.213
30	110	3	0.0465	85.0	43.0	0.211
30	110	3	0.0500	82.1	43.0	0.196
30	110	3	0.0600	75.6	43.0	0.164
30	110	3	1.0000	45.0	43.0	0.010
30	110	0.5	0.0350	53.4	43.7	0.049
30	110	0.5	0.0450	51.3	43.7	0.038
30	110	0.5	0.0455	51.2	43.7	0.038
30	110	0.5	0.0460	51.1	43.7	0.037
30	110	0.5	0.0465	51.0	43.7	0.037
30	110	0.5	0.0500	50.5	43.7	0.034
30	110	0.5	0.0600	49.4	43.7	0.029
30	110	0.5	1.0000	44.0	43.7	0.002

In Table 4.4, the effect of thermal conductivity on the thermal resistance is shown for both a relatively thick fabric and a thin fabric. From the results in Table 4.3 and 4.4, it can be seen that the cylinder's temperature increases as fabric thickness increases but decreases as thermal conductivity increases. Since there is no change in the fabric temperature for the thermal conductivity study and a relatively small change for the fabric thickness parametric study the thermal resistance follows a similar trend. This can also be inferred from equation (3.8). From Table 4.2, it can be seen that the largest thickness difference between the fabrics tested in this research is 4.19 mm (this is between the Fleece and cotton ensemble (4.73 mm) and the PBI Max fabric (0.54 mm)). From the parametric study in Table 4.3, this increase in fabric thickness yields a 159% increase in the thermal resistance of the fabric.

Also, from Table 3.1, the largest difference in the thermal conductivity of the fabrics tested is between the cotton material (0.06 W/m·K) and the thermal liner or moisture barrier (0.035 W/m·K). That is a 0.025 W/m·K difference in thermal conductivity. Although these fabrics were not tested individually, they have the largest difference in thermal conductivity and therefore, provide the best example for this parametric study. It can be seen in Table 4.4 that a 0.025 W/(m.K) increase in thermal conductivity yields a 53% reduction in the thermal resistance of the fabric for both the thick and the thin fabric. This reinforces the fact that since the thermal conductivities of protective clothing and cold weather apparel do not differ considerably, they do not influence the difference in thermal resistance of a fabric as much as the fabric's thickness.

In windy conditions, the air permeability of a fabric can have a major impact in determining its thermal resistance due to the presence of airflow. The air permeability of the fabric as well as the velocity of the airflow determines the rate at which air penetrates the fabric and makes direct contact with the surface of the cylinder, thereby enhancing overall heat loss (Wen et al., 2016). As air enters and exits the fabric, it enhances the heat transfer from the brass cylinder by creating additional pathways for energy transfer through advection, radiation and other means due to its interaction with the cylinder's surface, the fibers of the fabric and the air within the fabric ensemble. This further decreases the measured thermal resistance of the fabric. The effect of this can be seen from the results in Table 4.2. Although the fleece and cotton ensemble has a higher thickness than the firefighers' protective clothing, the thermal resistance of the firefighters' protective clothing is much higher than that of the fleece and cotton. This

could be due to the difference in permeability of the various ensembles. The fleece and cotton ensemble has an air permeability value that is more than three times higher than the air permeability of the firefighters' protective clothing (Table 3.2). Furthermore, the firefighters' protective clothing ensemble comprises of a moisture barrier that prevents air penetration after the first layer (as seen by its air permeability value of zero in Table 3.1). This minimizes the interaction of the flow with the cylinder's surface and hence the heat transfer through the fabric giving it the highest thermal resistance value of all the materials tested. Figure 4.8 shows how airflow impacts the intrinsic thermal resistance of the various fabrics/fabric ensembles.
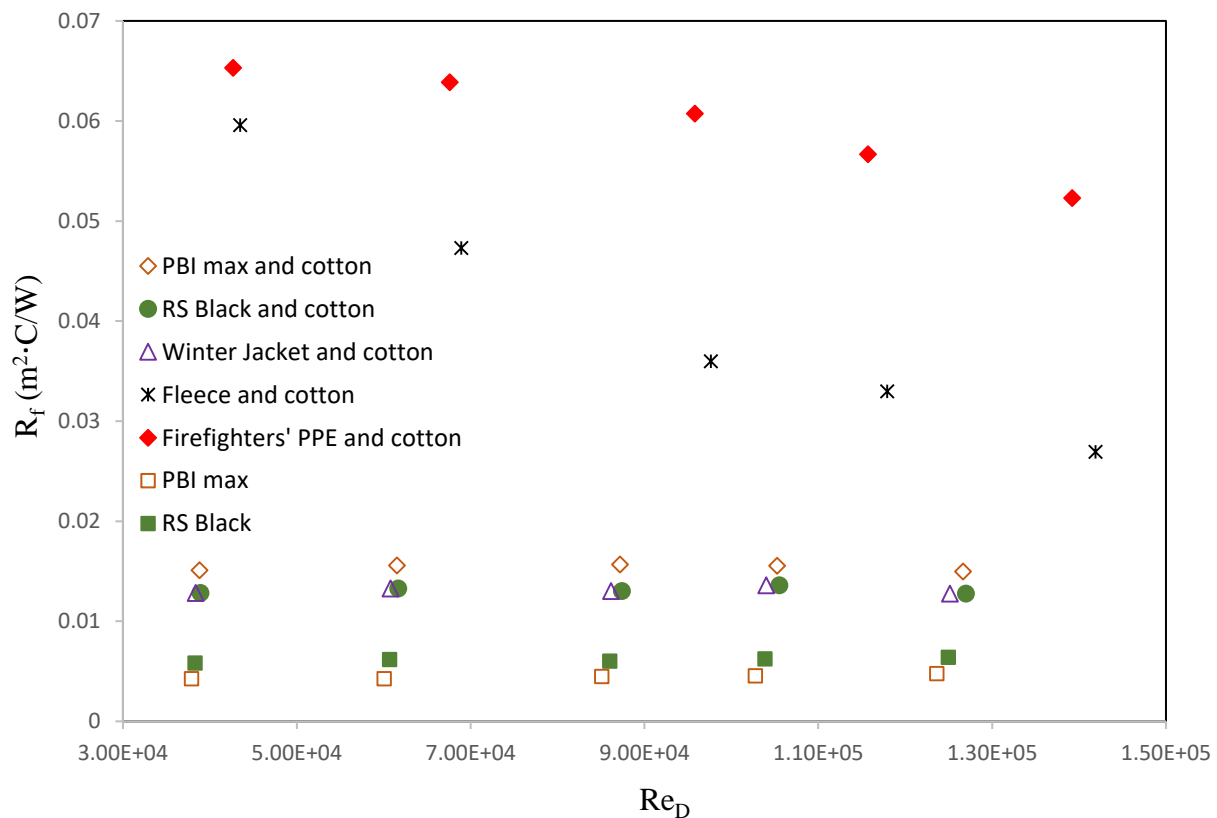
Figure 4.8: Effect of airflow on the thermal resistance of fabrics.

It can be seen that the thermal resistance for the single RS Black and PBI max fabrics, the two-layered PBI max and cotton, RS Black and cotton and winter jacket and cotton ensembles are relatively independent of Reynolds number. The largest difference between the thermal resistance values for each of these fabrics is 11% over the range of Reynolds number tested. A

22% reduction can be noticed in the thermal resistance of the four-layered Firefighters' PPE and cotton ensemble while an even more significant drop of 75% can be noticed in the thermal resistance values for the highly permeable fleece and cotton ensemble over the range of Reynolds number tested. Even though the outermost layer for the RS Black and cotton ensemble and the Firefighters' PPE and cotton is the same, the presence of multiple layers in the firefighters' PPE and cotton ensemble allows for more air gaps which aid in improving its thermal resistance in still conditions but enhances the variation of thermal resistance with changing wind speed. A similar trend can be noticed in the research by Morrissey and Rossi (2014) where a slight difference in thermal resistance was observed between two sets of ensembles tested at multiple airflow speeds with the same impermeable outer layer fabric but inner layer insulations of different air permeability values. A reason for this effect in the firefighters' PPE and cotton ensemble may be the presence of the impermeable moisture barrier as the second layer from the outside direction. This may prevent the airflow that penetrates the first layer from penetrating the rest of the ensemble; and due to the air gaps between the different layers, the airflow may cause the rest of the fabric layers to deform and hence reduce in thickness. As the airflow speed increases, the deformation increases and the effective thickness of the ensemble decreases. A reduction in thickness would lead to a reduction in the overall thermal resistance of the fabric ensemble. This can be seen in the parametric study shown in Table 4.3.

The high permeability of the fleece material yields an even greater variation in its thermal resistance value. As the airflow speed increases, there is higher air penetration into the fabric ensemble and the heat transfer rate from the cylinder and the fabric fibers increases leading to a reduction in the thermal resistance value measured. This reinforces the influence that the fabric air permeability has on its thermal resistance in windy conditions. Kosinski and Wojcik (2017) studied the impact of air permeability on heat transfer through partitions insulated with loose fibers and it was noticed that higher wind speeds caused a larger reduction in the thermal resistance of the materials tested than lower wind speeds and the airflow had a more significant effect on the thermal resistance of the material with less fibre density (higher permeability) than those with higher fiber density (lower permeability). The results shown in Gibson (2009) and Zhu et al. (2015) also support this.

The values of thermal resistance for the 2D and 3D heated cylinders were expected to be very similar, however this was not the case for the thicker fabric ensembles especially. There was a 49% difference between the thermal resistance values obtained from the 2D and 3D heated cylinders for the RS Black and cotton ensemble and a 42% difference for the PBI Max and cotton ensemble while an 83% difference was noticed for the firefighters' and cotton ensemble and a 91% difference for the fleece and cotton ensemble. This is due to the presence of the free end for the 3D cylinder that allows for more heat transfer from the top when the resistance to heat transfer due to the fabric wrapped around the side increases. This causes a reduction in thermal resistance values obtained for the fabric tested on the 3D cylinder. The difference in values between the hot plate and heated cylinder tests is due to the variation in geometry (cylinder versus plate) and testing conditions. The effect of fabric permeability magnified by airflow can also explain why the resistances from the hot plate test are significantly higher than those of the heated cylinder tests. The hot plate tests are performed in an environmental chamber with air flowing parallel to the surface of the fabric and the test plate at about 1 m/s while the heated cylinders are in cross flow with air speed ranging from about 10 m/s to 40 m/s thereby allowing more air penetration through the fabrics, which leads to more heat transfer and hence lower thermal resistance values measured. As compared to parallel airflow that is mainly utilized in hot plate tests, airflow that is normal to the surface of the testing model provides a thermal resistance testing scenario that better represents the general applications of outdoor clothing in everyday life or at least, the worst case scenario.

4.2.2 Summary of Thermal Resistance of Fabrics

Fabric thickness and thermal conductivity are important factors in determining thermal resistance in still conditions. However, in windy conditions, the thermal resistance is largely dependent on the permeability of the fabric. In this research, it was observed that fabrics with high air permeability allow some of the airflow through and onto the surface of the cylinder. This causes an additional path of heat transfer directly from the surface of the cylinder and the internal fibers of the fabric that is not always noticed in still or low airflow thermal resistance test methods such as the hot plate test. A reduction in thermal resistance with an increase in airflow speed can also be noticed for the fabric ensembles with higher permeability. This is because a higher airflow speed causes an increase in the rate of heat transfer that occurs directly from the surface of the cylinder and fabric fibers, thereby reducing its thermal resistance value further. In

addition to the difference in geometry between the models of the hot plate and heated cylinders, the concept of fabric permeability could be one of the reasons the results from the heated cylinder tests are much lower than those from the hot plate tests and the presence of the uncovered free end on the top of the 3D cylinder causes the difference in results between the thermal resistance measured by the 2D and 3D fabric-covered cylinders.

Chapter 5 – 1D Numerical Model

5.1 Finite-Difference Model

A finite-difference model (FDM) was developed to complement the experimental results obtained in this research. Although the data obtained from the experiment were all steady state, a transient model was developed in this section. Apart from being able to compare the steady state results of the experiment, the transient model has a larger range of applications in the fire service field, especially as it pertains to firefighters' protective clothing and skin temperatures in working environments.

The composite cylinder model was developed using the case scenario and the boundary conditions that were used in the experiment. A schematic of the model is shown in Figure 5.1.

(a) Top view of composite cylinder

(b) Segment of cylinder illustrating the finite-difference model
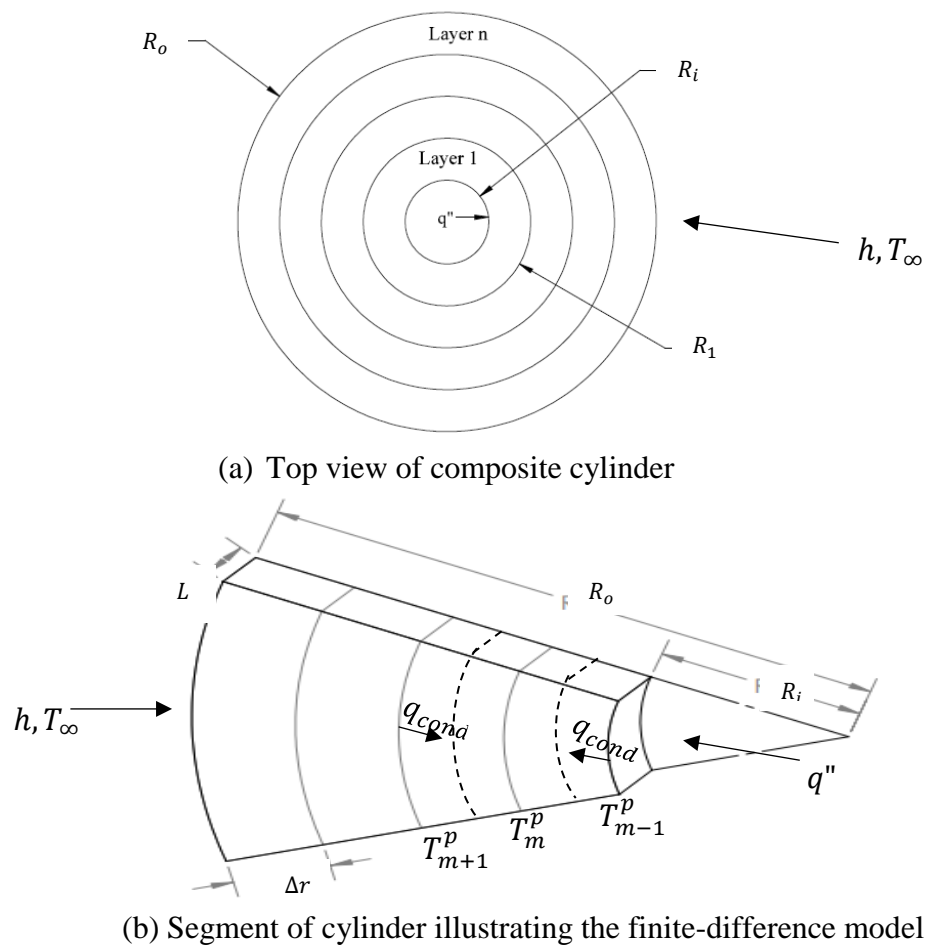
Figure 5.1: Problem description for the composite cylinder finite-difference model.

Figure 5.1 (a) shows the top view of a hollow n-layer composite cylinder where the thermal and physical properties of each layer vary. R_i and R_o represent the internal and external radius of the cylinder respectively and R_l represents the outer radius of the first layer. It is bounded internally by a constant heat transfer rate specified by the heat flux, q'' and externally by convection, (h, T_∞). Figure 5.1 (b) shows a segment of the cylinder that illustrates how the equation for the temperature at discrete radial positions and time steps was developed. T_m^p represents the temperature at a given radial position (m) and time step (p) while T_{m+1}^p and T_{m-1}^p represent the temperatures at the neighboring nodal points and Δr represents the radial distance between temperature nodes. The dotted lines in Figure 5.1(b) represent the boundary of the control volume pertaining to the node T_m^p and it represents the interface where conduction heat transfer between neighboring nodes (q_{cond}) occurs. For consistency purposes, all thermal energy is assumed to be going into the node. The model was developed using the backward-difference approximation. Therefore, an implicit method was used for computation.

In order to develop the equation for the heat transfer through the various layers, the energy balance at various important boundary conditions was analyzed similar to the process in Eppes and Burleson (1965) using the equation

$$q_{in} + q_g = q_{st}, \tag{5.1}$$

where q_{in} is the rate at which thermal energy goes into the control volume from both sides, q_g is the rate at which thermal energy is generated in the control volume and q_{st} is the rate at which thermal energy is stored in the control volume over a time step.

For the interior boundary that is exposed to a constant heat flux, the temperature was obtained as shown below:

$$q''A + q_{cond} = q_{st}, \tag{5.2}$$

$$q''A + kA\frac{\Delta T}{\Delta r} = mc_p\frac{\Delta T}{\Delta t}, \tag{5.3}$$

$$R_i\theta Lq'' + k(R_i + \tfrac{\Delta r}{2})\theta L(\tfrac{T_{m+1}^{p+1} - T_m^{p+1}}{\Delta r}) = \rho(R_i + \tfrac{\Delta r}{4})\theta L(\tfrac{\Delta r}{2})c_p(\tfrac{T_m^{p+1} - T_m^p}{\Delta t}), \tag{5.4}$$

where A is the area normal to the direction of heat transfer of the boundary surface of the control volume for a temperature node, L is the thickness of the node, θ is the angle of the cylindrical

segment used to derive the equations, m is the mass of the node, k, ρ and c_p are the thermal conductivity, density and specific heat capacity of the layer material respectively. ΔT is the difference between the temperature of neighboring nodes and Δt is the interval between two time steps.

Rearranging the above equation to solve for T_m^p, the result becomes:

$$T_m^p = T_m^{p+1} + \left(\frac{2k\Delta t\left(R_i+\frac{\Delta r}{2}\right)}{\rho c_p (R_i+\frac{\Delta r}{4})(\Delta r)^2}\right) T_m^{p+1} - \left(\frac{2k\Delta t\left(R_i+\frac{\Delta r}{2}\right)}{\rho c_p (R_i+\frac{\Delta r}{4})(\Delta r)^2}\right) T_{m+1}^{p+1} - \frac{2\Delta t R_i q''}{\rho c_p\left(R_i+\frac{\Delta r}{4}\right)(\Delta r)}, \tag{5.5}$$

letting

$$\varphi = \frac{2k\Delta t(R_i+\frac{\Delta r}{2})}{\rho c_p(R_i+\frac{\Delta r}{4})(\Delta r)^2}, \tag{5.6}$$

and

$$\gamma = \frac{2\Delta t R_i}{\rho c_p(R_i+\frac{\Delta r}{4})(\Delta r)}. \tag{5.7}$$

Therefore,

$$T_m^p = (1+\varphi)T_m^{p+1} - \varphi T_{m+1}^{p+1} - \gamma q''. \tag{5.8}$$

For any internal point within a particular layer, the energy balance was also applied to obtain the temperature distribution thus:

$$q_{cond(left)} + q_{cond(right)} = q_{st}; \tag{5.9}$$

$$kA_1\left(\frac{T_{m-1}^{p+1}-T_m^{p+1}}{\Delta r}\right) + kA_2\left(\frac{T_{m+1}^{p+1}-T_m^{p+1}}{\Delta r}\right) = \rho A\Delta r c_p\left(\frac{T_m^{p+1}-T_m^p}{\Delta t}\right).$$

For each internal node, the radial position varies. Therefore, the area of the entry and exit surfaces of the control volume depend on the location of the node in the radial direction. A_1 and A_2 represent the area of the left and right boundary surface of the control volume for a particular node. Rewriting the area, $A_1 = \left(R_i + m\Delta r - \frac{\Delta r}{2}\right)\theta L$ and $A_2 = \left(R_i + m\Delta r + \frac{\Delta r}{2}\right)\theta L$, then

$$k\left(R_i + m\Delta r - \frac{\Delta r}{2}\right)\theta L\left(\frac{T_{m-1}^{p+1}-T_m^{p+1}}{\Delta r}\right) + k\left(R_i + m\Delta r + \frac{\Delta r}{2}\right)\theta L\left(\frac{T_{m+1}^{p+1}-T_m^{p+1}}{\Delta r}\right)$$

$$= \rho(R_i + m\Delta r)\theta L\Delta r c_p\left(\frac{T_m^{p+1}-T_m^p}{\Delta t}\right). \tag{5.10}$$

Solving for T_m^p with $\alpha = \frac{k}{\rho c_p}$ and $Fo = \frac{\alpha \Delta t}{(\Delta r)^2}$,

$$T_m^p = (1 + 2Fo)T_m^{p+1} - Fo\left(1 - \frac{\Delta r}{2(R_i + m\Delta r)}\right)T_{m-1}^{p+1} - Fo\left(1 + \frac{\Delta r}{2(R_i + m\Delta r)}\right)T_{m+1}^{p+1}. \tag{5.11}$$

For a point that is at the interface of two layers (e.g. materials 1, 2), the temperature is obtained thus:

$$q_{cond(mat'l\ 1)} + q_{cond(mat'l\ 2)} = q_{st}; \tag{5.12}$$

$$k_1 A_1\left(\frac{T_{m-1}^{p+1}-T_m^{p+1}}{\Delta r_1}\right) + k_2 A_2\left(\frac{T_{m+1}^{p+1}-T_m^{p+1}}{\Delta r_2}\right) = \frac{1}{2}(\rho_1 c_{p1}\Delta r_1 + \rho_2 c_{p2}\Delta r_2)A_m\left(\frac{T_m^{p+1}-T_m^p}{\Delta t}\right)$$

$$k_1\left(R_i + m\Delta r_1 - \frac{\Delta r_1}{2}\right)\theta L\left(\frac{T_{m-1}^{p+1}-T_m^{p+1}}{\Delta r_1}\right) + k_2\left(R_1 + \frac{\Delta r_2}{2}\right)\theta L\left(\frac{T_{m+1}^{p+1}-T_m^{p+1}}{\Delta r_2}\right)$$

$$= \frac{1}{2}(\rho_1 c_{p1}\Delta r_1 + \rho_2 c_{p2}\Delta r_2)R_1\theta L\left(\frac{T_m^{p+1}-T_m^p}{\Delta t}\right). \tag{5.13}$$

Rearranging the above equation to solve for T_m^p,

$$T_m^p = \left(1 + \frac{2k_1\Delta t\left(R_1 - \frac{\Delta r_1}{2}\right)}{R_1\Delta r_1(\rho_1 c_{p1}\Delta r_1 + \rho_2 c_{p2}\Delta r_2)} + \frac{2k_2\Delta t\left(R_1 + \frac{\Delta r_2}{2}\right)}{R_1\Delta r_2(\rho_1 c_{p1}\Delta r_1 + \rho_2 c_{p2}\Delta r_2)}\right)T_m^{p+1} -$$

$$\left(\frac{2k_1\Delta t\left(R_1 - \frac{\Delta r_1}{2}\right)}{R_1\Delta r_1(\rho_1 c_{p1}\Delta r_1 + \rho_2 c_{p2}\Delta r_2)}\right)T_{m-1}^{p+1} - \left(\frac{2k_2\Delta t\left(R_1 + \frac{\Delta r_2}{2}\right)}{R_1\Delta r_2(\rho_1 c_{p1}\Delta r_1 + \rho_2 c_{p2}\Delta r_2)}\right)T_{m+1}^{p+1}, \tag{5.14}$$

letting

$$\varepsilon = \frac{2k_1\Delta t\left(R_1 - \frac{\Delta r_1}{2}\right)}{R_1\Delta r_1(\rho_1 c_{p1}\Delta r_1 + \rho_2 c_{p2}\Delta r_2)}, \tag{5.15}$$

and

$$\psi = \frac{2k_2\Delta t\left(R_1 + \frac{\Delta r_2}{2}\right)}{R_1\Delta r_2(\rho_1 c_{p1}\Delta r_1 + \rho_2 c_{p2}\Delta r_2)}. \tag{5.16}$$

Therefore,

$$T_m^p = (1 + \varepsilon + \psi)T_m^{p+1} - \varepsilon T_{m-1}^{p+1} - \psi T_{m+1}^{p+1}. \tag{5.17}$$

Finally, the temperature at the exterior boundary exposed to the freestream was obtained thus:

$$q_{conv} + q_{cond} = q_{st}; \tag{5.18}$$

$$hR_0\theta L\left(T_\infty - T_m^{p+1}\right) + k\left(R_0 - \frac{\Delta r}{2}\right)\left(\frac{T_{m-1}^{p+1} - T_m^{p+1}}{\Delta r}\right) = \rho c_p\left(R_0 - \frac{\Delta r}{4}\right)\left(\frac{\Delta r}{2}\right)\left(\frac{T_m^{p+1} - T_m^p}{\Delta t}\right). \tag{5.19}$$

Solving for T_m^p,

$$T_m^p = T_m^{p+1} + \left(\frac{hR_0\Delta t}{\rho c_p\left(R_0 - \frac{\Delta r}{4}\right)\left(\frac{\Delta r}{2}\right)}\right)T_m^{p+1} + \left(\frac{2k\Delta t\left(R_0 - \frac{\Delta r}{2}\right)}{\rho c_p\left(R_0 - \frac{\Delta r}{4}\right)(\Delta r)^2}\right)T_m^{p+1} -$$

$$\left(\frac{2k\Delta t\left(R_0 - \frac{\Delta r}{2}\right)}{\rho c_p\left(R_0 - \frac{\Delta r}{4}\right)(\Delta r)^2}\right)T_{m-1}^{p+1} - \left(\frac{hR_0\Delta t}{\rho c_p\left(R_0 - \frac{\Delta r}{4}\right)\left(\frac{\Delta r}{2}\right)}\right)T_\infty, \tag{5.20}$$

letting

$$\beta = \frac{hR_0\Delta t}{\rho c_p\left(R_0 - \frac{\Delta r}{4}\right)\left(\frac{\Delta r}{2}\right)}, \tag{5.21}$$

and

$$\delta = \frac{2k\Delta t\left(R_0 - \frac{\Delta r}{2}\right)}{\rho c_p\left(R_0 - \frac{\Delta r}{4}\right)(\Delta r)^2}. \tag{5.22}$$

Therefore,

$$T_m^p = (1 + \beta + \delta)T_m^{p+1} - \delta T_{m-1}^{p+1} - \beta T_\infty. \tag{5.23}$$

5.2 Summary of Finite-Difference Model

The finite-difference model was developed to obtain temperature values in the different layers of a multi-layered cylinder. The derivation shown in the above sections of this chapter is for a composite cylinder with an internal heat flux boundary condition and convection on the external surface. However, the model can be adapted to any type of heat transfer boundary condition by revising the equations on the boundary accordingly. To obtain results from the model as is, the heat flux on the internal boundary and the convection coefficient and freestream temperature on the external boundary need to be specified. Temperature-independent material properties such as density, specific heat and thermal conductivity pertaining to each layer of the composite cylinder are also necessary inputs for the model, as well as layer thickness. In this research, the model was only demonstrated for a maximum of a seven-layer cylinder, however, more layers can be easily added using equation (5.17).

For this research, a time step of $\Delta t = 0.5$ s was used. Since an implicit method was implemented for the computation, there was no restriction on the size of the time step and it was observed that the results obtained using $\Delta t = 5$ s were equally as accurate as the results obtained using $\Delta t = 0.5$ s for the boundary conditions tested. The number of temperature values obtained in a layer depended on the radial distance Δr between neighboring nodes, therefore to obtain a large number of values in the temperature distribution, a small Δr should be used. The model was implemented in the Microsoft Excel software. The equations for each boundary condition and temperature node were placed into a matrix as a system of linear equations and solved iteratively until steady state was attained. Steady state was said to be attained when the temperature at all the nodal points were within 0.001℃ of the temperature at the previous time step. The run-time of the model depends on the number of layers, and the size of Δt and Δr. More cylindrical layers, or small values of Δt and Δr may require longer run time for the model to get to steady state. This should not be a real problem for high speed processing computers as the run time for the seven-layer cylinder was less than 15 s. For this research, a Lenovo ThinkCentre computer with core i5 processing was used to run the model. Finally, it was assumed that there is perfect thermal and physical contact between neighboring layers of the composite cylinder and that all the layers of the composite cylinder have impermeable surfaces.

5.3 Comparison to Closed Form Transient Solutions

Yang and Liu (2016) developed closed form analytical solutions for transient heat conduction in hollow cylinders with multiple layers. Some examples were given to demonstrate the method developed. The model proposed in the current research was applied to the case scenarios stated in Yang and Liu (2016) and the results were compared. The parameters for each case scenario can be seen below. These parameters and the results for the examples were made non-dimensional in Yang and Liu (2016) to simplify the sample run.

i. A two-layer hollow cylinder with internal radius, $r_0 = 1$, constant inner and outer surface temperatures of $T_0 = 1$ and $T_2 = 0$, and layer properties shown in Table 5.1

Table 5.1: Properties of two-layer cylinder example stated in Yang and Liu (2016)

Layer	Radius, r (m)	Thermal diffusivity, α (m²/s)	Thermal conductivity, k (W/m·K)
1	2	4	4
2	4	1	1

ii. A seven-layer hollow cylinder with internal radius, $r_0 = 0.5$, variable heat flux at the inner surface ($q(t) = q_0(1 - e^{-0.2t})$), and convective heat transfer ($h = 2$) at the external boundary condition. The properties of the layers are shown in Table 5.2.

Table 5.2: Properties of seven-layer cylinder example stated in Yang and Liu (2016)

Layer	Radius, r (m)	Thermal diffusivity, α (m²·s)	Thermal conductivity, k (W/m·K)
1	1.5	6	2.0
2	3.0	8	3.0
3	5.0	10	5.0
4	6.5	14	5.0
5	8.5	11	3.0
6	9.5	9	2.0
7	10.5	7	1.5

The FDM model used was comprised of 40 data points for each cylindrical layer in both examples and time steps of $\Delta t = 0.01$ in example (i) and $\Delta t = 0.05$ in example (ii).

The results obtained from the FDM model proposed in this research were compared to the results stated in Yang and Liu (2016). Figure 5.2 shows the results for the two-layer cylinder while Figure 5.3 shows the results for the seven-layer cylinder.

(a) Result from Yang and Liu (2016) (reprinted with perimssion).

(b) Result from FDM model.

Figure 5.2: Comparison between results from current model and Yang and Liu (2016) for a two-layer cylinder.
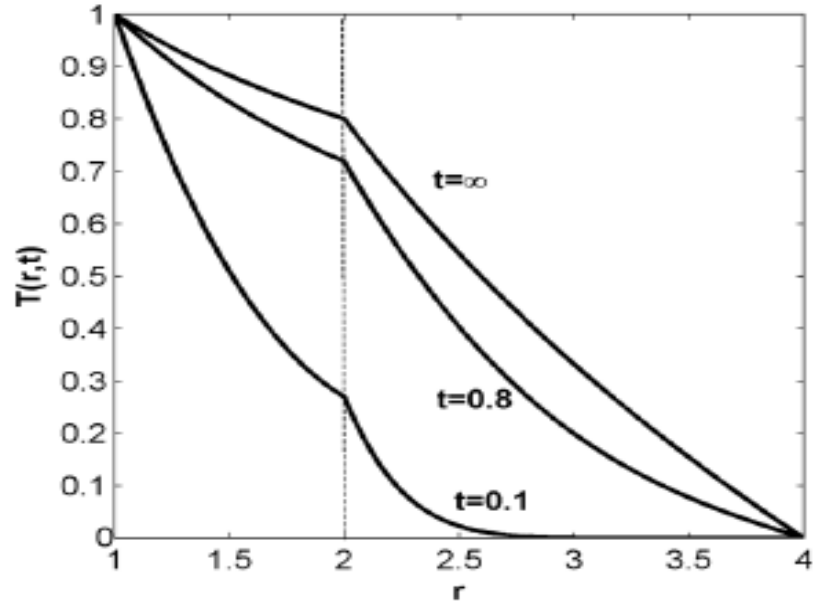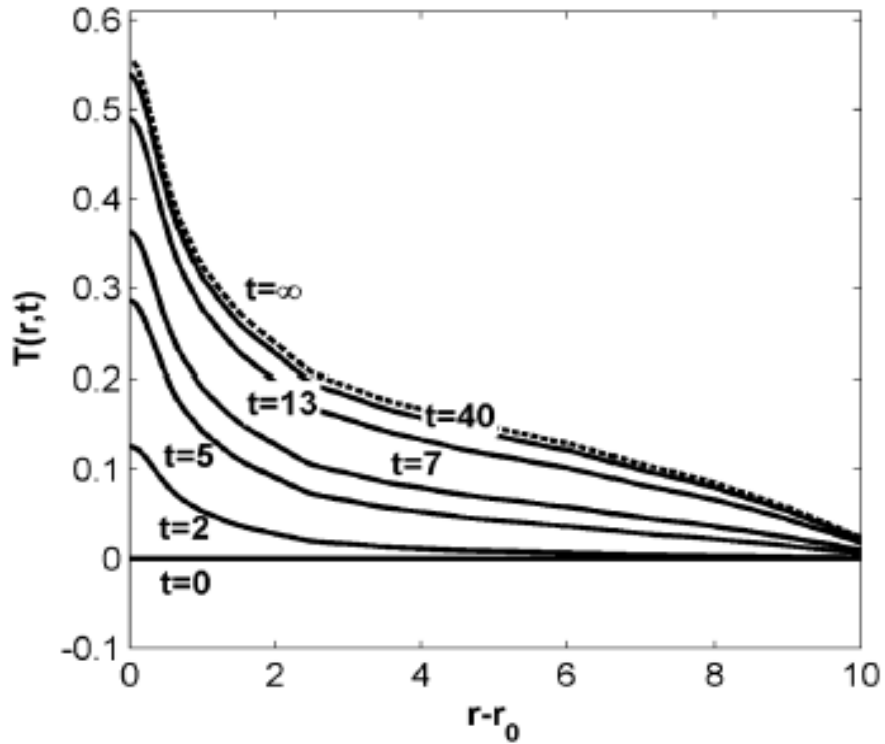
(a) Result from Yang and Liu (2016) (reprinted with permission).
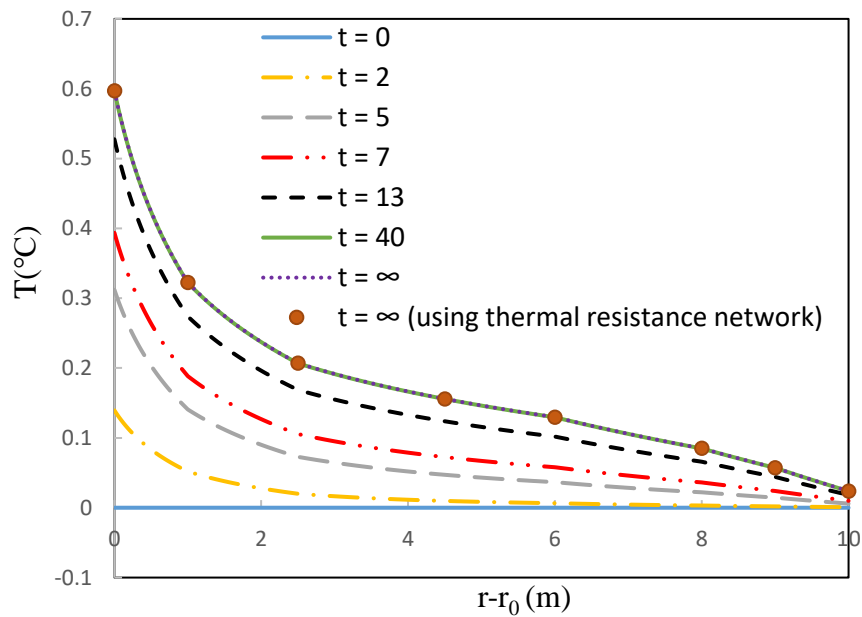
(b) Result from FDM model.

Figure 5.3: Comparison between results of example of seven-layer cylinder proposed by Yang and Liu (2016).

For the two-layer cylinder, the temperature values were recorded at times of $t = 0.1, 0.8$ and at steady state (t_∞), while the temperature values were recorded at times of $t = 2, 5, 7, 13,$ 40 and at steady state, (t_∞) for the seven-layer cylinder. From Figure 5.2 it can be seen that the results of the model proposed in this research and that documented in Yang and Liu (2016) are in good agreement. From Figure 5.3, for the seven-layer cylinder, it can be seen that the temperature values at the inner boundary layer (r-$r_0 = 0$) for the present model begin to deviate slightly from that stated in Yang and Liu (2016) as time increases to a maximum of 6% difference at steady state. While this difference is small, the effects of the grid size (Δr) and time step on the accuracy of the results were explored by performing grid sensitivity studies for the seven-layer composite cylinder. Results were obtained for 30, 40 and 50 nodal points in each layer and Δt values of 0.005, 0.01, 0.03 and 0.05. To further examine the temperatures closer to the internal boundary condition in the seven-layer cylinder, 80 temperature nodes were located in the first layer. There was no difference in the temperature values obtained for these variations. The thermal resistance network was also used to calculate the temperatures at steady state in the different layers of the seven-layer cylinder and as can be seen in Figure 5.3b, there is complete agreement between the result from the thermal resistance network and the and the steady state results of the present model.

Another example was used to test the accuracy of the model at steady state. A five-layer cylinder consisting of a brass layer and four layers of fabrics with parameters shown in Table 5.3 was tested. The case scenario consists of a constant heat flux ($q'' = 2000$ W/m^2) inner boundary condition with forced convection ($h = 100$ W/m^2·K, $T_\infty = 25$°C) on the outside The steady state temperature results from the present model were compared to the results obtained by evaluating the thermal resistance of each layer theoretically and combining them into a thermal resistance network. The closed-form solution in equation 3.10 was also compared to the the finite-difference model in this example. Since the closed-form solution was developed for only two layers, the properties of the four fabrics were combined into one as they have similar thermal properties. The results can be seen in Figure 5.4.

Table 5.3: Properties of five-layer cylinder example for comparison with the thermal resistance network method with references

Layer	Material	Radius, r (m)	Thermal diffusivity, α (m²/s)	Thermal conductivity, k (W/m·K)	References
1	Brass cylinder	0.024	3.45×10^{-5}	110	Bergman et al. (2011)
2	Cotton	0.0246	5.77×10^{-7}	0.06	Bergman et al. (2011)
3	Thermal liner – XE 189	0.02608	3.65×10^{-7}	0.036	Lawson et al. (2005)
4	Moisture barrier – Stedair 3000	0.02683	1.12×10^{-7}	0.036	Lawson et al. (2005)
5	Outer shell – RS Black	0.02763	3.45×10^{-5}	0.04	Torvi (1997)
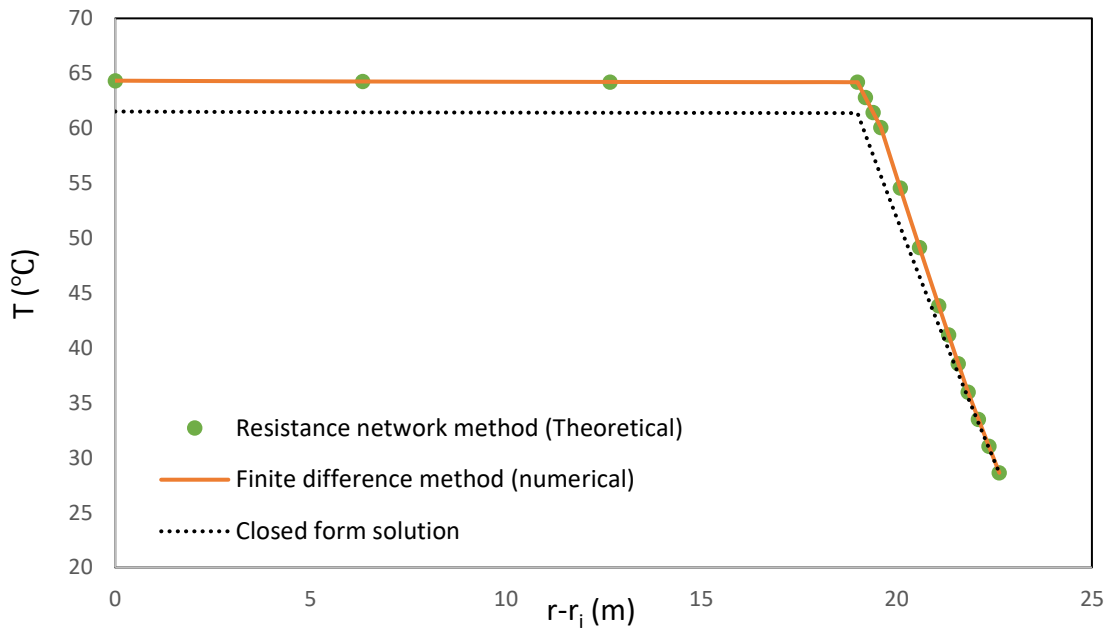
Figure 5.4: Steady state temperature comparison between results from FDM model and thermal resistance network.

From Figure 5.4, it can be seen that the steady state results obtained from the finite-difference method are in complete agreement with the results from the thermal resistance network. A maximum of 5% difference can be seen between the results of the closed form solution and the finite-diffence model. This is due to the fact that the entire fabric ensemble was

assumed to be one fabric in the closed form solution so small differences in the fabric properties would lead to the differerence between the results of the finite-difference model and the closed form solution. This increases the confidence in the model developed.

5.4 Comparison to Experimental Results

Since a high confidence in the model validity has been established, it was then used to model the results of the experiments. The physical and thermal properties of the cylinder and fabrics used for the modelling can be seen in Table 3.1 and Table 3.2. The parameters for specific tests performed in the wind tunnel were inputted into the finite difference model and the results of temperature at steady state were compared as seen in Figure 5.5, Figure 5.6, Figure 5.7 and Figure 5.8. Some examples of the transient response for the bare cylinder, a single-layer fabric-covered cylinder and mutiple-layer fabric-covered cylinders are shown in Appendix D. The steady state results are shown for the bare cylinder in Figure 5.5, the cylinder covered with the RS Black fabric (with and without an aluminum shimstock to show the effect of the air permeability of the fabric) in Figure 5.6, the cylinder covered by the fleece and cotton ensemble in Figure 5.7 and the cylinder covered by the four-layered Firefighters' PPE and cotton ensemble in Figure 5.8. The lines represent the results of the numerical model while the blue symbols represent the results obtained from the experiments.
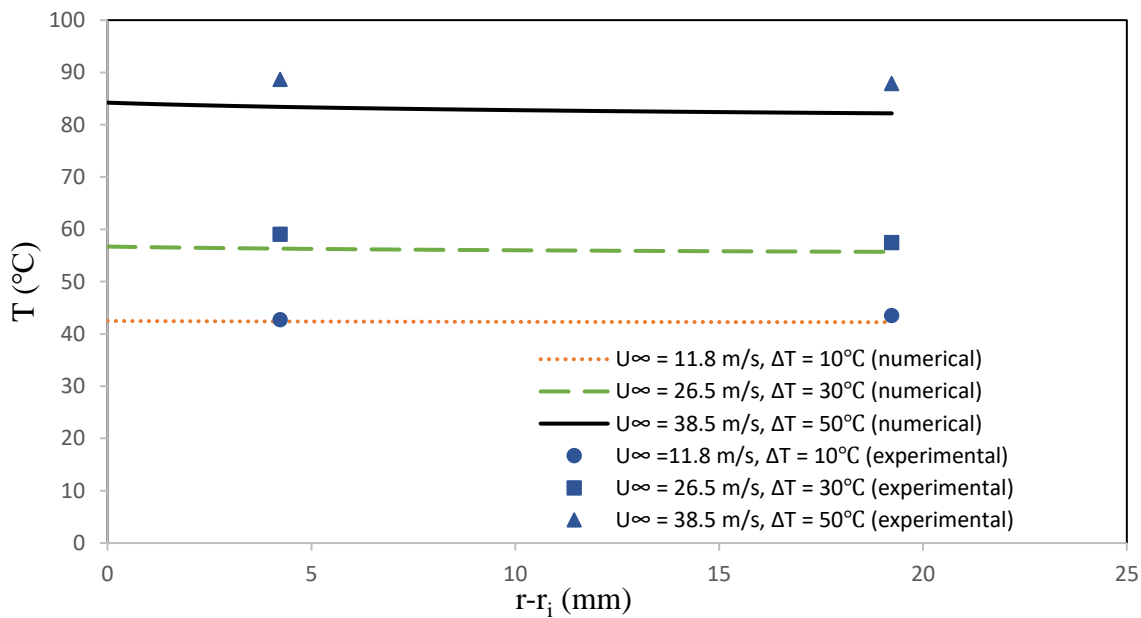
Figure 5.5: Comparison between the experimental and numerical results for the bare cylinder.
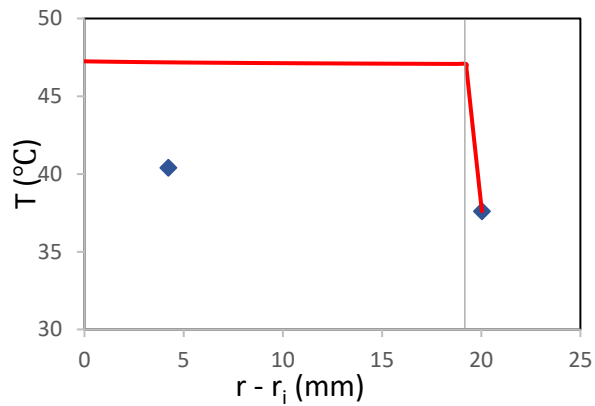
(a) $U_\infty = 11.8$ m/s, $\Delta T = 10°C$
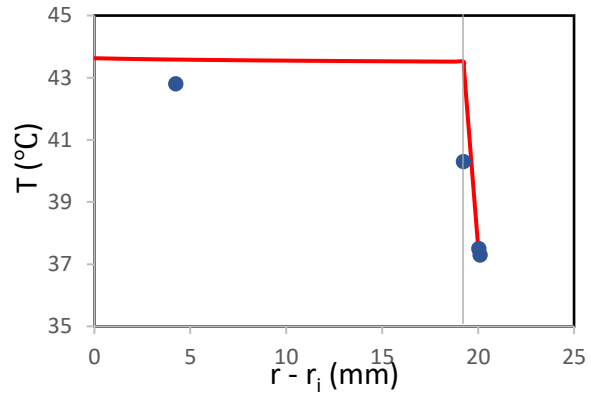
(b) $U_\infty = 11.8$ m/s, $\Delta T = 10°C$ (with shim stock)
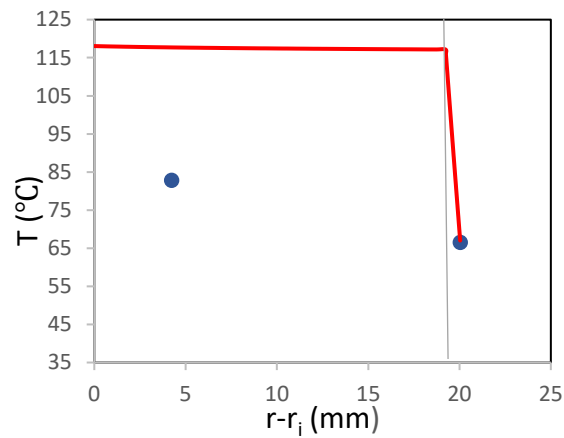
(c) $U_\infty = 26.5$ m/s, $\Delta T = 50°C$
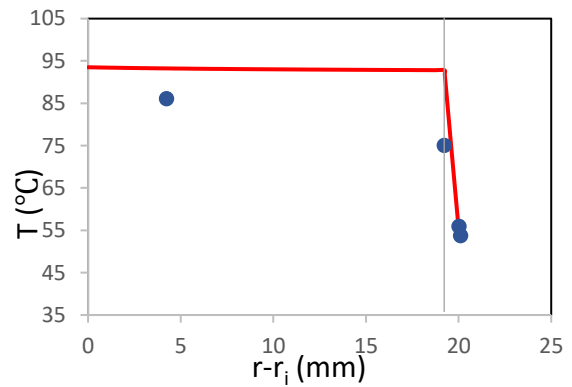
(d) $U_\infty = 26.5$ m/s, $\Delta T = 50°C$ (with shim stock)
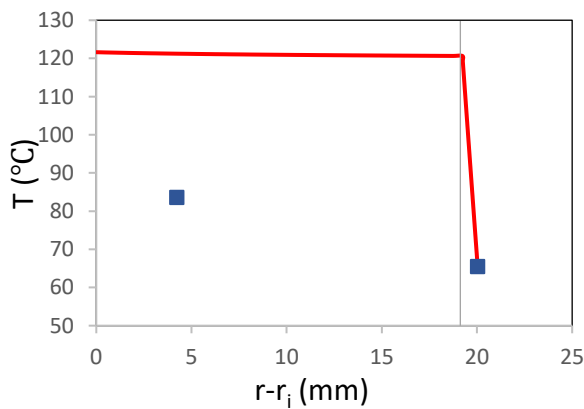
(e) $U_\infty = 32$ m/s, $\Delta T = 50°C$
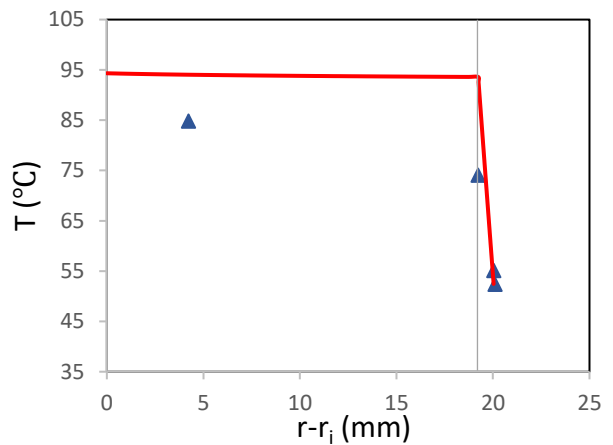
(f) $U_\infty = 32$ m/s, $\Delta T = 50°C$ (with shim stock)

Figure 5.6: Comparison between experimental and numerical results for RS Black covered cylinder (grey line represents the outer diameter of the brass layer).

◆ Experimental values

── FDM numerical results
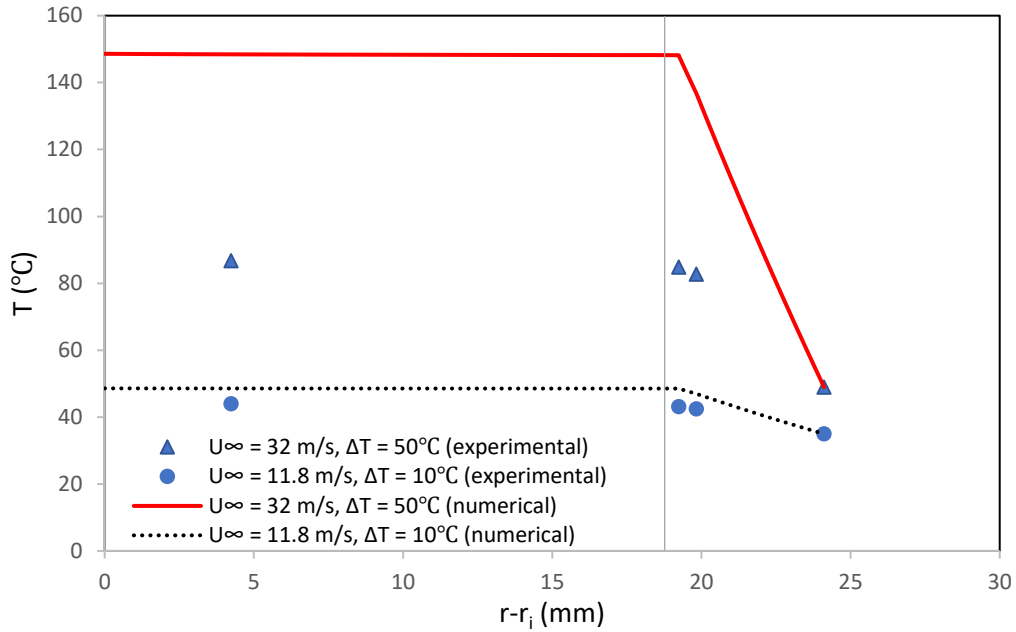
Figure 5.7: Comparison between experimental and numerical results for the fleece and cotton covered cylinder.
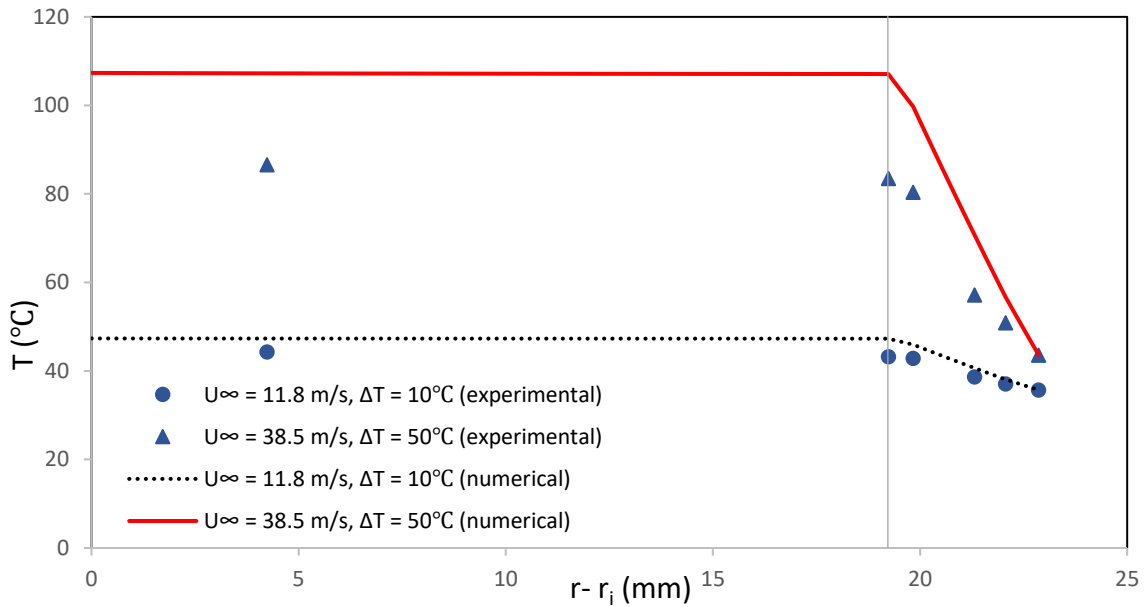
Figure 5.8: Comparison between experimental and numerical results for the four-layer Firefighters' PPE and cotton ensemble.

From Figures 5.5, 5.6, 5.7 and 5.8, it can be noticed that while there might be some variations between the temperature values within the bare or fabric covered cylinders, the temperatures on the external surface (i.e. at the highest radial position) are in agreement. This is

because the convection boundary condition on the external surfaces of the bare or fabric-covered cylinders was inputted into the model using the ambient temperature and the convection coefficient obtained from the cylinder's temperature in the experiment. This basically sets the temperature at the surface and the difference between the experimental and numerical results begin to be more apparent internally. For the bare cylinder shown in Figure 5.5, the temperature values obtained from the experiments and from the numerical model are in good agreement (within 7% difference) throughout the cylinder while significant variations can be noticed in the multi-layer cylinders in Figures 5.6 – 5.8. The reason for this can be explained with the aid of the results of the RS Black fabric-covered cylinder shown in Figure 5.6.

The experimental results of the fabric-covered cylinder shielded from the airflow with the shimstock are in better agreement with the the model (maximum of 22% difference) than those obtained from the unshielded fabric-covered cylinder tests (maximum of 37% difference). This is expected as the model was developed for a composite cylinder with an impermeable surface and the effects of fabric permeability on the heat transfer within the fabric-covered cylinder were not included in the model. Also, of all the fabric-covered cylinders tested, the fleece and cotton ensemble showed the most difference between the results of the model and the experiment (53%) for the high airflow speed case. This is because the fleece and cotton ensemble has the highest value of air permeability (Table 3.2) and at high airflow speeds, the effects of air permeability on the heat transfer within the fabric-covered cylinder is increased. As the airflow speed increases, the rate at which air infiltrates the fabric-covered cylinder increases. This leads to an even higher rate of heat transfer from the fabric-covered cylinder that is not accounted for in the numerical model. This can be seen in Figures 5.6, 5.7 and 5.8 as the results for the lower airflow speed tests are much closer to the numerical model than the results of the tests performed for high airflow speed.

Furthermore, although the fabrics used for the experiments were fitted as tightly as possible, it is very difficult to completely eradicate air gaps, as thermocouples were placed between the various fabric layers to measure the temperature. The presence of air gaps would increase the thermal resistance of the entire fabric-covered cylinder ensemble, thereby increasing the temperature within the cylinder and the fabric. This can be seen in Figure 5.9 where the relationship between air gap size and the temperature within the layers of a five-layer fabric-

covered cylinder is explored using the thermal resistance network. For this example, air gaps of equal sizes exist between all the layers of the ensemble.
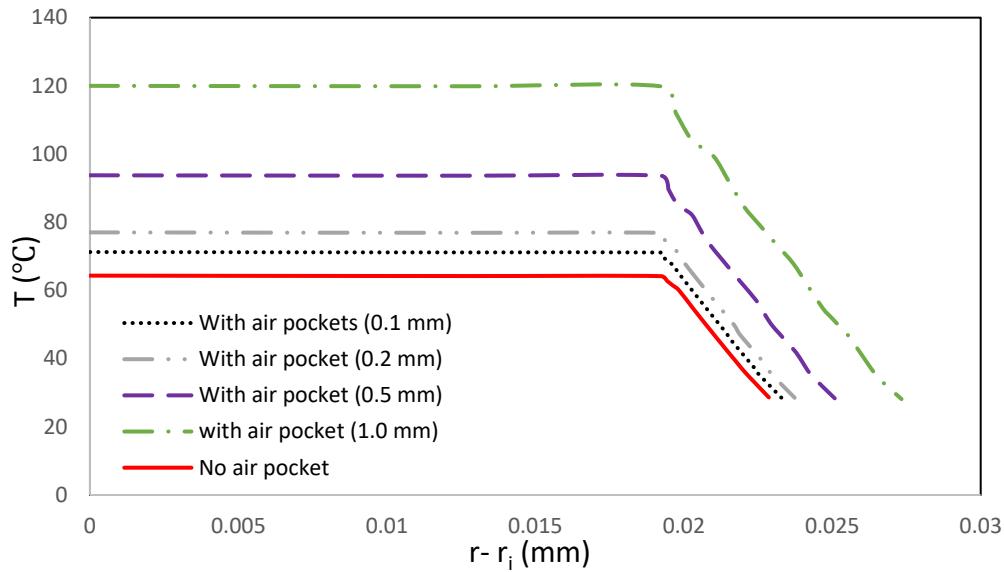

Figure 5.9: Effect of air gap on temperature within the cylinder obtained from the thermal resistance network method.

For this test run, a heat transfer rate of 18 W was input into the composite cylinder with convection on the outside ($h = 100$ W/m^2·K, $T_\infty = 25$°C). From Figure 5.9, it is expected that the temperature in the cylinder increases as the air gap size increases due to the increase in the resistance to heat transfer between each layer. However, from Figures 5.5 to 5.8, it can be seen that the temperature results of the finite-difference model which assumed perfect physical and thermal contact between all the layers of the composite cylinder are higher than the results from the experiment. This shows that the effect of air penetration through the fabric in decreasing the thermal resistance of the fabric is much larger than the effect caused by the increase in thermal resistance due to the air gaps that may have existed during the experiment. Other reasons for the differences in results between the experiment and the finite-difference model include the fact that the thermal properties of the fabrics were obtained from the literature and were not measured for the specific sample materials that were tested. This could contribute to the difference between the results of the experiment and the finite-difference model as can be seen from the sensitivity study for the effect of thermal conductivity on temperature in Table 4.4.

From the results shown in Figures 5.2 to 5.8, it can be concluded that the finite-difference model documented in this chapter can be used to calculate the temperature values at multiple radial positions and at a large number of time steps within a composite cylinder that is undergoing transient conduction and has an impermeable surface. It can also be used for cylinders with a permeable surface at low airflow speeds since the effect of fabric permeability is greatly reduced. Although the capability of the finite-difference model has been demonstrated on a maximum of a seven-layer cylinder, it can be adapted for use on a cylinder with an even greater number of layers.

The model was primarily developed to simulate the boundary conditions and test scenarios employed in the experiments performed for this research. However, it can easily be adapted to different boundary conditions and can also be used to calculate the heat transfer coefficient and the heat transfer rate through the cylinder given the other parameters. One interesting application of the model would be in the testing of firefighters' clothing. Along with a model of the skin and the physical and thermal properties of the the multi-layered firefighters' protective clothing, the time to different degrees of skin burn injury can be approximated. Several adjustments such as accounting for fit of clothing, effect of movement, contact resistance, and fabric permeability, would have to be made to the model to obtain values that are more representative of the actual situation. However, the model can be used almost as presently constructed to compare different fabric ensembles and obtain a ranking of which material combination provides better protection or thermal stress management in still or low wind speed conditions.

Chapter 6 – Conclusions and Recommendations

6.1 Conclusions

In this thesis research, a heated cylinder was used to evaluate parameters related to the thermal stress management of various clothing. A finite-height cylinder with a free end at the top causing three-dimensionality in the flow, and an infinitely long cylinder that spanned the height of the wind tunnel to promote two-dimensional flow, were used. The fabric specimens were wrapped around the heated sections of these two cylinder models and the Nusselt number and thermal resistance values for the 2D and 3D fabric-covered cylinders were obtained. Several conclusions were drawn from the results.

1) The Nusselt numbers obtained for the fabric-covered cylinders were significantly lower than the Nusselt numbers from the surface of the bare cylinder. Due to the difference in drag force coefficient at high Reynolds numbers between the bare cylinder and the cylinder covered with the most permeable fabric (fleece and cotton), the fabric air permeability seemed to be most responsible for the difference in Nusselt number results. The penetration of air into the layers of the fabric further disturbs the airflow in the fabric-covered cylinder's boundary layer compared to that for a bare cylinder and this may lead to a reduction in the rate of convective heat transfer from the surface of the fabric covered cylinder.

2) While fabric thickness and thermal conductivity are the most important factors in determining thermal resistance in still conditions, the air permeability of the fabric plays an important role in determining its thermal resistance in windy environments. The effect of air permeability could also be noticed in the thermal resistance results for the different fabric ensembles tested. Although the Nusselt numbers for the permeable fabric-covered cylinders are lower than the Nusselt numbers for the bare cylinder or an impermeable fabric-covered cylinder (indicating a decrease in heat transfer rate), a decrease in thermal resistance was noticed for fabrics with very high air permeability (indicating an increase in heat transfer). This is because as the air passes through the fabric, there is additional heat transfer through advection, radiation and other forms from both the surface of the cylinder as well as the fibers of the different fabrics. This leads to a reduction in the overall measured thermal resistance of the fabric ensemble that is not usually noticed in

singular low-speed airflow testing methods such as the hot plate. Furthermore, for the more permeable or multi-layered fabric ensembles, a reduction in thermal resistance values was noticed as the speed of airflow increased while the thermal resistance for the less permeable fabrics remained constant. This further confirms the impact of fabric permeability on thermal resistance.

3) A finite-difference numerical model was developed to complement the results of convective heat transfer obtained by the experiments. The model was developed using the backward-difference approximation and the energy balance at various important boundary points was analyzed to develop equations that approximate the temperature at multiple radial positions and time steps in a multi-layered cylinder. The composite cylinder was used to approximate the fabric-covered cylinder tests. The results of the model were in good agreement with the experiments for the bare cylinder as well as the fabric-covered cylinder that was protected from the effects of air penetration by an aluminum shimstock. The model results of fabric-covered cylinders at low airflow speed and temperature difference were significantly closer to the results of the experiment than for tests at high airflow speed and temperature difference. These are all expected as the effects of fabric permeability were not included in the development of the model and it was observed in the experiments to play a major role in determining the convective heat transfer coefficient for fabric-covered cylinders, especially at higher airflow speed. Other assumptions made for the numerical model, such as perfect thermal contact between all the layers of the composite cylinder could contribute to the higher temperature values obtained in the finite-difference model.

Although hot plate tests that measure the thermal resistance of fabrics under very low airflow conditions provide information for comparing the intrinsic thermal resistance of fabrics, the effects of wind penetration into the fabric are usually not apparent in these tests. From the results of the heated cylinder experiments and finite-difference model, it is understood that the effects of fabric permeability cannot be ignored as it plays a very significant role in the thermal resistance of fabrics in environments that involve relatively high speed airflow. While some firefighters' jobs are performed in low airflow speed environments, others are performed in environments where the individual would be subject to variations in wind conditions and the effects of air permeability would be more important.

76

6.2 Recommendations for Future Work

Although the results of the heated cylinder method developed in this thesis were shown to be comparable to the results from the hot plate test method, which is often used for ranking the thermal stress management of candidate clothing, some improvements can be made to this method. As the heat transfer from a person's body is not only sensible but is also influenced by sweat, the effect of this is important in quantifying the effects of clothing on thermal stress. This can be incorporated into the method of the heated cylinder, thereby enhancing the method to also be able to measure the evaporative resistance of different fabrics as well as the total heat loss through fabric layers. Furthermore, as individual pieces of clothing can be sized differently, the effect of fit can also be explored using the heated cylinder test method by allowing a range of air gaps between the cylinder's surface and the fabric to be considered, including the effects of air speed on the size of these air gaps. This would help to yield results that are more representative of real life situations.

For the finite-difference model developed, including the concept of fabric permeability as well as the effect of contact resistance between the layers of the multi-layered cylinder could help to yield more realistic results. Thermal properties could also be measured for the specific fabrics included in this study.

References

Achenbach, E. (1975). Total and local heat transfer from a smooth circular cylinder in cross-flow at high Reynolds number. *International Journal of Heat and Mass Transfer,* 18, 1387-1396.

Achenbach, E. (1977). The effect of surface roughness on the heat transfer from a circular cylinder to the cross flow of air. *International Journal of Heat and Mass Transfer*, 20(4), 359-369.

ASTM International (2012). ASTM E104, Standard Practice for Maintaining Constant Relative Humidity by Means of Aqueous Solutions, West Conshohocken, PA.

ASTM International (2016). ASTM F1291, Standard Test Method for Measuring the Thermal Insulation of Clothing Using a Heated Manikin, West Conshohocken, PA.

ASTM International (2016). ASTM D1776, Standard Practice for Conditioning and Testing Textiles, West Conshohocken, PA.

ASTM International (2017). ASTM F1868, Standard Test Method for Thermal and Evaporative Resistance of Clothing material using a Sweating Hot Plate, West Conshohocken, PA.

ASTM International (2019). ASTM D 123, Textiles – Standard Terminology Relating to Textiles, West Conshohocken, PA.

Bakshi, A., (2015). *Development and Study of Waterproof Breathable Fabric Using Silicone Oil and Polyurethane Binder,* M.Sc. Thesis, Technology Studies, Eastern Michigan University, Ypsilanti, MI.

Beitel, A., Heng, H., & Sumner, D. (2019). The effect of aspect ratio on the aerodynamic forces and bending moment for a surface-mounted finite-height cylinder. *Journal of Wind Engineering & Industrial Aerodynamics,* 186, 204-213.

Bergman, T., & Incropera, F. (2011). *Fundamentals of Heat and Mass Transfer.* Wiley, Hoboken, NJ.

Burleson, W., & Eppes Jr., R. (1965). *Solution of transient heat transfer problems for flat Plates, cylinders, and spheres by finite-difference methods*, US Army Missile Command, Madison County, AL.

CGSB (2013). CAN/CGSB-4.2, No.36-M89, Textile Test Methods, Air Permeability, Ottawa, ON.

Churchill, S., & Bernstein, M. (1977). A correlating equation for forced convection from gases and liquids to a circular cylinder in cross flow. *Journal of Heat Transfer – Transactions of the ASME*, 99(2), 300-306.

Chyu, M. K., & Natarajan, V. (1996). Heat transfer on the base surface of three dimensional protruding elements. *International Journal of Heat and Mass Transfer, 39*(14), 2925-2935.

Delouei, A., Kayhani, H. & Norouzi M. (2012). Exact analytical solution of unsteady axi-symmetric conductive heat transfer in cylindrical orthotropic composite laminates. *International Journal of Heat and Mass Transfer, 55*(15-16), 4427-4436.

Ding, D. (2010). *Characterizing the Performance of a Single-layer Fabric System through a Heat and Mass Transfer Model.* M.Sc. Thesis, Mechanical Engineering, University of Alberta, Edmonton, AB.

Fahy, R., Petrillo, J & Molis, J. (2020). NFPA – Firefighter fatalities in the United States – 2019, North Providence, RI.

Finnigan, J. J., & Longstaff, R. A. (1982). A wind-tunnel model study of forced convective heat-transfer from cylindrical grain storage bins. *Journal of Wind Engineering and Industrial Aerodynamics, 10*(2), 191-211.

Fonseca, G., & Breckenridge, J. (1965). Wind penetration through fabric systems. Part I. *Textile Research Journal, 35*(2), 95-103.

Fox, T., & West, G. (1990). On the use of end plates with circular cylinders in wind tunnel studies. *Research Report Series - University of Queensland, Department of Civil Engineering,* (118), 1-17.

Ganat, T., (2020). *Fundamentals of Reservoir Rock Properties*. Springer, Cham, Switzerland.

Garcia-Villalba, M., Palau-Salvador, G., & Rodi, W. (2014). Forced convection heat transfer from a finite-height cylinder. *Flow Turbulence and Combustion,* 93(1), 171-187.

Gibson, P. (2009). Modeling heat and mass transfer from fabric-covered cylinders. *Journal of Engineered Fibers and Fabrics,* 4(1), 1-8.

Giordano, R., Ianiro, A., Astarita, T., & Carlomagno, G. M. (2012). Flow field and heat transfer on the base surface of a finite circular cylinder in crossflow. *Applied Thermal Engineering,* 49, 79-88.

Gunesoglu, S., & Meric, B. (2006). Heat and mass transfer properties of 2-yarn fleece knitted fabrics. Indian Journal of Fibre and Textile Research, 31(3), 415-421.

Hilpert, R. (1933). Wärmeabgabe von geheizten drähten und rohren im luftstrom. *Forschung Auf Dem Gebiete Des Ingenieurwesens*, 4(5), 215-224. (German)

Holmer, I., & Nilsson H. (1995). Heated manikins as a tool for evaluating clothing. *The Annals of Occupational Hygiene,* 39(6), 809-818.

Huang, J. (2006). Sweating guarded hot plate test method. *Polymer Testing,* 25(5), 709-716

ISO (2004). Clothing - physiological effects - measurement of thermal insulation by means of a thermal manikin. ISO 15831, International Organization for Standardization, Geneva, Switzerland.

ISO (2014). Textiles - physiological effects - measurement of thermal and water-vapour resistance under steady-state conditions (Sweating guarded hot plate test). ISO 11092, International Organization for Standardization, Geneva, Switzerland.

Jacquemini, F., & Vautrin, A. (2004). Analytical calculation of the transient thermoelastic stresses in thick walled composite pipes. *Journal of Composite Materials,* 38(19), 1733-1751.

Jin, L., Cao, M., Yu, L., Hu, W., Yoon, J., Park, Y., & Li, K. (2018). New approaches to evaluate the performance of firefighter protective clothing materials. *Fire Technology,* 54(5), 1283-1307.

Kamata, Y., Kato, T., Ito, A., & Yahata, N. (1988). Convective heat transfer from human body. (Part 2. Effect of fabric on heat transfer). *Sen'i Gakkaishi, 44*(2), 78-87.

Kawamura, T., Hiwada, M., Hibino, T., Mabuchi, I., & Kumada, M. (1984). Heat transfer from a finite circular cylinder on the flat plate. *Bulletin of the JSME*, 27(233), 2430 – 2439.

Kim, J., Powell, J., Roberge, R., Shepherd, A., & Coca, A. (2014). Evaluation of protective ensemble thermal characteristics through sweating hot plate, sweating thermal manikin, and human tests. *Journal of Occupational and Environmental Hygiene, 11*(4), 259-267.

Kind, R., Jenkins, J., & Seddigh, F. (1991). Experimental investigation of heat transfer through wind-permeable clothing. *Cold Regions Science and Technology, 20*(1), 39-49.

Kline, S. (1985). The Purposes of Uncertainty Analysis. *Journal of Fluids Engineering – Transactions of the ASME*, 107(2), 153-160.

Kosiński, P., & Wójcik, R. (2017). An impact of air permeability on heat transfer through partitions insulated with loose fiber materials. *Applied Mechanics and Materials, 861*, 190-197.

Lawson, W., Bryner, N., & Amon F. (2005). Estimates of Thermal Properties for Fire Fighters' Protective Clothing Materials. *Govt Reports Announcements & Index (GRA&I)*, 14.

Lee, Z., Chen, C. & Hung, C. (2001). Transient thermal stress analysis of multilayered hollow cylinder. *Acta Mechanica, 151*(1-2), 75-88.

Lu, X., Tervola, P., & Viljanen, M. (2005). An efficient analytical solution to transient heat conduction in a one-dimensional hollow composite cylinder. *Journal of Physics A: Mathematical and General, 38*(47), 10145-10155.

Manshahia, M., & Das, A. (2014). Thermophysiological comfort characteristics of plated knitted fabrics. *The Journal of the Textile Institute, 105*(5), 509-519.

McLellan, T., & Selkirk, G. (2006). The management of heat stress for the firefighter: A review of work conducted on behalf of the Toronto fire service. *Industrial Health, 44*(3), 414-426.

Morrissey, M., & Rossi, R. (2014). The effect of wind, body movement and garment adjustments on the effective thermal resistance of clothing with low and high air permeability insulation. *Textile Research Journal,* 84(6), 583-592.

Najibi, A., & Talebitooti, R. (2017). Nonlinear transient thermo-elastic analysis of a 2D-FGM thick hollow finite length cylinder. *Composites Part B*, 111, 211-227.

Nazare, S., and Madrzykowski. (2015). A review of test methods for determining protective capabilities of fire fighter protective clothing from steam. NIST Technical Note 1861, National Institute of Standards and Technology, Gaithersburg, MD.

Okamoto, T., & Yagita, M. (1973). The experimental investigation on the flow past a circular cylinder of finite length placed normal to the plane surface in a uniform stream. *Bulletin of the JSME*, 16(95), 805-814.

OSHA (2015). Fire Service Features of Buildings and Fire Protection Systems. OSHA 3256-09R 2015. Occupational Safety and Health Administration, U.S. Department of Labor, Washington, DC.

Rodiger, T., Knauss, H., Gaisbauer, U., & Kramer, E. (2007). Pressure and heat flux measurements on the surface of a low-aspect-ratio circular cylinder mounted on a ground plate. *New Results in Numerical and Experimental Fluid Mechanics Vi,* 96, 121 – 128.

Sakamoto, H., & Oiwake, S. (1984). Fluctuating forces on a rectangular prism and a circular cylinder placed vertically in a turbulent boundary layer. *Journal of Fluids Engineering - Transactions of the ASME,* 106(2*)*, 160 – 166.

Sanitjai, S., & Goldstein, R. (2004). Forced convection heat transfer from a circular cylinder in crossflow to air and liquids. *International Journal of Heat and Mass Transfer*, 47(22), 4795-4805.

Saskatoon weather stats. (2018). "Saskatoon Historical Wind Speed". Amateur Weather Statistics for Saskatoon, Saskatchewan. Retrieved 13 October 2018, from https://saskatoon.weatherstats.ca/metrics/wind_speed.html.

Schmidt, E., & Wenner, K. (1943). Heat transfer over the circumference of a heated cylinder in transverse flow. *NACA Technical Memorandum* 1050.

Sobera, M., Kleijn, C., Van den Akker, H., & Brasser, P. (2003). Convective heat and mass transfer to a cylinder sheathed by a porous layer. *AIChE Journal,* 49(12), 3018-3028.

Sparrow, E., & Samie, F. (1981). Measured heat transfer coefficients at and adjacent to the tip of a wall-attached cylinder in crossflow – Application to fins. *Journal of Heat Transfer – Transactions of the ASME,* 103(4), 778-784.

Stansby, P. (1974). The effects of end plates on the base pressure coefficient of a circular cylinder. *Aeronautical Journal,* 78, 36, 37.

Su, Y., Li, R., Yang, J., Song, G., and Li, J. (2019). Developing a test device to analyse heat transfer through firefighters' protective clothing. *International Journal of Thermal Sciences* 138, 1-11.

Takeuchi, M., Isshiki, N., & Ishibashi, Y. (1982). Heat transfer on cylinder covered with close-fitting fabrics: Part I, wind penetration through fabrics. *Bulletin of the JSME,* 25(207), 1406-1411.

Takeuchi, M., Suzuki M., Kurosaki Y., & Isshiki N. (1984) Heat transfer on cylinder covered with close-fitting fabrics: Part 3, distribution of local heat transfer coefficients. *Bulletin of the JSME* 27(255), 483-489

Tamene, Y., Bougriou, C., & Bessaih, R. (2006). Thermal behavior of a composite cylinder in transient regime. *International Journal of Theoretical and Applied Mechanics*, 1, 1-12.

Torvi, D. (1997), "Heat Transfer in Thin Fibrous Materials under High Heat Flux Conditions," PhD Thesis, Mechanical Engineering Deptartment, University of Alberta, Calgary, Alberta.

Tsutsui, T., Igarashi, T., & Nakamura, H. (2000). Fluid flow and heat transfer around a cylindrical protuberance mounted on a flat plate boundary layer. *JSME International Journal, Series B: Fluids and Thermal Engineering*, 43(2), 279-287.

Tsutsui, T., & Kawahara, M. (2006). Heat transfer around a cylindrical protuberance mounted in a plane turbulent boundary layer. *Journal of Heat Transfer-Transactions of the ASME,* 128(2), 153-161.
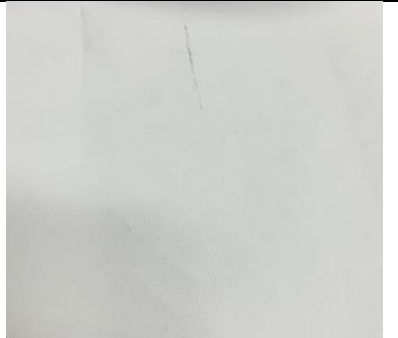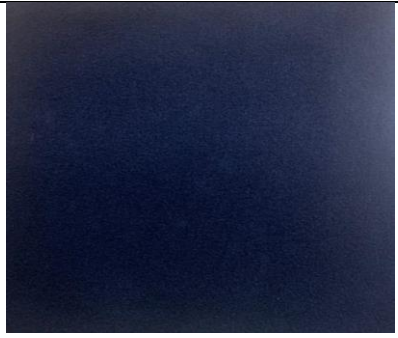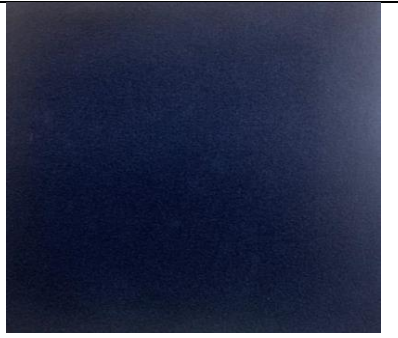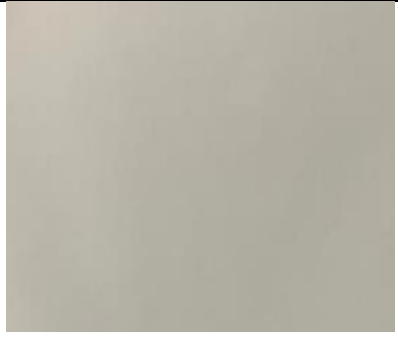
Ulijaszek, S., & Henneberg, M. (2012). Results of epidemiological studies of blood pressure are biased by continuous variation in arm size related to body mass. *Human Biology,* 84(4), 437-444.

University of Illinois Fire Service Institute (2008). "Firefighter fatalities and injuries: the role of heat stress and PPE", Urbana, IL. Accessed: January 8, 2020. https://www.fsi.illinois.edu/documents/research/FFLSRC_FinalReport.pdf.

Wen, S., Batcheller, J., & Petersen, S. (2016). Heat strain in chemical protective coveralls — are thermal sweating mannequin tests more informative than sweating hot plate tests? *Performance of Protective Clothing and Equipment: 10ᵗʰ Volume, Risk Reduction through Research and Testing,* ed. Shiels, B. & Lehtonen, K. (Eds.), (West Conshohocken, PA: ASTM International, 2016*). STP1593-EB *ASTM STP, 1593*, 296 – 312.

West, G., & Apelt, C. (1982). The effects of tunnel blockage and aspect ratio on the mean flow past a circular cylinder with Reynolds numbers between 10,000 and 100,000. *Journal of Fluid Mechanics,* 114, 361-377.

Yang, B., & Liu, S. (2017). Closed-form analytical solutions of transient heat conduction in hollow composite cylinders with any number of layers. *International Journal of Heat and Mass Transfer,* 108, 907-917.

Zhu, G., Kremenakova, D., Wang, Y., Militky, J., & Mishra, R. (2015). Study on air permeability and thermal resistance of textiles under heat convection. *Textile Research Journal,* 85(16), 1681-1690.

Appendix A: Pictures of Fabrics Tested

The pictures of the fabrics tested are shown in Table A.1.

Table A.1: Pictures of fabrics tested

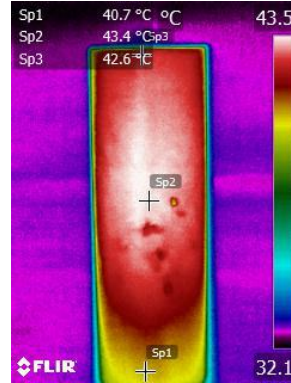| Name of fabric	Front	Back
PBI Max		
RS Black		
Cotton		

Winter jacket		
Fleece		
Thermal liner – XE – 289		
Moisture barrier – Stedair 3000		

Appendix B: Infrared Images for 3D and 2D Cylinder Tests

The infrared images for the various test scenarios of the 3D and 2D cylinders are shown in this appendix.
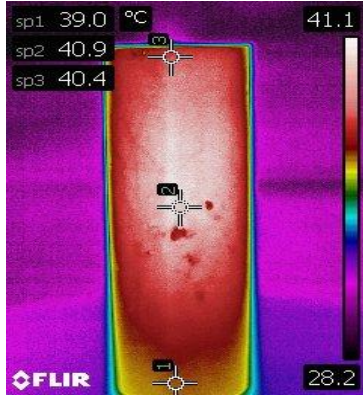
(a) $U_\infty = 11.8$ m/s, $\Delta T = 10°C$

(b) $U_\infty = 32$ m/s, $\Delta T = 10°C$
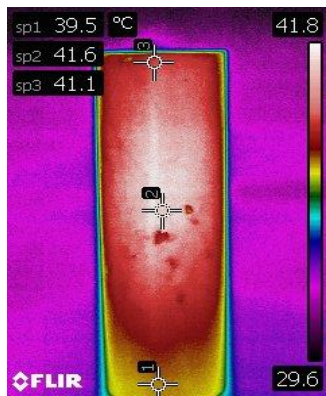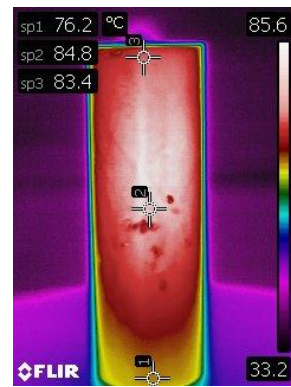
(c) $U_\infty = 18.7$ m/s, $\Delta T = 10°C$

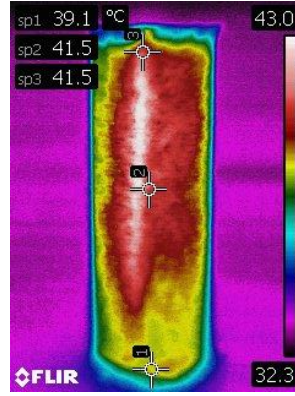(d) $U_\infty = 38.5$ m/s, $\Delta T = 50°C$
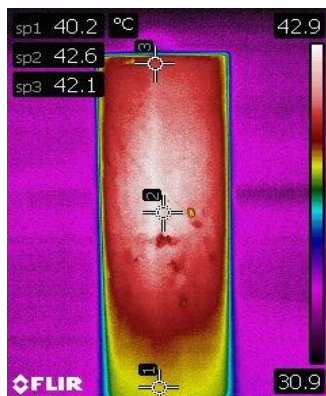
(e) $U_\infty = 26.5$ m/s, $\Delta T = 10°C$
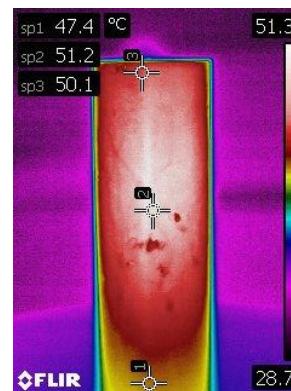
(f) $U_\infty = 18.7$ m/s, $\Delta T = 20°C$
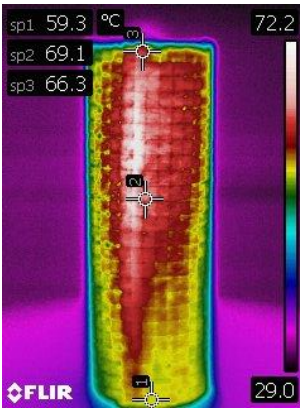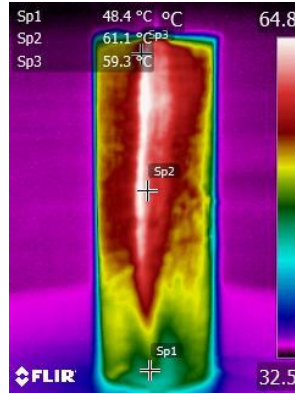
Figure B.1: Examples of infrared images for bare 3D cylinder.
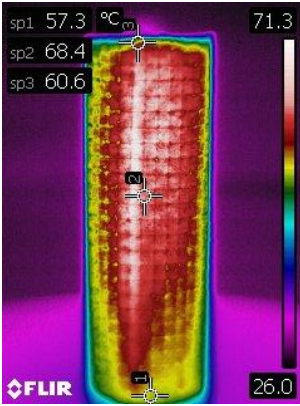
(a) RS Black fabric-covered cylinder

$(U_\infty = 11.8$ m/s, $\Delta T = 50℃)$

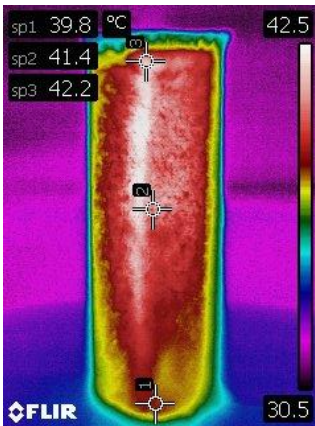

(b) Fleece and cotton fabric-covered cylinder $(U_\infty = 11.8$ m/s, $\Delta T = 50℃)$

(c) RS Black fabric-covered cylinder

$(U_\infty = 18.7$ m/s, $\Delta T = 50℃)$
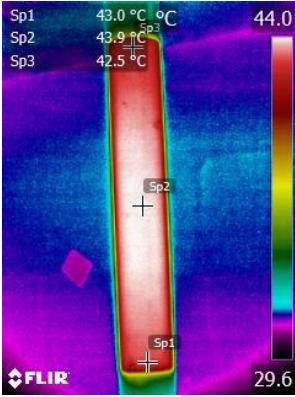

(d) Winter jacket fabric-covered cylinder

$(U_\infty = 26.5$ m/s, $\Delta T = 50℃)$

(e) Fleece and cotton fabric-covered cylinder

$(U_\infty = 26.5$ m/s, $\Delta T = 50℃)$

Figure B.2: Examples of infrared images for the 3D fabric-covered cylinder.

(a) $U_\infty = 11.8$ m/s, $\Delta T = 10°C$

(b) $U_\infty = 32$ m/s, $\Delta T = 10°C$
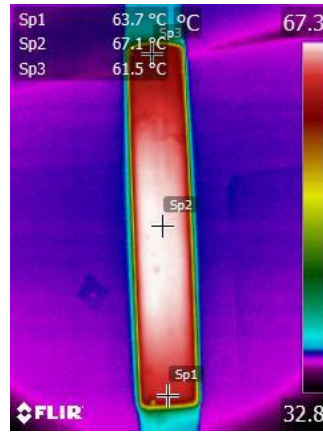
(c) $U_\infty = 18.7$ m/s, $\Delta T = 10°C$

(d) $U_\infty = 38.5$ m/s, $\Delta T = 30°C$
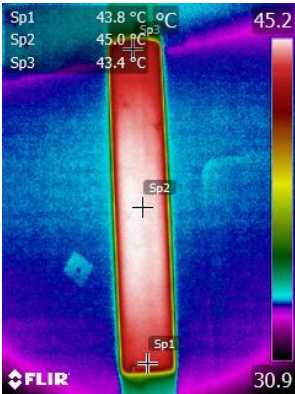
(e) $U_\infty = 26.5$ m/s, $\Delta T = 10°C$

Figure B.3: Examples of infrared images for bare 2D cylinder.
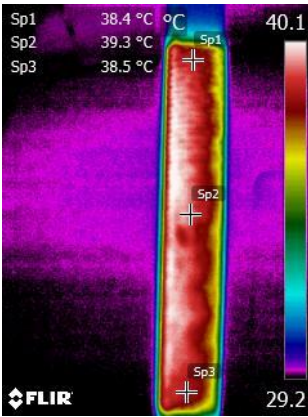
(a) RS Black fabric-covered cylinder
(U_∞ = 18.7 m/s, ΔT = 10℃)
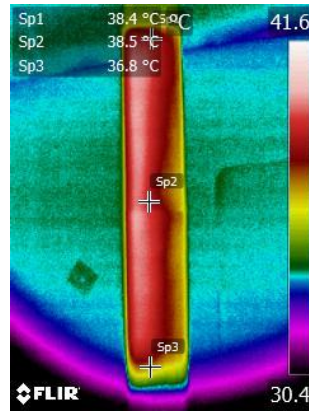
(b) RS Black covered with shim stock
(U_∞ = 32 m/s, ΔT = 10℃)
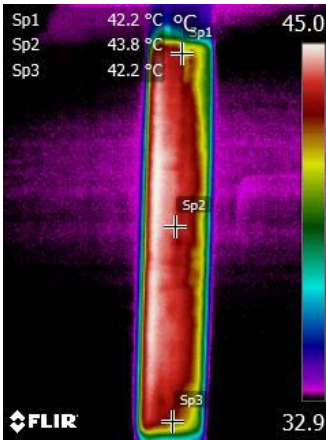
(c) PBI Max fabric-covered cylinder
(U_∞ = 18.7 m/s, ΔT = 10℃)

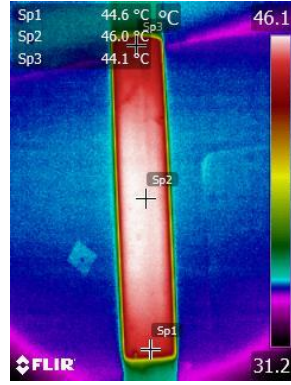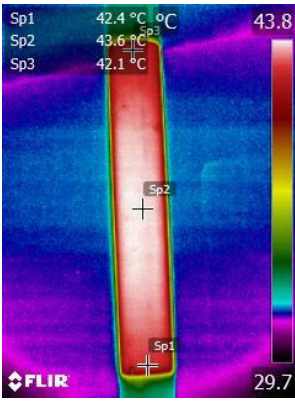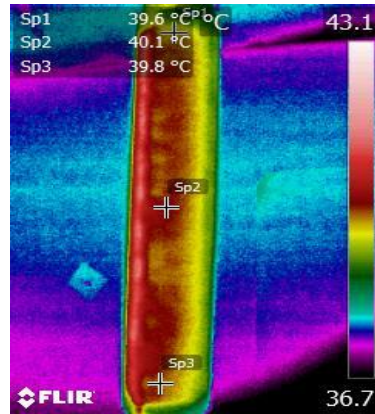(d) Firefighters' PPE and cotton fabric-covered cylinder (U_∞ = 11.8 m/s, ΔT = 50℃)
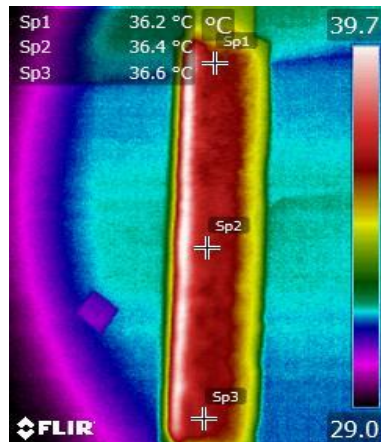
(e) Fleece and cotton fabric-covered cylinder (U_∞ = 11.8 m/s, ΔT = 10℃)

Figure B.4: Examples of infrared images for 2D fabric-covered cylinders.

Appendix C: Experimental and Numerical Values for the Cylinder and Fabric Surface Temperatures

In this appendix, the temperatures measured from the experiment and obtained from the finite-difference model are shown. Table C.1 shows the temperatures inside the bare cylinder measured from the experiment (T_{TC}) and calculated using the finite-difference model (T_c) as well as the percentage difference between them. The average temperature on the surface of the cylinder measured by the infrared camera (T_{avg}) is also shown.

Table C.1: Temperature inside bare cylinder from experiment and finite-difference model

U_∞ (m/s)	Intended ΔT (°C)	Experiment		Model	% difference	% difference
		T_{TC} (°C)	T_{avg} (°C)	T_c (°C)	(T_{TC} vs T_c)	(T_{TC} vs T_{avg})
	10	42.9	43.5	43.7	1.8	1.4
	20	50.3	52.8	53.1	5.5	4.8
11.8	30	65.0	64.5	65.0	0.1	0.8
	40	73.8	70.1	70.7	4.3	5.1
	50	84.2	82.3	83.1	1.3	2.3
	10	43.1	43.1	43.3	0.6	0.1
	20	50.9	52.4	52.8	3.8	3.0
18.7	30	63.5	63.8	64.4	1.4	0.6
	40	70.9	70.7	71.5	0.8	0.3
	50	83.5	80.9	81.9	2.0	3.2
	10	44.4	44.5	44.8	0.9	0.3
	20	52.8	54.0	54.5	3.2	2.3
26.5	30	61.3	57.5	58.2	5.1	6.3
	40	72.8	72.9	73.8	1.5	0.3
	50	84.9	82.6	83.8	1.3	2.7
	10	45.5	45.3	45.6	0.3	0.3
	20	54.7	56.2	56.7	3.7	2.8
32	30	64.5	62.2	63.0	2.4	3.6
	40	72.3	68.8	69.9	3.4	5.0
	50	85.7	83.4	84.7	1.1	2.7
	10	46.8	46.7	47.0	0.6	0.1
	20	57.7	58.0	58.6	1.6	0.5
38.5	30	67.2	65.2	66.1	1.7	3.0
	40	75.1	72.6	73.8	1.8	3.4
	50	88.9	85.4	86.8	2.3	4.0

Table C.2 shows the temperatures on the surface of the brass cylinder and on the surface of the fabric for the PBI Max fabric-covered cylinder measured from the experiment and calculated using the finite-difference model as well as the percentage difference between them.

Table C.2: Temperature on the surface of the brass cylinder and on the fabric for the PBI Max fabric-covered cylinder obtained from both the experiment and the finite-difference model

U_∞ (m/s)	Intended ΔT (°C)	T_c (°C)			T_f (°C)	
		Experiment	Model	% difference	Experiment	Model
11.8	10	45.7	50.8	10.5	43.9	43.9
	50	83.7	102.3	20.0	73.0	73.0
18.7	10	45.5	51.0	11.4	43.3	43.3
	50	86.2	108.0	22.4	73.6	73.6
26.5	10	42.0	47.7	12.6	39.3	39.3
	50	84.8	110.5	26.3	69.9	69.9
32	10	44.4	50.8	13.5	41.3	41.3
	50	86.3	113.4	27.2	69.9	69.9
38.5	10	46.9	54.1	14.2	43.3	43.3
	50	87.5	117.2	29.0	69.9	69.9

Table C.3 shows the temperatures on the surface of the brass cylinder and on the surface of the fabric for the RS Black fabric-covered cylinder measured from the experiment and calculated using the finite-difference model.

Table C.3: Temperature on the surface of the brass cylinder and on the fabric for the RS Black fabric-covered cylinder obtained from both the experiment and the finite-difference model

U_∞ (m/s)	Intended ΔT (°C)	T_c (°C)			T_f (°C)	
		Experiment	Model	% difference	Experiment	Model
11.8	10	40.4	47.1	15.3	37.6	37.6
	50	84.6	112.2	28.0	73.1	73.1
18.7	10	41.4	48.5	15.8	38.3	38.3
	50	84.4	115.8	31.3	70.6	70.6
26.5	10	44.3	52.8	17.6	40.6	40.6
	50	86.2	121.1	33.7	70.1	70.1
32	10	47.1	55.8	16.9	42.7	42.7
	50	83.6	120.6	36.3	65.5	65.5
38.5	10	48.5	58.0	17.8	43.2	43.2
	50	88.5	128.1	36.6	69.5	69.5

Table C.4 shows the temperatures on the surface of the brass cylinder and on the surface of the fabric ensemble for the PBI Max and cotton fabric-covered cylinder measured from the experiment and calculated using the finite-difference model.

Table C.4: Temperature on the surface of the brass cylinder and fabric for the PBI Max and cotton fabric-covered cylinder obtained from both the experiment and the finite-difference model

U_∞(m/s)	Intended ΔT (°C)	T_c (°C)			T_f (°C)	
		Experiment	Model	% difference	Experiment	Model
11.8	10	40.0	45.6	13.0	37.5	37.4
	50	72.4	98.7	30.7	63.5	63.2
18.7	10	41.0	48.5	16.7	39.7	39.6
	50	72.2	100.8	33.0	61.7	61.4
26.5	10	42.4	48.9	14.2	39.4	39.3
	50	74.1	104.5	34.0	61.5	61.2
32	10	45.5	52.9	15.1	42.7	42.6
	50	68.1	102.2	40.0	54.6	54.4
38.5	10	40.5	49.9	20.8	37.0	37.0
	50	74.4	109.8	38.4	59.1	58.9

Table C.5 shows the temperatures on the surface of the brass cylinder and on the surface of the fabric ensemble for the RS Black and cotton fabric-covered cylinder measured from the experiment and calculated using the finite-difference model.

Table C.5: Temperature on the surface of the brass cylinder and fabric for the RS Black and cotton fabric-covered cylinder obtained from both the experiment and the finite-difference model

U_∞ (m/s)	Intended ΔT (°C)	T_c (°C)			T_f (°C)	
		Experiment	Model	% difference	Experiment	Model
11.8	10	41.6	46.9	12.0	38.7	38.7
	50	76.4	100.9	27.7	63.2	63.2
18.7	10	42.8	48.8	13.2	39.3	39.3
	50	74.7	100.8	29.7	59.6	59.6
26.5	10	43.9	50.5	13.9	40.1	40.1
	50	76.3	104.8	31.5	58.7	58.7
32	10	44.7	51.9	14.9	40.7	40.7
	50	76.5	107.2	33.5	57.0	57.0
38.5	10	48.8	57.2	15.9	44.3	44.3
	50	74.7	105.1	33.8	53.6	53.6

Table C.6 shows the temperatures on the surface of the brass cylinder and on the surface of the fabric ensemble for the fleece and cotton fabric-covered cylinder measured from the experiment and calculated using the finite-difference model.

Table C.6: Temperature on the surface of the brass cylinder and fabric for the fleece and cotton fabric-covered cylinder obtained from both the experiment and the finite-difference model

U_∞ (m/s)	Intended ΔT (°C)	T_c (°C)			T_f (°C)	
		Experiment	Model	% difference	Experiment	Model
11.8	10	43.1	48.7	12.2	35.0	35.0
	50	82.6	103.6	22.5	49.1	49.1
18.7	10	43.8	50.7	14.6	36.4	36.4
	50	81.4	116.9	35.8	47.9	47.9
26.5	10	46.3	56.7	20.2	38.6	38.6
	50	85.1	136.7	46.5	50.0	50.0
32	10	46.3	61.1	27.5	38.6	38.6
	50	84.8	149.4	55.2	49.0	49.0
38.5	10	44.2	65.5	38.9	36.5	36.5
	50	85.4	162.2	62.0	47.9	47.9

Table C.7 shows the temperatures on the surface of the brass cylinder and on the surface of the fabric ensemble for the firefighters' PPE and cotton fabric-covered cylinder measured from the experiment and calculated using the finite-difference model.

Table C.7: Temperature on the surface of the brass cylinder and fabric for the firefighters' and cotton fabric-covered cylinder obtained from both the experiment and the finite-difference model

U_∞ (m/s)	Intended ΔT (°C)	T_c (°C)			T_f (°C)	
		Experiment	Model	% difference	Experiment	Model
11.8	10	43.2	47.8	10.1	35.7	35.7
	50	79.7	103.2	25.7	43.6	43.6
18.7	10	44.1	48.9	10.4	36.2	36.2
	50	82.5	104.1	23.1	44.1	44.1
26.5	10	45.2	51.2	12.4	36.6	36.6
	50	83.2	107.8	25.8	42.9	42.9
32	10	45.2	53.3	16.5	36.5	36.5
	50	81.9	110.0	29.3	40.8	40.8
38.5	10	49.0	57.3	15.6	39.9	39.8
	50	83.5	110.0	27.4	43.6	43.6

Appendix D: Examples of Transient Results from Finite-difference Model

This appendix shows some examples of the transient response for the bare cylinder, the RS Black covered cylinder, the fleece and cotton covered cylinder, and the firefighters' PPE and cotton covered cylinder.
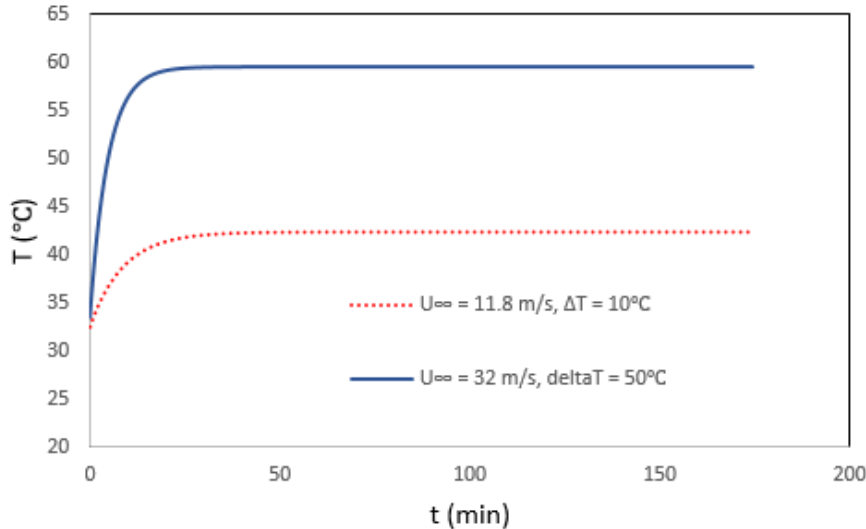

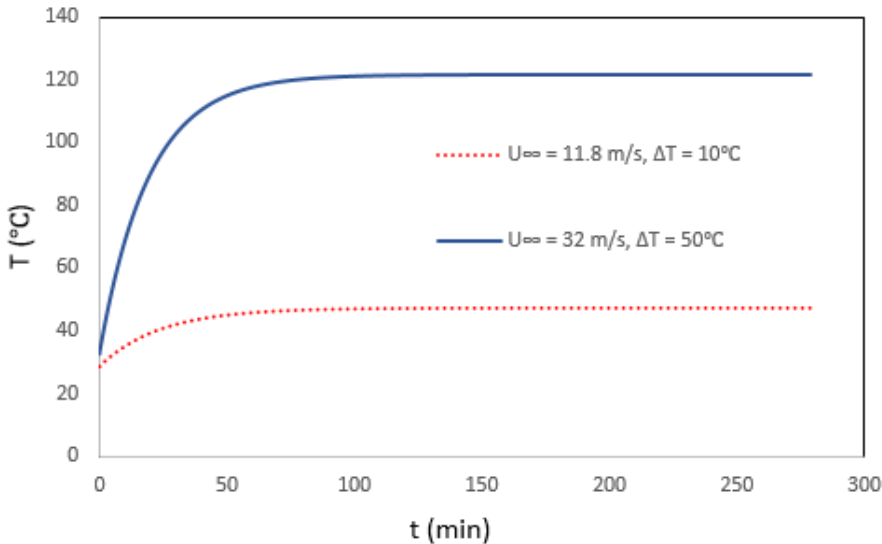Figure D.1: Transient response of the internal temperature of the bare cylinder.

Figure D.2: Transient response of the internal temperature in the brass cylinder for the RS Black fabric-covered cylinder.
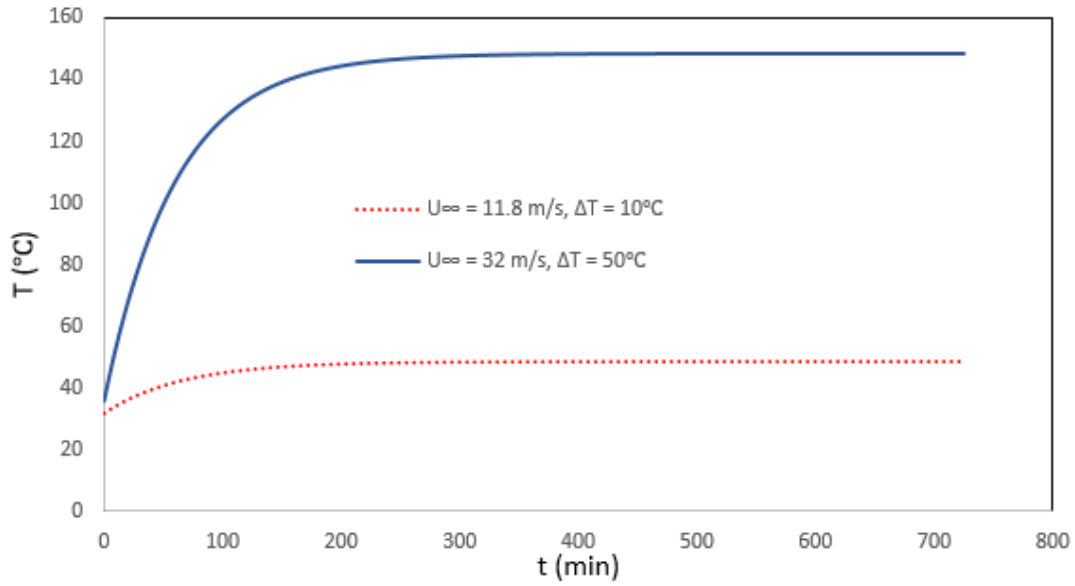
Figure D.3: Transient response of the internal temperature in the brass cylinder for the fleece and cotton fabric-covered cylinder.
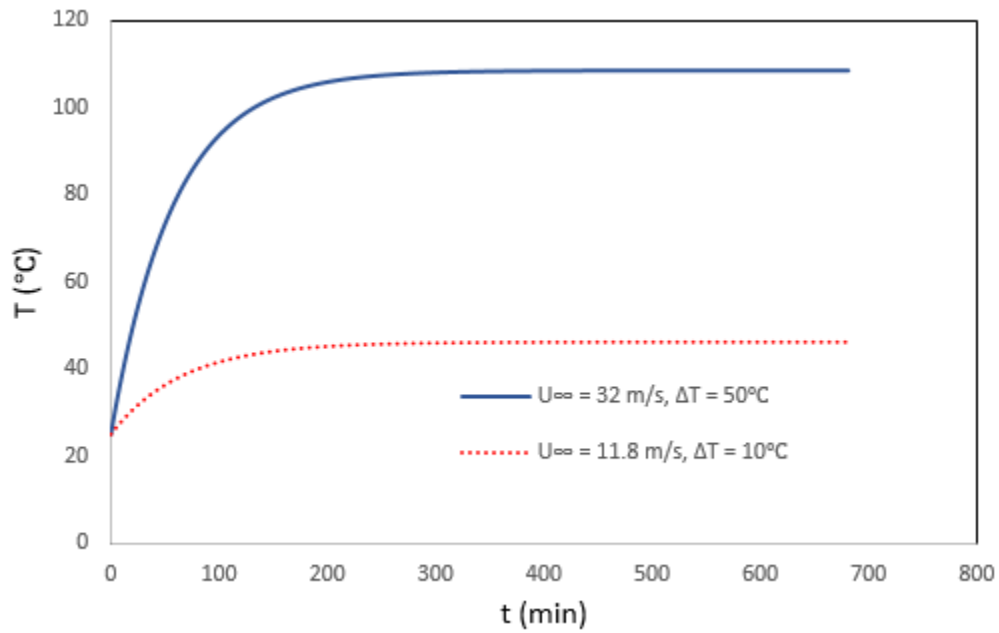

Figure D.4: Transient response of the internal temperature in the brass cylinder for the firefighters' PPE and cotton fabric-covered cylinder.

Appendix E: Permission from Elsevier

ELSEVIER LICENSE
TERMS AND CONDITIONS

Mar 26, 2021

This Agreement between University of Saskatchewan -- Tamsaki Asawo ("You") and Elsevier ("Elsevier") consists of your license details and the terms and conditions provided by Elsevier and Copyright Clearance Center.

License Number	5036320197862
License date	Mar 26, 2021
Licensed Content Publisher	Elsevier
Licensed Content Publication	International Journal of Heat and Mass Transfer
Licensed Content Title	Closed-form analytical solutions of transient heat conduction in hollow composite cylinders with any number of layers
Licensed Content Author	Bingen Yang,Shibing Liu
Licensed Content Date	May 1, 2017
Licensed Content Volume	108
Licensed Content Issue	n/a
Licensed Content Pages	11
Start Page	907

Type of Use	reuse in a thesis/dissertation
Portion	figures/tables/illustrations
Number of figures/tables/illustrations	2
Format	electronic
Are you the author of this Elsevier article?	No
Will you be translating?	No
Title	A Method to Evaluate the Thermal Stress Management of Firefighters' Protective Clothing
Institution name	University of Saskatchewan
Expected presentation date	Apr 2021
Portions	Figure 2 and Figure 5
Requestor Location	University of Saskatchewan 8 - 104 104th St Saskatoon, SK S7N 1M8 Canada Attn: University of Saskatchewan
Publisher Tax ID	GB 494 6272 12
Total	0.00 CAD